PV Module Integrated Converter for Distributed MPPT PV Systems

Acanski, Milos

DOI
10.4233/uuid:95f37723-f452-4e05-95a3-e6693638d8d5

Publication date
2019

Document Version
Final published version

Citation (APA)
Acanski, M. (2019). *PV Module Integrated Converter for Distributed MPPT PV Systems*. [Dissertation (TU Delft), Delft University of Technology]. https://doi.org/10.4233/uuid:95f37723-f452-4e05-95a3-e6693638d8d5

PV Module Integrated Converter for Distributed MPPT PV Systems

Miloš Ačanski

PV Module Integrated Converter for Distributed MPPT PV Systems

Dissertation

for the purpose of obtaining the degree of doctor
at Delft University of Technology
by the authority of the Rector Magnificus, prof.dr.ir. T.H.J.J. van der Hagen
Chair of the Board for Doctorates
to be defended publicly on
Thursday 31 January 2019 at 10:00 o'clock

by

Miloš AČANSKI
Master of Science in Electrical Engineering, University of Belgrade, Serbia
Born in Kula, Serbia

This dissertation has been approved by the promotor.

Composition of the doctoral committee:

Rector Magnificus	chairperson
Prof.dr. J.A. Ferreira	Delft University of Technology, promotor

Independent members:

Prof.dr G.Q. Zhang	Delft University of Technology
Prof.dr A. Smets	Delft University of Technology
Prof.dr A. Weeber	Delft University of Technology
Prof.dr P. Pejović	University of Belgrade, Serbia
Dr. J. Popović	Klimop Energy

This research was funded by IOP (Innovatiegerichte Onderzoeksprogramma) program of the Dutch government, within the EMVT framework (ElektroMagnetische VermogensTechniek).

Printed by Ridderprint, Ridderkerk, Netherlands
ISBN 978-94-6375-307-4

Mojoj porodici
To my family

Acknowledgements

The work presented in this thesis would not be possible without the help and support of many people to whom I would like to express my gratitude.

I would like to thank my promotor, Prof. Braham Ferreira, for the opportunity to do a PhD at TU Delft and for his support. I would like to thank my daily supervisor Jelena Popović for the help and guidance she gave me throughout my studies. For my enthusiasm for power electronics, and for his recommendation for this PhD position, I am thankful to Prof. Predrag Pejović.

The presented research was funded by IOP-EMVT program and sincere thanks go to its committee for the support through our meetings and provided courses. I would like to thank Leonie Stigter from Helianthos for the support with flexible PV modules, and Rob Schaacke from Betronic for the technical support regarding the converter design. For the support on magnetic design and simulations, I am thankful to Ziwei Ouyang. I would like to thank the Netherlands for all the cycling paths and for providing me with a pretty careless everyday life outside the University.

I had an excellent time while working with many great colleagues: Ilija Pecelj, Dalibor Čvorić, Ivan Josifović, Todor Todorović, Johan Wolmarrans, Silvio Fragoso Rodrigues, Jinku Hu, Aleksandar Borisavljević, Rodrigo Teixeira Pinto, Wembo Wang, Tsegay Hailu, Xun Gong, Marcelo Gutierrez Alcaraz, Balazs Czech, Anoop Jassal, Martin van der Geest, Zhahui Juan and Venugopal Prasanth. I would like to thank Rob Schoevaars, Joris Koeners, and Harrie Olsthoorn for the technical help, and to Sharmila Rattansingh and Laura Bruns for the administrative support.

I am thankful to many people with whom I spent many enjoyable moments outside the university. Big thank you goes to Ilija Pecelj for all the time spent in technical and philosophical discussions, for our cycling tours, and for the support during the hardest times when finishing writing the thesis. For countless pleasant moments, and especially for our gym, roller skating and kebab sessions, I am thankful to my best man Dalibor Čvorić and his wife Ljubica Veljković. I have enjoyed many late nights, travels and celebrations laughing together with Ivan Josifović and Sanja Petrović. I would like to thank Todor Todorčević, Emanuele Cannella, Teddy Zhai, Shan Yang, Nikola Stanić and Vlada Milovanović for all the fun times we spent together. I am grateful to Jelena, Mark, Una and Nestor Gerber for the enjoyable parties, and for helping me to adjust after coming to the Netherlands. A special thanks goes to Zgembo Adislić for his uplifting monologues during my hardest times.

I would like to thank my father Vojislav, mother Stojanka, brother Marko and sister Biljana for their support. For all the pleasant moments during my time spent in Serbia, I would like to express my gratitude to Milenko, Borislava and Andrej Vujanović, and Stojadin and Snežana Spasić.

Most importantly, I would like to thank my wife Jelena Spasić for her endless love, patience and encouragement. I am fortunate to have her by my side. She is my role model when it comes to discipline and responsibility, and without her this thesis would not see the light of day.

Table of Contents

Chapter 1 Introduction

1.1 Introduction

1.1.1 Global Energy Consumption

As the human population grows and technologically prospers the demand for energy is constantly increasing. In 2016 alone the total world energy consumption was close to 160 PWh [1-1]. Approximately one sixth of the total energy production goes to electricity production, which translates to close to 4 MWh of average annual electrical energy consumption per capita. On the global level, electrical energy consumption lately had a relatively steady annual growth of up to 1% and this trend is likely to continue [1-2].

It may not look apparent, but almost all of the world energy today is, directly or indirectly, the nuclear energy coming from the Sun. It seems that the ancient people appreciated this fact much more than a modern man, often personifying the Sun as a deity, a practice which is today almost completely abandoned. Before the industrial revolution started, the direct energy from the Sun was the dominant energy source, providing a man with warmth and food. Nowadays, most of the Sun's energy comes in a preserved state as a fossil energy and to a much smaller extent directly or indirectly as solar, wind or hydro energy. As of 2017, fossil sources (oil, coal and gas) comprised almost 85% of the world energy supply [1-3]. If the current pace of fossil fuel consumption continues, alternative energy sources will be needed for the following reasons:

1. The reserves of fossil fuel are limited. It is only a matter of time when they will be exhausted. This period is difficult to estimate since it can be extended by new harvesting methods, which already happened a few times in the past. With the current rate of consumption, the fossil reserves are expected to diminish at one point, oil, for example, in 50 years [1-3].
2. As the reserves of fossil fuel are reduced, fuel prices increase. Furthermore, fossil fuel is not uniformly distributed, but rather concentrated in certain parts of the world, which is a reason for frequent price manipulations and even international conflicts.
3. Fossil fuels are not considered as clean energy sources. The global CO_2 and warming emissions resulting from such an energy production are a serious global environmental threat.

Direct solar energy can address all of these issues:

1. Amount and reserve of solar energy is virtually unlimited, at least for the next several billion years.
2. Solar energy is abundant and free in its primary form. This makes the price of solar energy more dependent on technology and less dependent on availability.
3. Solar energy is significantly cleaner than the energy that is obtained using fossil fuels.

Many nations have agreed to prevent the dangerous impact of fossil fuel on the world's climate. Climate change concerns, coupled with high fossil fuel prices are driving renewable energy legislations, incentives and commercialization. In Europe for example, the so-called “20-20-20” targets (20% increase in energy efficiency, 20% reduction of emissions, and 20% share of renewable energy in consumption by 2020), set by European Commission, require improved electricity grid infrastructure, smart metering, but also a larger share of renewable energies on the market [1-4].

Renewable energies (renewables) come from natural resources such as sunlight, wind, water, tides, and geothermal heat, which are renewable, or naturally replenished. When it comes to electricity production, renewables are currently far behind the fossil fuels. Figure 1.1 shows the electricity generation by source type for OECD countries in 2016 [1-5]. As it can be seen, the renewables constitute only around 24% of the electricity production. The main renewable energy sources are hydro and wind energy. As already mentioned, these sources are in fact indirect Sun’s energy. In the end, only a small part of the total renewable electricity is obtained directly from the Sun, only around 2%. However, looking at the annual growth rates, the solar energy had experienced the highest growth among the renewables, averaging at 43% between 1990 and 2016.

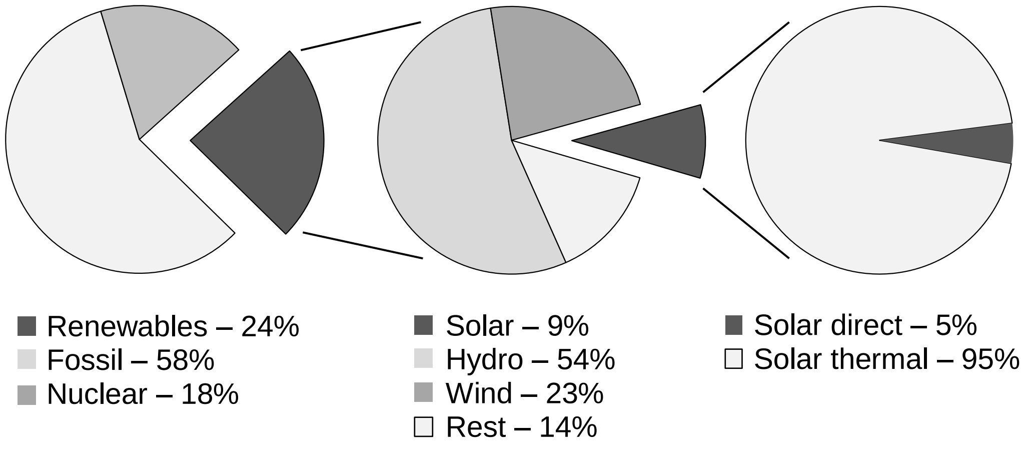

Figure 1.1: Electricity generation by source type for OECD countries in 2016 [1-5]

1.1.2 Solar Energy Potential

The estimates of remaining non-renewable worldwide energy resources vary, with the remaining fossil fuels totaling an estimated 12 EWh, and the available nuclear fuel such as uranium reaching up to 3 EWh of thermal energy [1-6] [1-7]. In reality, the available energy is lower due to conversion losses. The total annual energy reaching the Earth's surface from the Sun is close to 800 EWh, dwarfing all non-renewable resources in just one week. To get the feeling how large the solar energy potential is, by the time you read this sentence enough sunlight will reach the Earth's surface to power the whole world for 1 day. Of course, due to limited space, and losses in energy conversion and transportation not all the energy can be used directly. Still, with the current technology, it takes the area size of the Netherlands to cover the energy demand of Europe. It would take about 5% of the Earth dry area to power the whole world. This means that the solar energy can support the total world energy demand, however it would require vast areas and strong electrical infrastructure. Sun-rich desert areas are good candidates for such purposes, as proposed by Desertec foundation [1-8].

Nowadays, only a small part of total produced energy is obtained using the solar energy directly. Furthermore, a large part of this energy is used to obtain hot water, not electricity. In 2016, solar energy produced enough electricity to cover nearly 4% of the EU electricity demand which corresponds to the annual power consumption of the Netherlands. Based on current market trends, solar energy could meet up to 8% of the EU electricity demand by 2020 and depending on some conditions up to 15% by 2030, dramatically reducing the emissions of greenhouse gases that harm the environment [1-9].

One of the disadvantages of solar energy is low energy density. Nowadays, a typical large solar electric power plant can produce the amount of electrical energy in the order of 100 kWh per 1 m^2 in a year. In comparison, for the same surface area some nuclear plants can produce more than 100 times more energy. With constant technological advances, improvements in efficiency of the components are expected, but certainly not an order of magnitude more. With constantly increasing land prices, alternatives to stand alone power plants are already being searched for, for example incorporating solar energy sources into the existing infrastructure.

The potential of PV energy has already been recognized by many countries, with many government incentive programs to boost the solar energy production. Still, most of the today's world energy production comes indirectly from the Sun, but with constant technological advances this trend is expected to change. As discussed later, direct solar energy generation is very elegant and clean way to produce electricity, without involving moving parts, mechanical energy or harmful emissions. This makes solar energy a promising renewable energy source for the future.

1.1.3 Photovoltaic Technology

Not until recently man was able to use the solar energy directly in order to obtain electrical energy. The **photovoltaic** (PV) effect, generation of electric current in a material upon exposure to light, was first observed in 19th century. However, the practical PV generators started to emerge in the second half of 20th century, with the advances in microelectronic industry. First PV generators, or so called **PV cells**, were based on silicon wafers and the same technology used for IC manufacturing. Recently, PV cells based on other materials such as Gallium, Indium, Arsenide or even organic compounds have being developed. For practical reasons, PV cells are grouped into **strings** and encapsulated in a housing forming **PV modules**. With technological improvements the efficiency of such devices is being constantly improved, and now lies in the range from 5% to 20% for typical commercially available PV cells, and more than 40% for PV cells for special purposes, such as satellites [1-10]. PV modules combined in arrays are the main part of a **PV system**, a power system designed to supply usable electrical energy to the electricity grid by means of the photovoltaics.

Together with efficiency improvements, the price of PV modules is decreasing as well. Looking at the average PV module price per watt in the last few decades, every time the cumulative production doubled, the price was reduced by more than 20% [1-11]. Reduced prices allowed for PV energy to be used in smaller systems in residential sector, for example small buildings or single households. Prior to that, PV energy was mostly reserved for large utility scale PV plants or where there were no alternatives. The price drop, driven by economies of scale and technological improvements, combined with substantial government incentives has led to almost exponential growth of the installed PV power. In 2016 the global cumulative installed PV power surpassed 300 GW mark, with annual growth rate of more than 30% (Figure 1.2) [1-12].

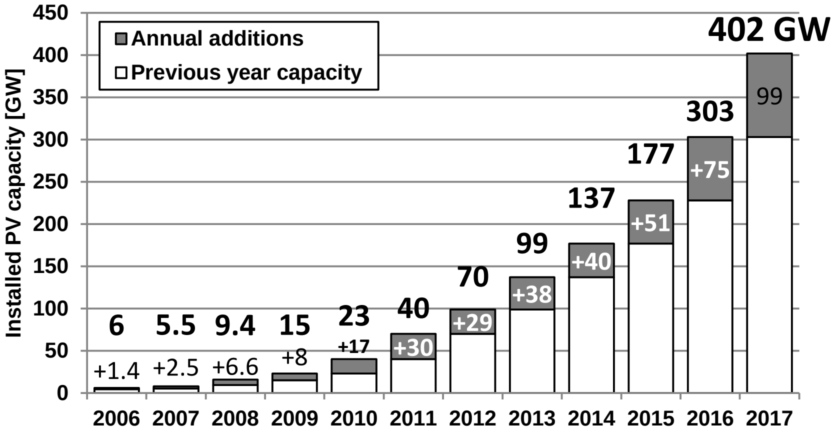

Figure 1.2: Global cumulative installed PV energy [1-12]

As the land area in urban environment becomes limited and expensive, there is a transition from ground PV systems to roof mounted or so called building applied PV systems (BAPV) or even further to **building integrated PV systems** (BIPV) where PV modules are integrated part of building elements such as facades, semi-transparent windows or roof tiles (Figure 1-3) [1-13]. This transition also shifted the focus from efficiency to other properties of PV cells, such as ease of installation, resistance to environmental conditions, and even esthetic aspects.

To fully enable BIPV systems, a PV module should be able to adapt its shape to any building element. This can be achieved with **novel flexible PV modules** instead of **traditional rigid PV modules**. Beside flexibility and light weight, another advantage of flexible PV modules is their potential to lower manufacturing costs through low-cost manufacturing [1-14]. Furthermore, such lightweight and flexible PV modules can offer additional cost benefits in terms of transportation, installation and structural frames for the modules. In other words, they have potential to significantly reduce the so-called "balance of system" costs, which cover all components of a PV system other than PV modules.

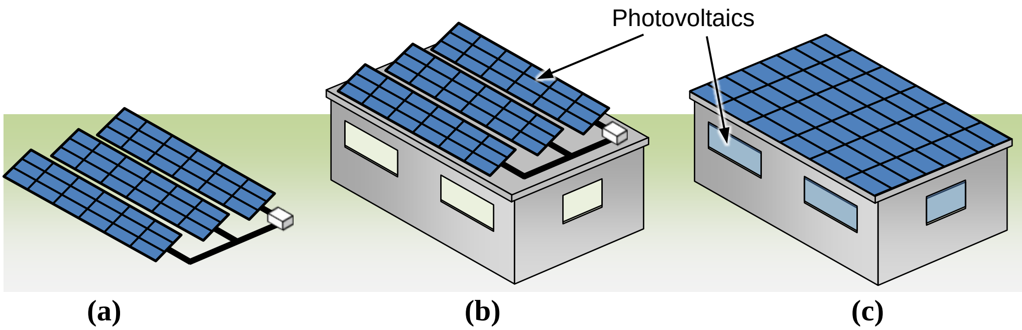

Figure 1.3: (a) Conventional, (b) building-applied, (c) building-integrated PV system

1.1.4 Power Electronics for PV

Being a very nonlinear and intermittent power source, PV modules usually cannot be used directly as a power supply. The output voltage and, more importantly, the output power will depend significantly on the electrical profile of the load and the environmental conditions. Typically, there is a **power electronic converter** as an electronic interface between the power source and the load, providing two functions:

1. Maximum power point tracking (MPPT) – Power converter will force the non-linear PV power source to work under conditions where the maximum available power can be extracted.
2. Power conversion – Power converter will increase/decrease the voltage of a PV source or perform DC-AC conversion in order to meet the electrical specifications of the load.

These functions can be achieved using two separate stages or with a single stage, depending on system specifications. Standard power converter topologies are usually employed to satisfy these goals, for example, a boost converter to track the maximum power point and to boost the low voltage output from the PV source to high enough voltage required for AC grid connection. Apart from meeting the design specifications, the power converter has also to satisfy three design goals, the same ones that are applicable to the whole PV system:

1. High conversion efficiency,
2. Low specific price,
3. High reliability and long lifetime.

These goals are sometimes mutually exclusive, usually with “pick two out of three” rule. Regarding the efficiency, a typical PV converter has efficiency of more than 95%. The power converter is therefore significantly more efficient than even the most efficient PV module. Still the converter efficiency is constantly being improved in order to decrease the losses, size and cost of thermal management. The efficiency is also a strong marketing point. The specific price of the power converter is much lower compared to PV sources. As of 2017, a power converter for PV applications can cost below 0.2 €/W, depending on the system power level [1-10]. However, if the converter reliability is low, the initial price advantage can be compromised by high maintenance costs. Ideally, a converter in a PV system should match the life time of a PV module of usually 20 years or more, which is a challenging task.

The **PV system architecture** defines the way in which PV modules and power converters are connected in a PV system. In a typical PV system, PV sources and the power converter can be separately identified when looking at the PV system architecture. Usually there is an array of PV sources and a single power converter as an interface to the electricity grid (Figure 1.4a), the so-called central inverter architecture [1-15]. This architecture was proven as efficient in large utility scale PV systems (>100 kW). Here, the key for efficient operation is to provide uniform operating conditions for the whole PV array. In residential sector, PV systems are facing environmental and installation limitations which impose non-uniform operating conditions on the PV module network. As a result, MPPT tracking becomes less efficient, decreasing the system yield [1-16]. To overcome this, the PV network has to be divided into sections with locally-uniform operating conditions with independent power processing. This leaded to the development of more **granular architectures** where power electronics partially penetrate into the PV network (Figure 1.4b), the so-called string and multistring architectures [1-17]. As the PV system further moves into residential areas, integrates into built environment and penetrates into the grid, the granularity, or level of penetration of power electronics into the PV array, has to increase in order to maintain high system yield. At some point, this will lead to a system where PV sources and the power electronics are indistinguishably integrated from the system point of view (Figure 1.4c).

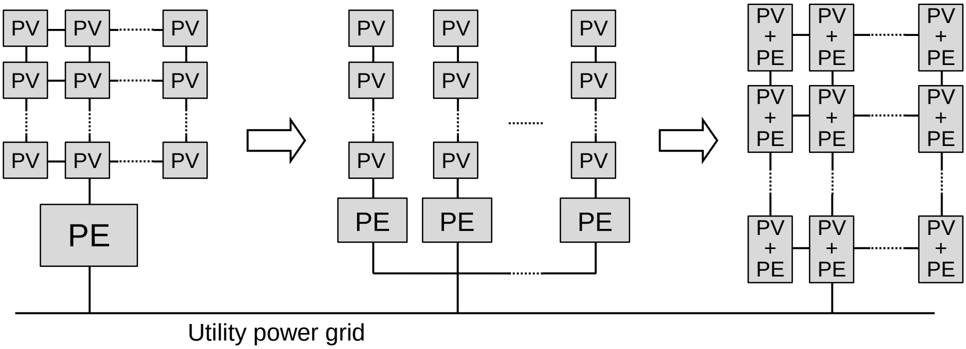

Figure 1.4: Increased granularity of power electronics (PE) in residential PV systems: (a) centralized, (b) string/multistring, (c) distributed MPPT system

1.1.5 PV Systems with Distributed Power Processing

Increased penetration level of PV systems into electrical grid and urban environment brings a transition from standard ground systems to BAPV/BIPV systems. Being exposed to urban environment and non-uniform operating conditions, traditional PV system architectures start to show its shortcomings. Improved PV system architectures has been proposed since, with even more granular power processing by means of **distributed maximum power point tracking** (DMPPT) [1-18]. This is achieved by connecting a power converter to each PV module in the PV system and performing the power processing on a PV module level. Depending on the specific application, DMPPT approach can significantly increase the system yield [1-19]. From the system point of view, the DMPPT system corresponds to Figure 1.4c. The related losses are effectively eliminated, but the additional cables and labor are required to connect the PV module and the converter. Furthermore, to make this approach viable the cost of added electronics should be compensated by the cost of recovered energy. This calls for novel technologies that could reduce the price of power electronics for PV systems.

To summarize, constant improvements are still needed to keep the PV energy as one of the most promising renewable energy sources in the future, even in DMPPT systems. These are:

1. Improving PV system overall energy yield,
2. Improving the cost, reliability and performance of power electronic interface,
3. Improving system architectures and adaptability to build environment and smart grids.

Being a link in the power processing chain, an improved power electronic converter can bring positive impact on all three points through distributed power processing.

1.2 Problem Description

Looking at Figure 1.4c, from the system point of view the PV module and the power converter in a DMPPT system represent together a single unit, although they are in reality physically separated. Additional cables are required to connect the power converter to the PV module and the rest of the system. Sometimes the converter is mounted on the PV module itself, but more often on the supporting structure for PV modules, especially when retrofitting it to the existing PV systems. In case of BIPV systems, the problem of finding a suitable place for the converter is much harder.

On the other hand, looking at the PV module and the converter individually, despite their fundamentally different functions, we can draw some physical similarities. We can classify all their construction components into functional and packaging elements [1-20], as shown in Figure 1.5. In case of PV modules, the functional elements are strings of PV cells, while the packaging parts are encapsulation and interconnections elements. In case of power converters, the functional elements are electronic, magnetic and thermal components, while the packaging components are printed circuit board (PCB) and the housing. Note that some parts of the converter can have secondary role, for example housing may be used for encapsulation and as a heatsink.

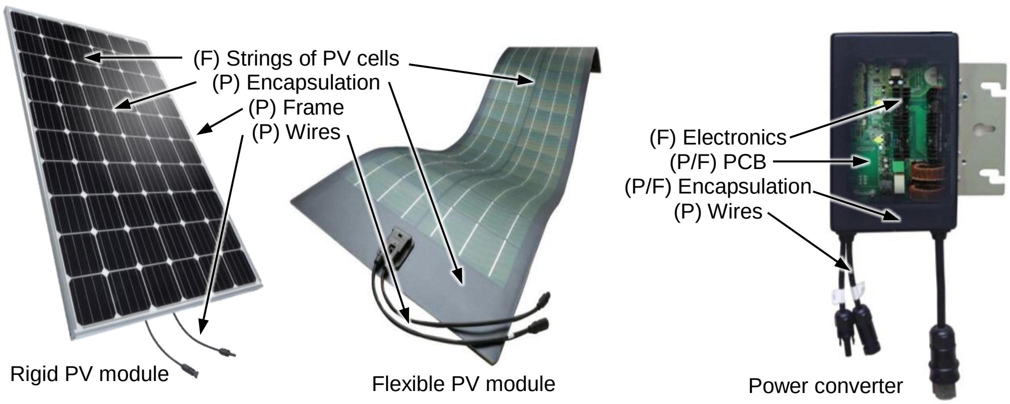

Figure 1.5: (F) Functional and (P) packaging elements in PV modules and converters

Looking at the structure, it can be seen that the PV modules and the majority of power converters are 3-dimensional devices with 1-dimensional structure where functional and packaging parts are arranged in layers. While functional parts are unique, the packaging parts are made using similar materials. Here, the question arises if the packaging layers can be shared by **integrating the converter into the PV module**. We can also consider different **levels of integration**, depending on how many layers are shared. In case of the highest level of integration, only the functional layer of the converter is retained within the PV module, as shown in Figure 1.6.

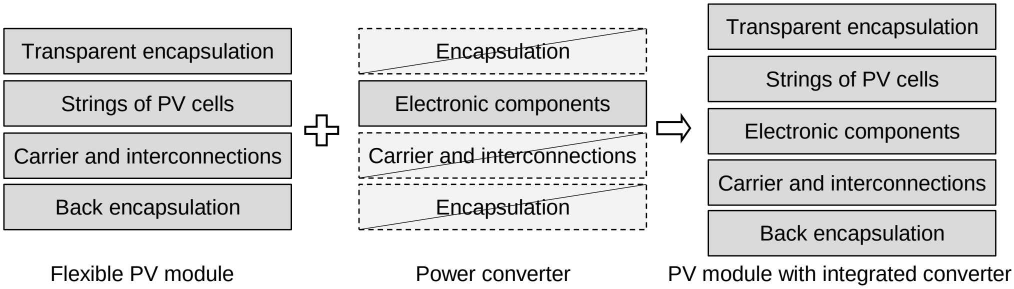

Figure 1.6: Sharing packaging layers to integrate power converter into PV module

Integration of the converter into the PV module presents a step further in the DMPPT, allowing for an automated manufacturing process and optimal design of the converter for the particular PV module. By making a single integrated product, the installation cost can be decreased further, eliminating additional wires between the PV module and the converter. This does not come without a price however, as the specific design requirements increase the complexity of the design procedure.

First, being a buffer between the PV module and the rest of the system, the converter has to satisfy the **electrical** specifications on both sides, and it has to do it in the most efficient way. Thermal and mechanical requirements will limit the range of possible solutions, leading towards more efficient and spatially distributed topologies to reduce the power loss density and towards higher operating frequencies to reduce the size of the converter by reducing the size of passive elements.

Second, in case of the PV module integration, special **technologies** are required to achieve low profile and flexible design. Not all currently available technologies intended for power converters and components will be suitable for such an application. This is especially true in case of materials for magnetic components and packaging for semiconductor devices.

Third, since PV modules are relatively inefficient devices, a large amount of the absorbed light energy is transformed into heat. Under operating condition commonly encountered in BIPV systems PV modules can easily reach high temperatures. With its presence, the integrated converter will change the heat flows from the PV module but also act as an additional heat source caused by power losses in its components, changing the temperature profile of the system. Without proper **thermal management** the excess heat will cause negative effects on the reliability and performance of both the PV module and the converter.

To summarize, three main domains can be identified when designing the PV module integrated converter, each with its own trade-off parameters and sets of boundary conditions:

- Electrical integration – with the goal of selecting system architectures and converter topologies suitable for high switching frequency operation, in order to achieve small size limited by spatial restrictions and low power loss generation limited by thermal capabilities.
- Spatial construction and technology – with the goal of selecting the most suitable technologies and materials to allow for low profile, flexible construction, in particular for magnetic components with their size determined by the electrical design.
- Integrated thermal management – with the goal of efficiently removing heat loss from the converter, while being limited by spatial constraints, device packaging, operating requirements and the amount of power losses from the converter and the PV module.

When designing conventional converters, the abovementioned design areas are usually loosely coupled. In the case of PV module integration, a tight thermal coupling between the converter and the PV module and the technology requirements for thin and flexible construction will introduce strong **design interdependencies**. Overcoming these limitations presents a challenge, but can lead to a cost effective, reliable solution for PV systems with improved energy yield, integration level and power density. This thesis is intended to tackle these challenges and present a step toward reliable integration of power electronics into PV modules.

1.3 Research Questions and Approach

Taking into account the foregoing problems, the goal of the thesis is:

To investigate the limits of physical integration of a power converter into a flexible PV module through an integrated interdependent electrical, thermal and technological design.

The approach to reach this goal consists of several steps providing solutions to the following questions:

- What are the limits of integration and possible system architectures for distributed power processing and which converter topologies are most suitable for the PV module integration?
- What are the best technology platforms for integrating the power electronic converter into the PV module?
- Which thermal management strategies are suitable for heat extraction and converter operation under stringent thermal and spatial requirements?
- What are the interdependences between the electrical, technological and thermal design domains, and can a multi-objective design procedure be developed?

1.4 Thesis layout

The thesis layout is shown in Figure 1.7.

Chapter 2 gives an overview of the PV technology, PV systems and power electronics for PV applications. With the focus on residential PV systems, it is shown that a high level of PV system penetration into electrical grid and built environment needs to be followed by a high level of granulation of power electronics into the PV system. The chapter introduces distributed maximum power point tracking in PV systems as a way to improve the efficiency in urban environment, and presents the current state-of-the-art converters for such applications.

Chapter 3 presents a new PV module integrated converter concept as the next step to implement distributed maximum power point tracking in PV systems. Advantages and limitations introduced into the converter design are identified. The converter design is presented as a tightly coupled unity consisting of electrical, technological and thermal design domains. This chapter introduces design domain constraints and goals as well as the design interdependences between them.

Chapter 4 classifies and ranks the existing topologies on the basis of electrical performance and suitability for integration into PV module in order to come to the most suitable topologies. Different possible system architectures will be considered, which will result in different topologies selected for the PV module integrated converter.

Chapter 5 gives an overview of existing technologies and defines new packaging and integration concepts as the most suitable platforms to implement a PV module integrated converter. Existing suitable technologies are ranked on the basis of thermal, electrical and mechanical performances, limitations, cost and reliability. Special attention is given to ability for high switching frequency operation and the enabling semiconductor devices based on GaN and SiC technologies, and to magnetic components as the most critical part for achieving low profile integration.

Chapter 6 reviews the existing thermal management strategies suitable for low profile converters and categorizes them on the basis of technological and electrical requirements. The thermal model of the combined PV module and the integrated converter is presented, from the system down to the component level.

Chapter 7 combines the results from Chapters 4, 5 and 6 into a unified design procedure. The design of the converter circuit is based on defining converter electrical specifications and detailed analytical electrical design, choosing the technology platform and defining thermal requirements using the developed thermal model. In this chapter previous results are combined together to create a set of possible converter designs. Based on the optimization parameters the most suitable combination of topology, technology and thermal management parameters is obtained. As the result, the chapter presents the assembly, experimental validation and performance evaluation of the integrated converter design.

Chapter 8 revisits the problem objectives by summarizing the major contributions of the thesis and giving recommendations for future research on the subject.

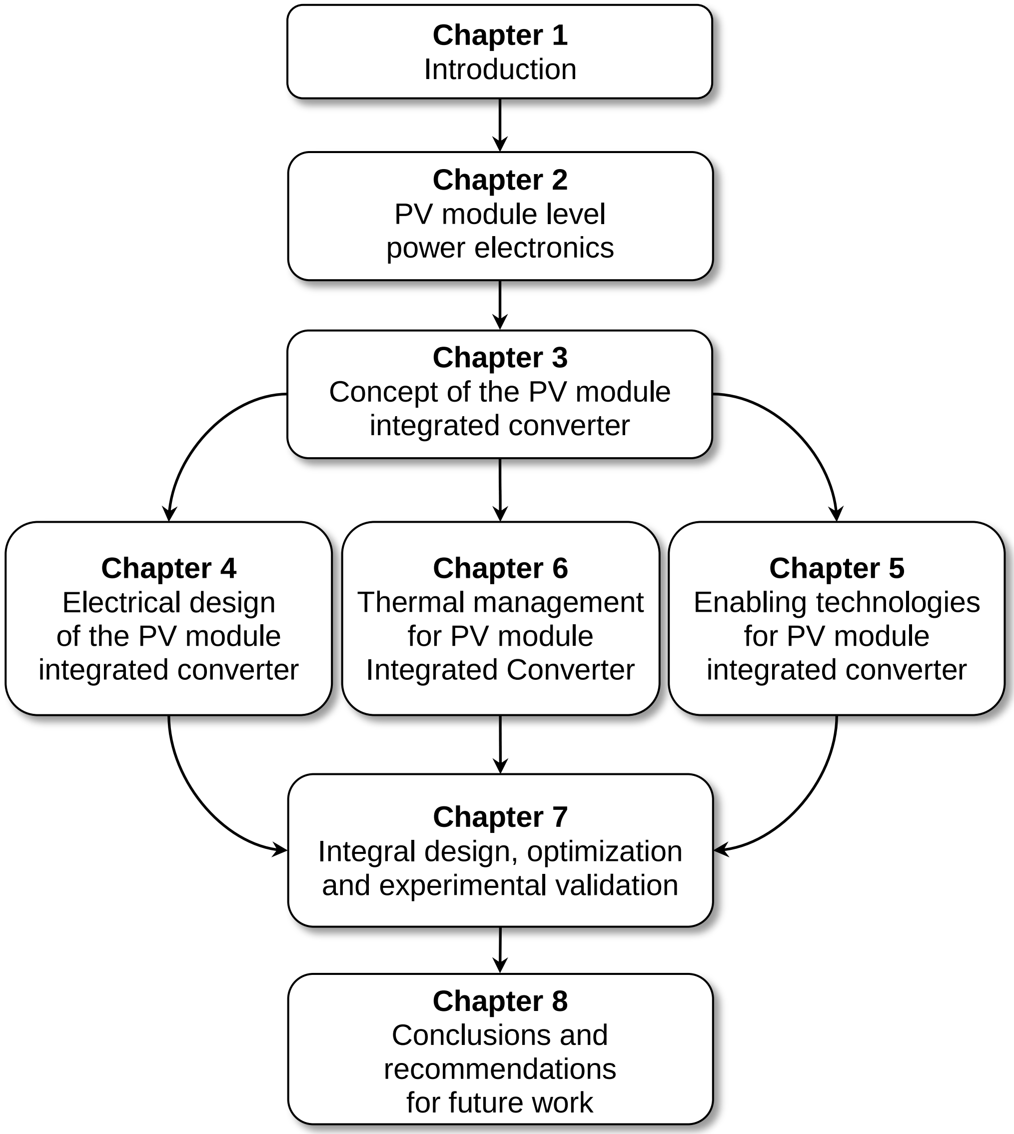

Figure 1.7: Thesis layout

1.5 References

[1-1] International Energy Agency, "Key World Energy Statistics 2017," 2018

[1-2] Enerdata, "Global Energy Statistical Yearbook 2018," available online, *www.yearbook.enerdata.net/*

[1-3] British Petroleum, "BP Statistical Review of World Energy," 2018

[1-4] European Parliament, Council of the European Union, "Directive 2009/28/EC of the European Parliament and of the Council," 2009

[1-5] International Energy Agency, "Renewables Information: Overview 2017," 2017

[1-6] World Energy Council, "World Energy Resources 2016," 2016

[1-7] M. Perez, R. Perez, "A Fundamental Look at Supply Side Energy Reserves for the Planet," Newsletter of the International Energy Agency Solar Heating and Cooling (IEA-SHC), Vol. 62, 2015

[1-8] L. Esmeralda, G. Moreno, "Concentrated Solar Power (CSP) in DESERTEC - Analysis of Technologies to Secure and Affordable Energy Supply," Intelligent Data Acquisition and Advanced Computing Systems (IDAACS), 2011

[1-9] Solar Power Europe, "Global Market Outlook for Solar Power 2017-2021" 2017

[1-10] "Research Cell Record Efficiency Chart," available online, *www.nrel.gov*

[1-11] Fraunhofer ISE, "Photovoltaics Report," 2017

[1-12] REN21, "Renewables 2018 – Global Status Report," 2018

[1-13] H. Kaan, T. Reijenga, "Photovoltaics in an Architectural Context," Progress in Photovoltaics: Research and Applications, 2004

[1-14] E. Hamers, M. van den Donker, B. Stannowski, R. Schlatmann, G. Jongerden, "Helianthos: Roll-to-Roll Deposition of Flexible Solar Cell Modules," Plasma Processes and Polymers, 2007

[1-15] S. Kjaer, J. Pedersen, F. Blaabjerg, "A Review of Single-Phase Grid-Connected Inverters for Photovoltaic Modules," IEEE Transactions on Industry Applications, Vol. 41, No. 5, 2005

[1-16] A. Chouder, S. Silvestre, "Analysis Model of Mismatch Power Losses in PV systems," Journal of Solar Energy Engineering, Vol. 131, No. 2, 2009

[1-17] M. Meinhardt, G. Cramer, “Multi-String-Converter, the Next Step in Evolution of String-Converter Technology,” European Conference on Power Electronics and Applications (EPE), 2001

[1-18] R. H. Wills, S. Krauthamer, A. Bulawka, J. P. Posbic, “The AC Photovoltaic Module Concept,” Energy Conversion Engineering Conference (ECE), 1997

[1-19] L. Linares, R.W. Erickson, S. MacAlpine, M. Brandemuehl, “Improved Energy Capture in Series String Photovoltaics via Smart Distributed Power Electronics,” Applied Power Electronics Conference and Exposition (APEC), 2009

[1-20] J. Popović, “Improving Packaging and Increasing the Level of Integration in Power Electronics,” PhD thesis, Delft University of Technology, 2005

Chapter 2 — PV Module Level Power Electronics

2.1 Introduction

In the introductory chapter it was noted that there is a trend of changing the PV system architectures and the way the power electronics is implemented in a PV system. The installed PV power in small systems in the residential sector experienced steep increase in the past years, as a follow up to the price drop of PV energy and increased demand for cleaner energy generation.

As the PV energy penetrates into the grid and urban environment, there is a transition from large ground PV systems to small rooftop or BIPV systems. Facing new operating conditions, traditional system architectures start to show its shortcomings and the PV system architectures need to change to maintain high yield.

The goals of this chapter are:

- To show the evolution of PV systems, from large utility scale to residential and BIPV sector.
- To identify future trends in PV system architectures and power electronics technology for PV converters.

The chapter starts with presenting basics of PV energy generation, and the way the PV sources are built, characterized and used in PV systems. This will give insight into limitations that the PV systems face in built environment. Special attention is given to novel flexible thin-film PV technology with a potential to greatly reduce the cost of the PV system and to ease the integration of PV sources into building structures. After that, through a classification of PV systems with focus on residential systems, it is shown that high level of PV system penetration into electrical grid and built environment has to be followed by high level of penetration of power electronics into the PV array. As a consequence, new PV system architectures are introduced, with distributed power processing in order to overcome the environmental issues met in the urban areas. To show the advantage of such distributed architectures, some case studies are presented. The chapter ends by presenting the state-of-the-art in power converters for distributed architectures, and identifying drawbacks that still exist in the current solutions.

2.2 PV System Fundamentals

Approximately 1000 W/m^2 of the Sun's irradiance reaches the Earth surface around noon at clear sky conditions, mostly in visible and infrared range of the spectrum. If wasted, most of this energy will only end up heating the Earth. The plants found a way to use this energy through photosynthesis, using approximately 5% of light energy to obtain sugar from carbon dioxide and water. This is however chemical energy. For a modern man, obtaining electrical energy directly from Sun would be more suitable.

2.2.1 PV Cells

Photovoltaics (PV) is direct conversion of light into electricity and is based on the photovoltaic effect – generation of electric voltage between two electrodes attached to a solid or liquid system and exposed to radiation (light). Practically all modern photovoltaic devices are made of semiconductor materials and contain one or more p-n junctions where the photo-voltage is generated. These devices are known as PV cells. A typical single junction PV cell and its structure are shown in Figure 2.1 [2-1]. Aside from the p-n junction, there are some additional layers, for example, conductive layers to collect and transport photo-generated carriers and anti-reflection layers to increase the amount of absorbed photons.

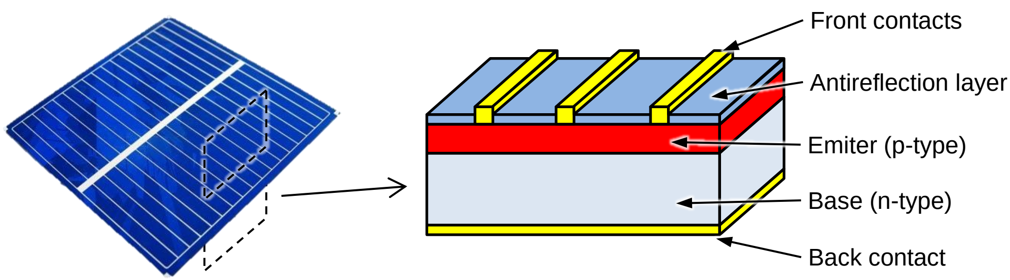

Figure 2.1: Typical semiconductor-based PV cell and its cross-section

The previous figure shows that a semiconductor based PV cell is in principle an exposed large-area diode. Illumination of the cell creates free charge carriers, which allow photo-generated current to flow through the connected load. This diode and the photo-current source can be represented in the equivalent circuit diagram (Fig. 2.2a). Additional resistors in the equivalent circuit model the internal and external conduction and leakage losses.

For specific operating conditions (solar irradiation and temperature), the current-voltage characteristic is shown in Figure 2.2b. It can be seen that it resembles a diode characteristic, offset by photo-generated, or short circuit, current I_{SC}, which in absence

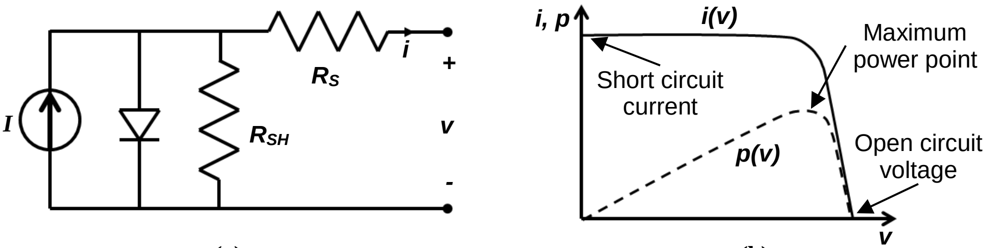

(a) **(b)**

Figure 2.2: (a) PV cell equivalent electrical circuit, (b) PV cell V-I curve

of a connected load generates open circuit voltage V_{oc}. Multiplying current and voltage point by point, a power curve can be obtained. There is one particular current-voltage combination where the extracted power reaches its maximum, called the maximum power point (MPP). Naturally, it is desirable that the maximum power is sourced from the PV cell under all operating conditions.

Only a part of the solar radiation incident to the PV cell is converted to electricity. The ratio of the output photo-generated electrical power to the input solar irradiation power is defined as efficiency. The efficiency (and also the maximum output power) of the PV cell is measured under internationally specified standard test conditions (STC) [2-2]. The efficiency of PV cells depends primarily on the technology being used, and ranges from a few percent for certain thin-film or organic types up to more than 40% for special PV cells consisting of several junctions. Following technological advances, the efficiency is being constantly improved, as it can be seen in Figure 2.3 for several different PV cell technologies as of 2017 [2-3].

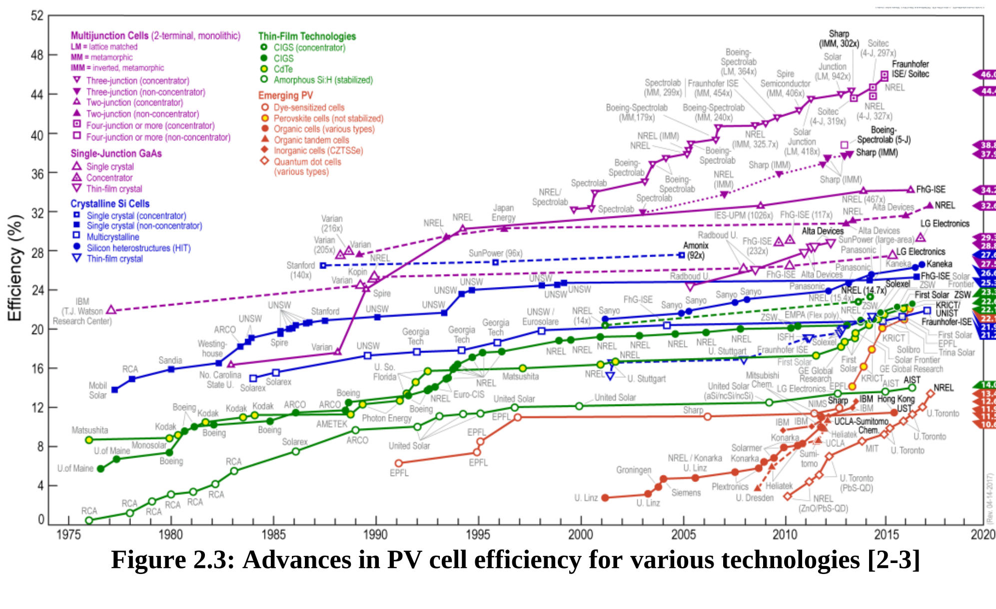

Figure 2.3: Advances in PV cell efficiency for various technologies [2-3]

The generated electrical power of a PV cell depends primarily on the solar radiation energy (irradiation) being absorbed and transformed. To a lesser extent, it also depends on the PV cell operating temperature. As the operating temperature increases, the output power decreases, for example by 0.4%/°C in case of silicon-based PV cells. The Sun's irradiance is only partially converted into electrical energy, one part of the cell reaching irradiance is reflected back from the PV cell surface and the remaining part continues its way through the front layers of the cell until it reaches the active semiconductor layer. Under realistic conditions, reflective losses are very low due to the structured surface which can dramatically reduce the amount of reflected light [2-4]. Only one part of the absorbed radiation is converted to electrical energy, while the rest is converted into heat. The output electrical power of the PV cell is determined by cell efficiency, but also by load profile according to Fig 2.2b. Therefore, the processes and parameters that determine the energy balance are reaching irradiance and cell temperature, optical properties of the PV cell, photovoltaic conversion efficiency, balance of heat flows, and electrical characteristic of the load (Figure 2.4).

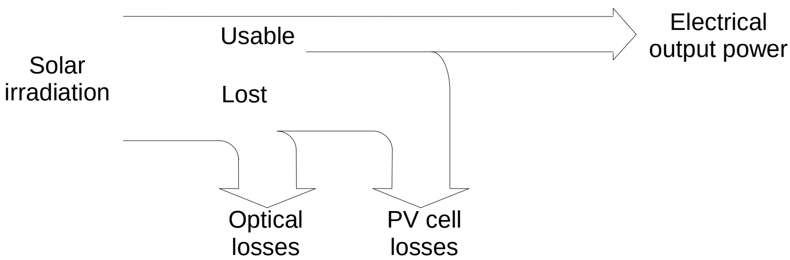

Figure 2.4: Energy balance in a PV cell

2.2.2 PV Modules, Technology and Manufacturing

Various types of silicon-based PV cells exist, depending on the technology and materials used. The most common types are crystalline PV cells. They are made out of mono- or multi-crystalline silicon wafers sewed from a silicon ingot. Crystalline silicon PV cells as of 2016 still dominate the PV cell market share, despite their expensive and energy consuming manufacturing process. One of the reasons for this is the existing understanding of crystalline silicon physics and properties, and the fact that they are using similar process and manufacturing equipment as the production lines for standard integrated circuits.

Thin-film PV cells represent another major technology, and are made by depositing extremely thin layers of photosensitive materials onto a low-cost backing such as glass, stainless steel or plastic. Production costs can be lower compared to the more material-intensive crystalline Si technology, but the efficiency is lower as well due to internal energy losses since they have no crystal structure. A description and comparison of major PV cell types can be found in [2-6] and is shown in Table 2.1.

Table 2.1: Comparison of technologies for commercial PV cells

Technology	Thin film				Crystalline wafer based	
Type/material	a-Si	CdTe	CIGS	a-Si/m-Si	Mono c-Si	Multi c-Si
Cell efficiency	6-8%	21%	23%	12%	26%	22%
Area needed per kW	14m^2	6 m^2	5 m^2	8 m^2	4 m^2	5 m^2

Global PV cell production has so far involved mostly crystalline silicon, owing to economies of scale, with around 95% of the market share as of 2017 [2-6]. However, current and future plans still have a strong focus on thin-film technology which is expected to gain a larger share of the PV market (Fig. 2.5). In this moment, it is difficult to foreseen which technology will prevail in the future, but according to current trends, it will most probably be the one that is most cost effective, and not the one that is most efficient.

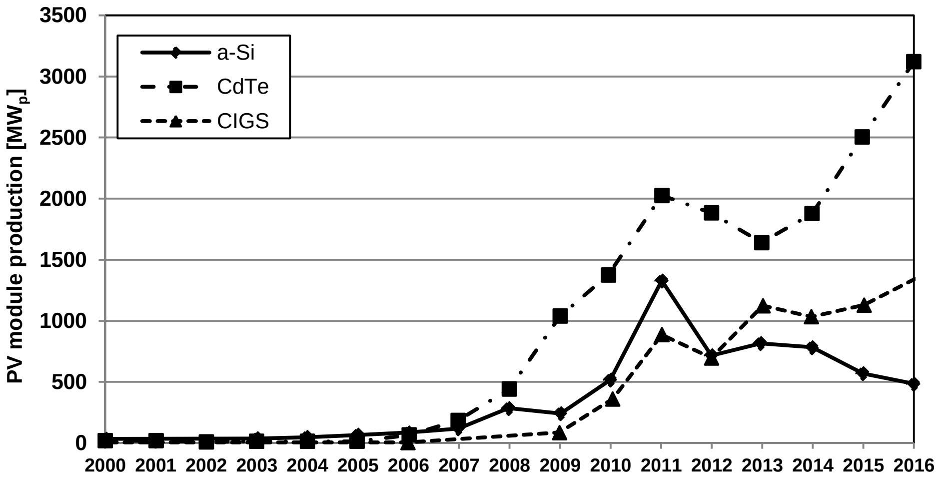

Figure 2.5: Annual global module production for leading thin-film technologies [2-6]

For practical use, PV cells are packaged into PV modules containing either a number of crystalline Si cells connected in series or a layer of thin-film material cells which are internally connected (Figure 2.6). The cells are connected in series in order to achieve high voltages which are suitable for power electronic systems and conversion. For the construction of crystalline PV modules, cells need to be connected in series, and this is separated process that is sometimes done by hand, therefore expensive. In case of thin-film cells serial connection can take place simultaneously during module assembly, which gives a great advantage to the thin-film technology. The cells are then encapsulated using glass or plastic layers to protect them from the environment.

Finally, additional elements are added to connect the PV modules into PV systems, such as structural frame reinforcement and a junction box with electrical contacts.

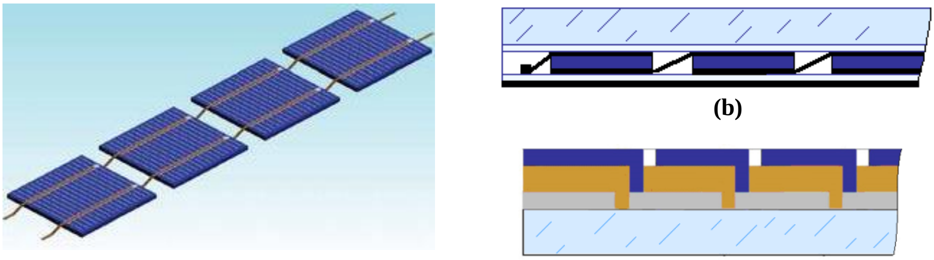

(a) (b) (c)

Figure 2.6: PV module construction: (a) Connection of crystalline cells, (b) Typical construction of crystalline PV module and (c) thin-film PV module on glass

In a new roll-to-roll production process, flexible thin-film amorphous silicon (a-Si) solar cells are produced on long pieces of foil in a number of roll-to-roll steps (Figure 2.7) [2-7]. The process uses a temporary substrate in the form of metal foil. Thin semiconductor layers are applied to this carrier by means of vapor deposition. The layers are applied homogeneously over long lengths of foil in layers just a couple of micrometers thick. Laser scribing techniques are used to divide the thin layers into stripe-shaped cells and to connect them in series. Then a permanent carrier is applied and the temporary carrier foil is removed. In the final process steps, the solar cell laminate is cut into pieces, encapsulated and fitted with contact points (Figure 2.7b). The whole module has a thickness of half a millimeter, width of 30 cm and length of 6 m. The advantage of this process is that it enables large-scale, low-cost production and easy integration into building products such as roofing and facade materials.

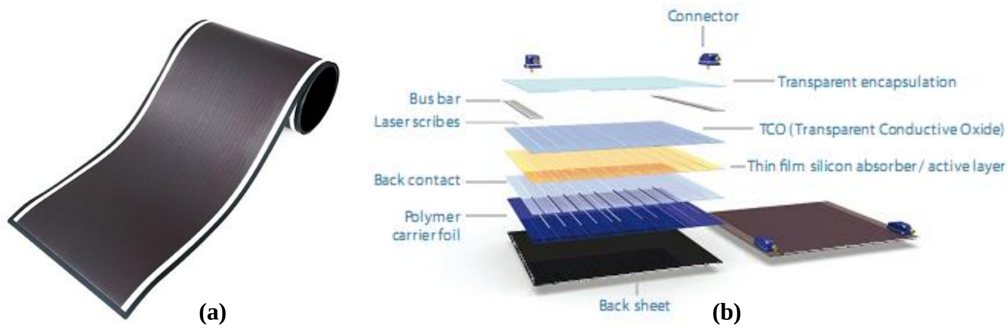

(a) (b)

Figure 2.7: (a) Flexible thin-film a-Si PV module, (b) PV foil composition

Series connection of the PV cells (and also PV modules) causes an undesired effect when one or more PV cells are partially or completely shaded. Since the weakest link in the chain determines the quality of the system, the effect is the same as if all cells were shaded. In this situation, the resistance of the cell is significantly higher than the resistance of the load and most of the voltage generated by the rest of the cells appears at the shaded diode. This can overheat the shaded cell, creating a hot-spot, which might further lead to a breakdown. To avoid this, anti-parallel diodes are connected to the cells in order to take over the string current of the shaded cell. As it will be shown later, the same can be applied to larger scale, as a single underperforming PV module can bring down the performance of the whole system.

2.2.3 PV Systems

To provide usable electrical power, PV modules are arranged together into arrays, and interfaced to a power converter, forming a PV system. The role of the power converter is to convert the DC power from the PV array into DC or AC power at appropriate voltage level. Depending on how is this energy further distributed, PV systems can be divided into [2-1]:

- Grid connected PV systems,
- Standalone (off-grid) PV systems.

Standalone PV systems do not have a connection to an electricity grid. To ensure the supply of the standalone system with electric power also in the times without or with very low radiation, such as at night or cloudy weather, standalone systems usually have an integrated storage system. Standalone systems can also be implemented with auxiliary power sources, as so-called hybrid systems, where additional generators employing fossil fuel or other renewable energy source complement the PV energy production.

Grid connected PV systems always have a connection to the electricity grid via a suitable inverter (DC/AC power converter), since PV modules deliver only DC power. Grid-connected PV systems can be subdivided into:

- Decentralized grid-connected PV systems,
- Central grid-connected PV systems.

Decentralized grid-connected PV systems are usually small power systems installed on the roof of buildings or integrated into building facades and connected to the low voltage AC grid.

Central grid-connected PV systems have larger installed power, up to several MW. With such central PV power stations it is possible to feed the power directly into the medium or high-voltage grid. The basic grid-connected PV system has changed little despite advances in PV cell technology and is shown in Figure 2.8. The PV system consists of PV modules, inverters for DC/AC conversion, electrical cables and additional installation components between them. On the DC side of the PV system there are junction boxes for parallel/serial connections of the PV modules, protection diodes and additional safety components. On the AC side of the PV system there are switches, grid connectors and additional safety components.

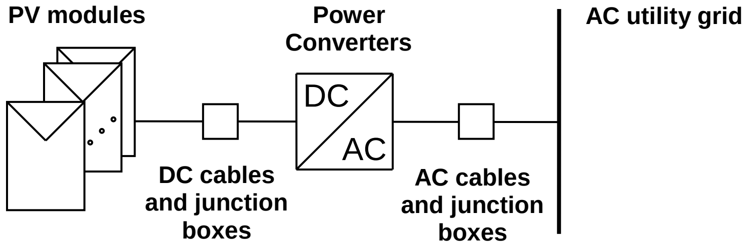

Figure 2.8: Grid-connected PV system

2.2.4 MPPT and Mismatch Losses

As noted before for Figure 2.2, PV cells are nonlinear power sources with load dependent output power, and the same applies to PV modules and their networks. A PV system should be designed to operate at the maximum available power under all operating conditions. To accomplish this, the converter performs maximum power point tracking (MPPT). This is accomplished by successively adjusting the PV module current in order to reach the maximum power point (MPP). Maximum power point tracking is always performed in the first (and sometimes the only) stage of the PV converter by implementing one of the MPPT algorithms. Many MPPT methods have been developed and they all vary in complexity, convergence speed, range of effectiveness, cost and other respects [2-8].

Unfortunately, when MPPT is performed centrally, or at one place over the whole PV network, the actual extracted power can be lower than the maximum available power. Series connection sets the same current for all PV modules in a string. This means that it will not be possible to individually track the maximum power point for each PV module, therefore, if the electrical parameters of the PV modules differ, mismatch will occur and a part of the available power will be lost. Mismatch can be caused by non-uniform solar irradiation due to shading, dirt or non-uniform PV module orientation, but can also be caused by aging or damage to the PV module. Some mismatch inducing situations are shown in Figure 2.9.

As an example, consider the system in Figure 2.10a [2-9]. In a string of five serial connected PV modules one is uniformly shaded, for example by a cloud or dirt, reducing the irradiation by 50% and causing mismatch between the PV modules. Figure 2.10b shows the power curve for normal and mismatch conditions. It can be seen that under normal, unshaded conditions, the maximum available power is 800 W, while the maximum power under non-uniform irradiation is 640 W, assuming that the MPPT algorithm succeeds in finding the global maximum. However, looking at the

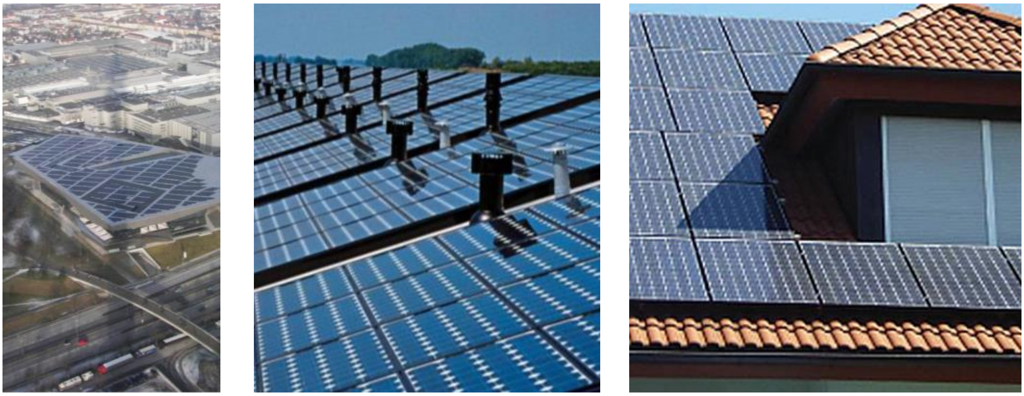

Figure 2.9: Shading examples: shade caused by nearby towers, pipes or building elements

individual power curves for each module, it can be seen that the maximum available power under partial shading conditions is 720 W. Therefore, if the MPPT was performed on a PV module level instead of on the string level, 80 W could be recovered – an increase of almost 13%. Under heavier shading, the difference can be even larger. This might not be an issue in large systems where all PV modules are mounted uniformly and cleaned regularly. In urban environment, where there are limitations in the way the PV modules are oriented or if the shading is more likely to happen due to dirt or shadows, power can be reduced significantly.

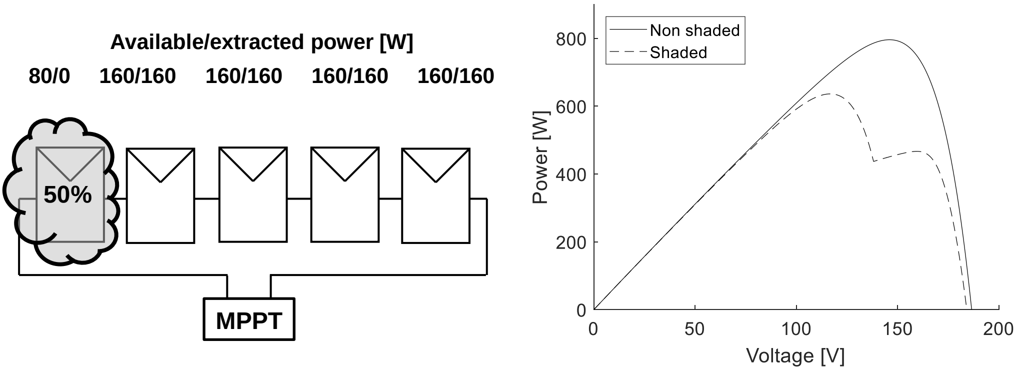

(a) (b)

Figure 2.10: Mismatch losses caused by centralized MPPT

The scenario mentioned above also applies to PV cells within a PV module. It should be noted that under some conditions, referring to Figure 2.2, the operating point of underperforming PV modules or cells can be forced into 2nd or 4th quadrant where they will operate as a load instead of a generator, dissipating power which can cause excess temperatures and even failure. For these reasons, anti-parallel bypass diodes are usually placed across PV modules or groups of PV cells within the module, to bypass the current, and cut out the underperforming elements, as in the example above.

2.2.5 PV System Architectures

Depending on the configuration of PV modules and power converters, different PV system architectures can be formed. A number of architectures for PV installations have been commercially implemented and yet more proposed by the academic community. Each of these approaches has advantages and disadvantages, and trade off various attributes such as complexity, efficiency, safety, reliability, cost or flexibility. In today's PV systems, three most common configurations can be identified, as showed in Figure 2.11 [2-10, 11]:

1. Central inverter system,
2. String inverter system,
3. Multistring inverter system.

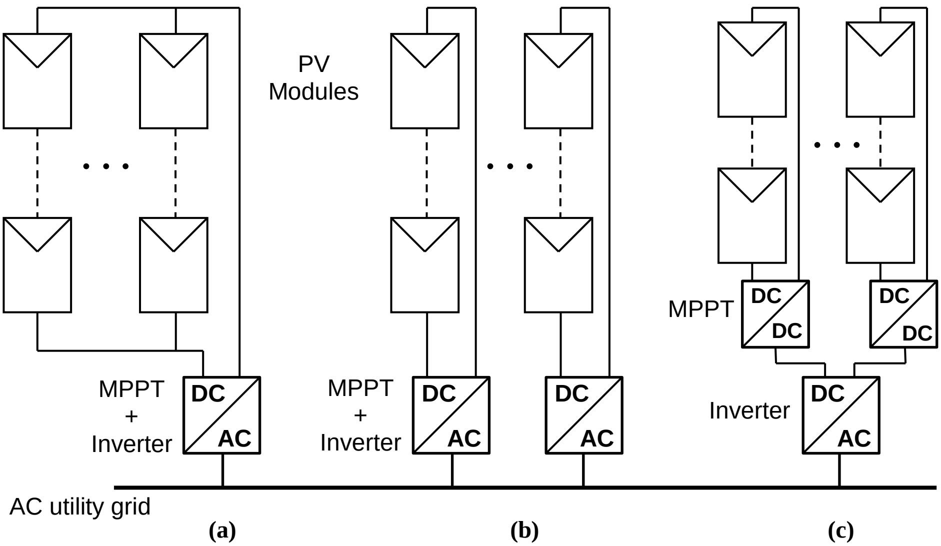

Figure 2.11: PV system architectures: (a) central, (b) string, (c) multistring system

The central inverter configuration illustrated in Figure 2.11a relies on a single inverter for the entire array of serial-parallel connected PV modules. This architecture is today widely used from large utility-scale systems to small residential systems. For large-scale and high-power applications this inverter is often divided in several master-slave units. Centralized inverter configuration includes some severe disadvantages, such as high-voltage DC cables between modules and inverter, power loses due to centralized MPPT (due to large mismatch losses), loses in the string diodes, and a nonflexible design. On the other hand, this configuration has advantages such as lowest specific inverter cost and high inverter efficiency because of the high power level. They are still number one choice for high power, large scale applications, where the converter is usually connected directly to the medium-voltage AC grid.

For smaller applications the drawbacks of the central inverter configuration, in the first place centralized MPPT, become more eminent. For such applications the string inverter configuration (Figure 2.11b) is more suitable. This configuration does not have parallel connected strings; instead, a smaller inverter for each string is used. In that way strings are completely independent from each other, and each string has its own maximum power point tracking. This decreases mismatch losses and increases overall system efficiency compared to the central inverter configuration. The disadvantage of string inverters is the higher inverter price per kW because of the lower inverter power level. Additionally, mismatch losses are still present, because of the series connection of modules within the string.

A variation of the string inverter system is the multistring inverter system illustrated in Figure 2.11c. Multistring inverter concept combines advantages of the string inverter, such as high energy yield, with the lower costs of central inverter. Each PV string has its own DC/DC converter with maximum power point tracker and each converter is connected to a common high power inverter through a common DC bus. Therefore, the multistring converter is a central inverter with per-string maximum power point tracking, but as in the string architecture, the mismatch losses are still present.

The quality of a PV system can be reflected in its performance ratio – the ratio of the electricity measured on the ac side of the electricity meter, compared to the amount of electricity generated by the PV modules, over a certain period. The performance ratio depends on each part of the PV system, as well as on the actual operational and environment conditions, and is typically 70% or higher. The main properties of the three conventional architectures are summarized in Table 2.2.

Table 2.2: Comparison of standard PV system architectures

System	**Central inverter**	**Multistring inverter**	**String inverter**
Inverter power level	>100 kW	<100 kW	<100 kW
Inverter specific cost	~0.06 €/W	~€0.07-0.2 €/W	~€0.07-0.2 €/W
Inverter efficiency	up to 98.5%	up to 98%	up to 98%
Impact of mismatch	high	medium	medium
Flexibility	small	small - medium	medium - high
Application	large PV systems	medium PV systems	small - medium PV system

The inverter does not always operate at its maximum efficiency, but according to an efficiency profile as a function of input power. The “european efficiency” η_{EU} is an averaged efficiency over a yearly power distribution corresponding to middle-Europe climate. The value of this weighted efficiency is obtained by assigning a percentage of time the inverter resides in a given operating range, according to Equation 2.1. Otherwise, the peak efficiency of an inverter can reach above 99% [2-12].

$$\eta_{EU} = 0.03\eta_{5\%} + 0.06\eta_{10\%} + 0.13\eta_{20\%} + 0.1\eta_{5\%} + 0.48\eta_{10\%} + 0.2\eta_{20\%} \quad (2.1)$$

It is worth noting the discrepancy between the efficiencies of the PV modules and inverters. The PV modules are relatively inefficient devices, while the efficiency of inverters approaches 100%. Still, large efforts are being invested into improving the converter efficiency by fractions of a percent. The converter has to process the total generated power in a relatively small volume, and every reduction of conversion losses will reflect on the required thermal management, and therefore the cost.

The choice of the most suitable architecture for a particular PV system depends upon many factors. The central inverter architecture is still the most used approach in large utility scale installations. These systems are usually built on locations that do not have problems with shadings, and with equally oriented PV modules that are regularly cleaned and maintained. As we are going towards smaller commercial and residential PV installations in urban areas with PV modules mounted on roofs, walls and other not so easily accessible places, the disadvantage of centralized maximum power point tracking becomes more prominent. String and multistring architectures become more suitable for these systems, although not completely solving the issue.

Going from large to smaller PV systems, it can be seen that there is a trend toward distributing the maximum power point tracking from the whole PV array towards individual strings of PV modules. But still, as long as the power tracking is performed on groups of PV modules and not individually, there is a risk of high mismatch losses. To address these problems new architectures with per-module maximum power point tracking were recently proposed.

2.3 Distributed Maximum Power Point Tracking

In conventional PV systems with PV modules connected in strings, it is often not possible to extract the maximum power from the modules, for the following reasons:

1. There are always small differences between the modules, even if they came from the same product line and from the same manufacturer.
2. Even if a single cell in the string is shaded its MPP current will decrease significantly. The string current will be forced to flow through bypass diodes, passing by the whole module whose power is lost even though there are still cells in the module which can generate power.
3. Sometimes modules do not have the same orientation, and this is especially the case in the building integrated PV modules, for example if the modules are mounted on the curved roof.

As shown in Figure 2.9, the power curves of different PV modules are not of the same shape, due to the different operating conditions or manufacturing tolerances. Since the current is forced to be equal for all modules in one string, modules cannot be operated at their own maximum power point, hence mismatch losses occur [2-13].

2.3.1 DMPPT Architectures

Recently, new architectures were proposed where each PV module has its own MPPT unit. Contrary to the central inverter architecture where MPPT is centralized, here MPPT is distributed throughout the PV array. Hence the name – distributed maximum power point tracking (DMPPT). In this way the power output of each module can be optimized regardless of the performance of other modules connected in the same PV array. Among new proposals [2-14], the two most perspective solutions are:

1. Architecture with PV module joined inverters (AC DMPPT) [2-15]
2. Architecture with PV module joined DC/DC converters (DC DMPPT) [2-16]

A significant advantage that both of these distributed converters technologies have over traditional central or string inverter technology is the ability to perform maximum power point tracking (MPPT) at the PV module level. This is achieved by isolating PV module from other modules connected in the same array. Another advantage of this approach is the ability to reconfigure PV arrays without additional complex string calculation, and possibility to combine modules with different power ratings and even different technologies, something that was not imaginable in conventional central or string inverter systems. With the per-module power tracking and implementing communication protocols, it is also possible to monitor module performance and easy and quick localization of faulty or underperforming modules.

DMPPT architecture with PV module joined inverters is shown in Figure 2.12. Each PV module has its own inverter that is attached to the module or to the module supporting structure. This combination of the PV module and adjoined inverter is often called AC module, while the converter is called microinverter or, somewhat ambiguously, module integrated converter, although the converter is not physically integrated into the PV module. A great advantage of this approach is the modularity. A system can be built starting with only one AC module and later, as the power requirements increase, additional modules can be simply added.

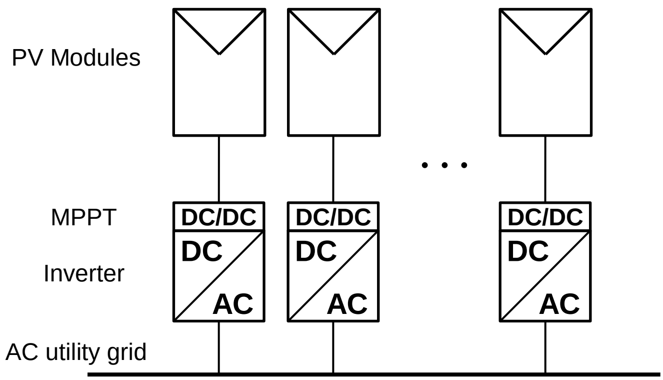

Figure 2.12: Distributed MPPT PV system with AC modules

Although a promising architecture, AC modules still have relatively low acceptance, mainly due to the low power level per unit which leads to lower inverter efficiency and higher specific costs when compared with conventional inverters. Another problem is high component count per PV module and, in the case of single phase applications, necessity for large electrolytic capacitors. This can significantly decrease the reliability and reduce the life time of the AC module.

In distributed architecture with module integrated DC/DC converters each module has its own integrated DC/DC maximum power point tracker which routes the optimized DC power to a central inverter over a common DC bus (Figure 2.13). These converters are sometimes mentioned as power optimizers. In comparison with the AC module architecture, this approach has lower flexibility due to the lower modularity.

Furthermore, a central inverter is retained and still presents a single point of failure, although, it can be a simplified and cost reduced version that performs DC/AC conversion only, without MPPT. On the other hand lower component count of the DC/DC converters gives the inherent reliability of the approach for integration into the PV module. In Chapter 4, two variants of this architecture will be shown, depending on the way the converters are connected, leading to two different converter topologies.

In order to make distributed MPPT architecture cost competitive with current architectures, several problems have to be solved. Mounting a converter on each PV module is not an easy task since it will be exposed to harsh environmental conditions. Being a simple device with a guaranteed lifetime of typically over 20 years, it is a challenge to construct a converter that can match the lifetime and reliability of a PV module. Regarding the reliability and life time, DC/DC distributed architecture has advantage over AC modules because of the simpler converter design. Another challenge is to match high efficiency and low specific cost of the central inverters. This could be possible with new design techniques and through the mass production respectively.

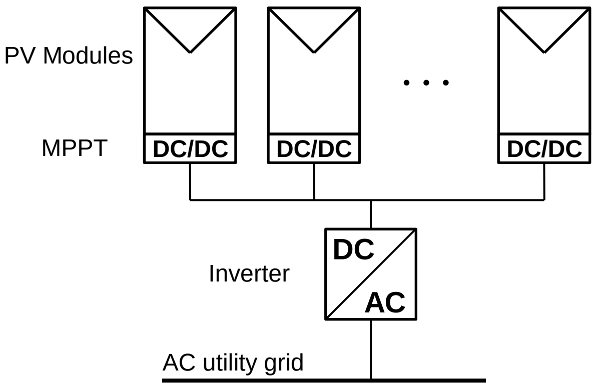

Figure 2.13: Distributed MPPT PV system with DC/DC converters

2.3.2 Case Studies for DMPPT Systems

Comparing DMPPT systems with traditional centralized MPPT (CMPPT) might not be appropriate, at least not for all situations. Clearly in some cases where mismatch is unavoidable, as it was shown in the case of the example from section 2.2.4, DMPPT will always have advantages when it comes to the system efficiency [2-9]. In case of the well oriented and maintained PV system, such as large ground PV power plants, even taking into account age related mismatch, DMPPT might not offer better efficiency.

Several manufacturers of the DMPPT converters have conducted field studies of their products, showing advantages over the conventional PV systems, although these data should be taken with a grain of salt. In a study performed by Texas instruments [2-17], the manufacturer of SolarMagic converters, it was shown that using DMPPT architecture can bring considerable gain in system performance. Depending on the specific scenarios, these gains can range from 5%-37%, as shown in Figure 2.14. The converter used in the study is intended for DC DMPPT systems, corresponding to Figure 2.13, and is mentioned in Section 2.4.2. Two independent studies presented in [2-18] and [2-19] also examined the performance of DMPPT systems using the same converters. The first study examines only the effects of shading on the performance of a small 2.6 kW PV system. Depending on the type of shading, the improvement in energy yield ranges from 29% to 71%. The second study also examined only effects of shading on a single string 1 kW PV system. Two scenarios were considered, with variable amount of horizontal and vertical shade cast on a single PV module. Depending on the situation, up to 30% of losses of a single PV module could be recovered when using DMPPT approach.

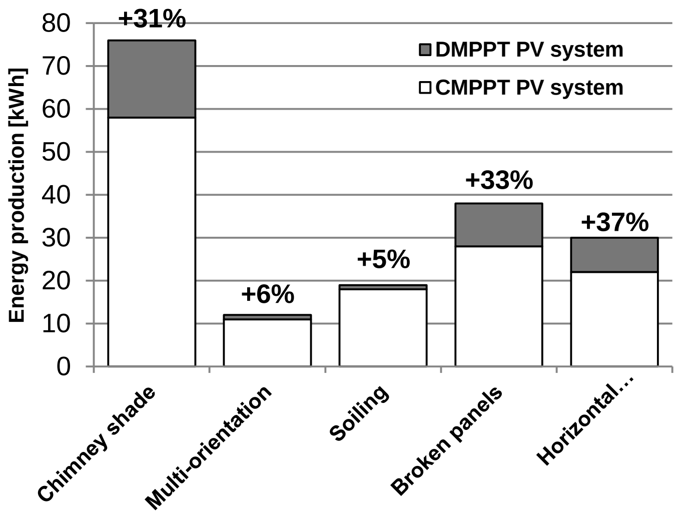

Figure 2.14: Energy gains in a DC DMPPT PV systems for various scenarios [2-17]

Another study presented in [2-20] examines the effects of shading in a ground based PV system with PV modules arranged in inclined ground-mounted rows. During the winter months, when the Sun spends more time low on the horizon, shading between rows of PV modules can significantly decrease the energy output of the PV system. Using the DC DMPPT approach, gains in monthly energy production can go up to 38% during the winter months (Figure 2.15).

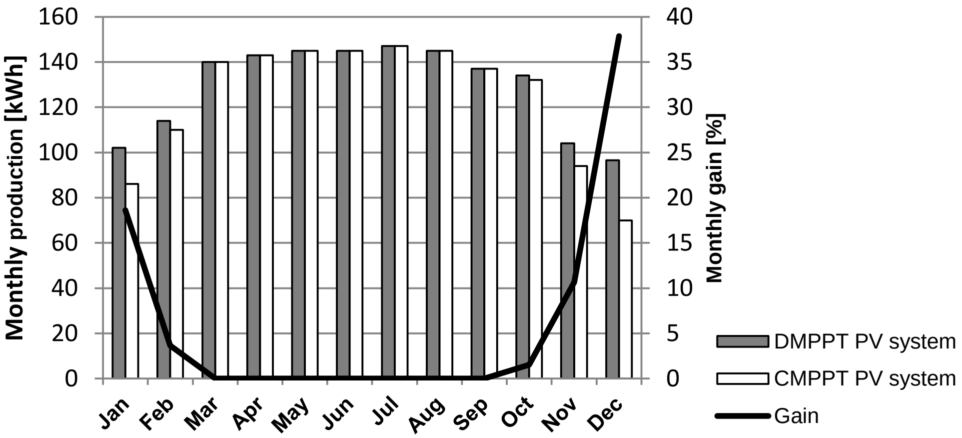

Figure 2.15: Monthly energy gains in a DC DMPPT PV systems [2-20]

In a study presented in [2-21], an AC DMPPT system is analyzed in two scenarios. The converter used is mentioned in Section 2.4.1 and is shown in Figure 2.16b. The first scenario investigated the effects of partial shading of the PV array. For the considered case, the increase of energy yield of the DMPPT system compared to the CMPPT system is 28%. In the second scenario, the PV array consists of two differently oriented groups of PV modules, which could be the case in BIPV applications. In this case, the increase in energy yield compared to the CMPPT system is 12%.

Other comparisons between DMPPT and CMPPT PV systems can be found in literature, for both DC [2-16, 2-22, 2-23] and AC [2-24..26] DMPPT systems. It should be noted that the majority of case studies take into account only shading effects which, as already noted, can be minimized if the modules are well placed and oriented. In some cases the shading scenarios are exaggerated or unrealistic leading to large performance advantages of DMPPT systems. In any case, the DMPPT systems will always have advantage over CMPPT systems when constant shading is present. However, it should be stressed again that DMPPT systems enable more surface area to be used for PV panels, even if that will introduce mismatch losses, which can be compensated by higher overall energy production. Moreover, whether the DMPPT system is more cost effective than CMPPT system will depend on the actual cost of the added converter, which might not be offset by higher energy yield.

2.4 State-of-the-Art in DMPPT Converters

DMPPT converters are relatively young technology, with first commercially available converters starting to appear by the end of 20th century [2-27], although with modest success due to the small market size and sometimes unreliable field performance. With the rapid expansion of the PV market at the beginning of 21st century, many solutions for DMPPT systems appeared, both for AC and DC variants. However, the period around 2010 included unprecedented price reductions in the PV market for PV modules and inverters for conventional PV systems. Converters for DMPPT systems on the other hand remained relatively immune to these price declines due to the small market, being approximately two to three times more expensive per watt than conventional inverters. This has led to losses as the suppliers struggled to remain competitive, with many players in the DMPPT market losing the pricing battle. However, some manufacturers remained. In the following some notable examples of converters for DMPPT systems will be listed.

2.4.1 AC DMPPT Converters

As of 2017, there are several manufacturers of small inverters for PV modules, and their price is in the range of 0.3 €/W, with an estimated market share of 1% [2-6]. At the time of writing, the most successful manufacturer in the AC DMPPT market, notably in the US, is Enphase with its microinverters, one of which is shown in Figure 2.16a [2-28]. It is a single phase inverter with the output power of 250 W. It should be noted that for a single phase inverter, a large capacitors are required to deal with pulsating power. In this case, electrolytic capacitors are being used, and despite the manufacturer's warranty of 20 years, the long term reliability is yet to be proven. A three-phase inverter can be used to avoid electrolytic capacitors, as was the case with PV-MIPS project [2-29] and the converter shown in Figure 2.16b. Here, lower value film capacitors were used, however, together with a special high voltage PV module to avoid additional boost stage. Another notable example is the Enecsys, shown in Figure 2.16c, with its converter which uses high voltage film capacitors coupled with transformers to avoid using electrolytic capacitors [2-30].

(a) (b) (c)

Figure 2.16: State-of-the-art converters for AC DMPPT systems

2.4.2 DC DMPPT Converters

Simple battery chargers, sometimes even without implemented MPPT, existed ever since the first commercial PV modules emerged. However, true DC DMPPT solutions appeared in recent years, long after the first AC DMPPT converters. As of 2016, there are several manufacturers of DC/DC converters for PV modules, and their price is in the range of 0.1 €/W, with an estimated market share of 3% [2-6]. It should be noted that DC DMPPT converters although being considerably cheaper their AC counterparts, still require a central inverter. Moreover, there are several variants of DC MPPT architectures, which will be covered in Chapter 4. Depending on the architecture, converters differ in output voltage and the way the outputs are connected and interfaced to the central inverter. Figure 2.17a shows the SolarMagic (TI, [2-31]) converter which has buck-boost topology and can decrease and increase the voltage from the PV module. This type of converters can be easily retrofitted in existing PV systems, with serial connected outputs to form strings which are then connected in parallels to the central inverter. Another solution is to have either low or high output voltage converters, with outputs connected in parallel to the central inverter. An example of former solution is SolarEdge converter [2-32], shown in Figure 2.17b, where the outputs of the converters are connected in parallel to the 50 V DC bus. This however requires a boost stage in the central inverter, which can affect the final system efficiency. Figure 2.17c shows the Femtogrid converter [2-33], which boosts the PV module voltage to 380 V which is more suitable for the central inverter.

(a) **(b)** **(c)**

Figure 2.17: State of the art in converters for DC DMPPT systems

The abovementioned AC and DC DMPPT converters are listed in Table 2.3, with some main properties.

Table 2.3: Comparison of state-of-the-art converters for DMPPT systems

Name	Enphase	PV-MIPS	Enecsys	SolarMagic	SolarEdge	Femtogrid
Output	AC			DC		
Efficiency	97 %	96 %	92.1 %	98.5 %	98.8 %	>97 %
Notes	1-phase, Electrolytic capacitors	3-phase, Film capacitors	1-phase, Film capacitors	Buck-Boost, Low voltage	Boost, Low voltage	Boost, High voltage

2.5 Conclusions

As the PV technology progresses, expands and enters into the residential area, new challenges arise. With limited space, environmental impact and design constraints, mismatch between PV modules caused by non-uniform irradiation can significantly decrease the yield of a PV system. Using centralized MPPT in traditional PV systems it is not possible to extract the maximum power from each PV module individually under all conditions. New distributed MPPT architectures not only provide consistent maximum power from the PV array, but can also enable flexible PV modules to be used in traditionally inaccessible places such as curved surfaces. However, instead of large conventional converters, DMPPT systems uses small converters joined to each PV module in the system. The number of manufacturers producing converters for DMPPT PV systems has been constantly increasing in recent years. However, in all current state-of-the-art converters some drawbacks still exist:

- The converters are external to the PV module, that is, additional cables, connectors and labor are required to connect the converter and the PV module.
- The price of the converters is still high, and can be only justified in small and medium systems with large mismatch losses.
- Electrical characteristics of the converters usually limit their usage to only several types of PV modules.
- Converters for DMPPT systems are relatively young technology and their field performance and reliability are not yet proven. PV modules are simple devices and it will be difficult to match their reliability and life time.

In the following chapter, a new concept of a DMPPT converter intended to tackle the abovementioned limitations will be presented.

2.6 References

[2-1] A. Goetzberger, V. Hoffmann, “Photovoltaic Solar Energy Generation,” Springer, 2005

[2-2] “IEC 61853, Photovoltaic (PV) module performance testing and energy rating,” IEC standard, 2011

[2-3] “Research Cell Record Efficiency Chart,” available online, *www.nrel.gov*

[2-4] International Energy Agency – Photovoltaic Power Systems (IEA-PVPS), “PV Performance Modeling Methods and Practices: Results from the 4th PV Performance Modeling Collaborative Workshop,” 2017

[2-5] European Photovoltaic Industry Association (EPIA), “Solar Generation 6,” 2011

[2-6] Fraunhofer ISE, “Photovoltaics Report,” 2018

[2-7] E. Hamers, M. van den Donker, B Stannowski, R Schlatmann, G. Jongerden, “Helianthos: Roll-to-Roll Deposition of Flexible Solar Cell Modules,” Plasma processes and Polymers, 2007

[2-8] T. Esram, P. Chapman, “Comparison of Photovoltaic Array Maximum Power Point Tracking Techniques,” IEEE Transactions on Energy Conversion, 2007

[2-9] M. Acanski, J. Popović-Gerber, J. A. Ferreira, “Next Generation Power Electronic Technology for Photovoltaic Systems,” Young Researcher Symposium (YRS), 2010

[2-10] F. Schimpf, L.E. Norum: “Grid Connected Converters for Photovoltaic, State of the Art, Ideas for Improvement of Transformerless Inverters,” Nordic Workshop on Power and Industrial Electronic, 2008

[2-11] S. Kjaer, J. Pedersen, F. Blaabjerg: “A Review of Single-Phase Grid-Connected Inverters for Photovoltaic Modules,” IEEE Transactions on industry applications, Vol. 41, No. 5, 2005

[2-12] I. Josifović, J. Popović-Gerber, J. Ferreira, “Power Sandwich industrial drive with SiC JFETs,” European Conference on Power Electronics and Applications (EPE), 2011

[2-13] B. Koirala, B. Sahan, N. Henze: “Study on MPP Mismatch Losses in Photovoltaic Applications,” European Photovoltaic Solar Energy Conference and Exhibition (EU-PVSEC), 2009

[2-14] G. Walker, J. Pierce, “Photovoltaic DC-DC Module Integrated Converter for Novel Cascaded and Bypass Grid Connection Topologies – Design and Optimization,” Power Electronics Specialists Conference (PESC), 2006

[2-15] H. Oldenkamp, I. de Jong, “The Return of the AC-Module Inverter,” European Photovoltaic Solar Energy Conference (EU PVSEC), 2009

[2-16] G. Walker, P. Sernia: “Cascaded DC–DC Converter Connection of Photovoltaic Modules,” IEEE Transactions on Power Electronics, Vol. 19, No. 4, 2004

[2-17] Texas instruments, “New Analog IC Technology Support Safety, High Efficiency and High Reliability of Today's PV Solar System,” available online at *www.ti.com*

[2-18] “Seltener Zauber,” Photon Profi Magazine, September 2009

[2-19] E. Zentgraf, “Study of shaded PV-Modules without and with the so-called Power Optimizer Solar Magic,” TEC Institute for Technical Innovations, 2010

[2-20] C. Deline, B. Sekulic, J. Stein, S. Barkaszi, J. Yang, S. Kahn, “Evaluation of Maxim Module-Integrated Electronics at the DOE Regional Test Centers,” Photovoltaic Specialist Conference (PVSC), 2014

[2-21] B. Sahan, R. Burger, W. Belschner, N. Henze, “A novel AC module with high-voltage panels in CIS technology,” European Photovoltaics Solar Energy Conference Exhibition, 2008

[2-22] E. Roman, V. Martinez, J. Jimeno, R. Alonso, P. Ibanez, S. Elorduizapatarietxe, “Experimental Results of Controlled PV Module for Building Integrated PV Systems,” Solar Energy, vol. 82, 2008

[2-23] L. Linares, R. W. Erickson, S. MacAlpine, M. Brandemuehl, “Improved Energy Capture in Series String Photovoltaics via Smart Distributed Power Electronics,” Applied Power Electronics Conference and Exposition (APEC), 2009

[2-24] O. Arráez-Cancelliere, N. Muñoz-Galeano, J. Lopez-Lezama, “Performance and Economical Comparison Between Micro-Inverter and String Inverter in a 5.1 kWp Residential PV-System in Colombia,” Power Electronics and Power Quality Applications (PEPQA), 2017

[2-25] S. Harb, M. Kedia, H. Zhang, R. Balog, “Microinverter and String Inverter Grid-Connected Photovoltaic System - A Comprehensive Study,” Photovoltaic Specialists Conference (PVSC), 2013

[2-26] S. Krauter, J. Bendfeld, “Cost, Performance, and Yield Comparison of Eight Different Micro-Inverters,” Photovoltaic Specialist Conference (PVSC), 2015

[2-27] C. Verhoeve, C. Frumau, E. de Held, W. Sinke, “Recent Test Results Of AC-Module Inverters,” Netherlands Energy Research Foundation ECN, 1997

[2-28] “Enphase C250 microinverter datasheet”, available online, *www.enphase.com*

[2-29] N. Henze, A. Engler, B. Sahan, "Performance of a Novel Three-Phase Photovoltaic Inverter for Module Integration," Institut für Solare Energieversorgungstechnik (ISET), 2014

[2-30] “Enecsys SMI-S200W-72 Datasheet,” available online, *www.enecsys.com*

[2-31] “Solar Micro-Converter DC-DC Power Optimizer,” available online, *www.ti.com*

[2-32] “SolarEdge Power Optimizer Datasheet,” available online, *www.solaredge.com*

[2-33] “Femtogrid Solar Power Optmizer PO310 Datasheet,” available online, *www.femtogrid.com*

Chapter 3 Concept of the PV Module Integrated Converter

3.1 Introduction

The DC DMPPT PV market has evolved rapidly over a short period of time and a number of companies are now offering power converters for DC DMPPT PV systems. This is still a young market with a lot of room for improvements. The existing solutions are usually designed to be more flexible in terms of electrical specifications in order to accommodate a certain range of available PV modules. This imposes additional constraints on the converter design optimization and has negative effect on the conversion efficiency. Another consideration is the installation cost, since additional cables and connectors together with providing a place for the converter requires additional installation material and labor. In a highly competitive market such as PV, the initial investment costs are sometimes more important than the improved system performance.

For the best system performance, a DMPPT converter should be optimally designed for the particular PV module which is going to be used. This puts the converter in a position that is from electrical point of view closer to the PV module than to the inverter or grid. To decrease the cost, it would be desirable to increase the level of integration by positioning the converter as close as possible to the PV module not only from electrical point of view but also mechanical, combining functional and physical with electrical integration. By integrating the converter directly into the PV module, the PV-module-converter system could be considered as a single building block in a PV system. By specifying which encapsulation and packaging layers can be shared among the PV module and the converter, one could also consider different integration levels.

As a continuation of Chapter 2, this chapter presents a high level PV module integrated converter concept as the next step in integration of power electronics into the PV array. Possible approach to achieve PV module converter integration is visualized, and some of the converter specifications are set. The analysis of the proposed concept from the point of view of different design areas will result in a set of boundary conditions for the design procedure for the integrated converter, but will also set some relations between the design areas.

The goals of this chapter are as follows:

1. Presenting the concept of the PV module integrated converter as the next generation power electronics technology for DMPPT systems,
2. Defining the scope of this thesis, that is, the considered system architecture, the level of integration, and some of the converter specifications,
3. Identifying the main design areas, their boundary conditions and interdependences between them.

It will be shown that on top of the standard requirements for a PV converter, the integration concept will bring in additional limitations into the main design areas, namely electrical, thermal and technological design. These will be addressed separately in their own chapters and combined all together in the final chapter when the converter is finally designed.

3.2 Concept of the PV Module Integrated Converter

By integrating a converter directly into a PV module it is possible to reduce its cost and to improve the level of integration in the system. A factory pre-mounted converter eliminates additional wires and connectors found in conventional DMPPT systems, making the installation process easier and cheaper. The converter can also be optimized for the specific PV module, enabling optimal components values, lower cost and higher conversion efficiency.

Further improvements in system cost and flexibility can be achieved using thin-film flexible PV modules. As noted in Chapter 2, flexible PV modules eliminate heavy and expensive glass and other encapsulants found in standard PV modules, leading to decreased manufacturing and installation costs. The physical properties of flexible PV modules make them an excellent candidate for BIPV applications. Furthermore, owing to the manufacturing process similar to printing, the number and size of PV cells in flexible PV modules can be easily scaled to achieve different electrical properties. In this way flexible PV modules can be customized to meet the converter specifications, instead of other way around.

Figure 3.1 illustrates the concept of a converter integrated into a flexible thin-film PV module. After the component placement, the converter is encapsulated for protection using the same back encapsulation material as the PV module, therefore sharing one or more structural layers with the PV module. With a converter placed between the PV module and the supporting surface, flexibility and very low profile become main construction design goals for the PV module integration. This will have impact throughout the design procedure for the integrated converter introducing certain design interdependencies.

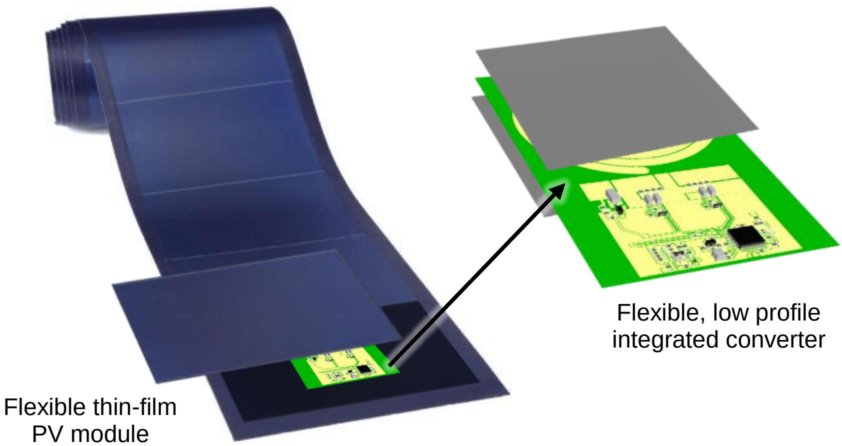

Figure 3.1: Concept of the PV module integrated converter

3.3 Scope of the Thesis – System Architecture and Level of Integration

As mentioned in Chapter 2, there are two main architectures for DMPPT PV systems, AC and DC, depending on the type of voltage generated on the converter output. From the point of view of PV module integration, the DC approach is more feasible for two reasons:

1. Magnetic materials – Conventional grid tied inverters require large filtering magnetic components for the grid connection. As it will be shown in Chapter 5, with the available magnetic materials for low profile flexible construction, the values of achievable inductances are severely limited.
2. Capacitors – Conventional 1-phase inverters require bulky capacitors for energy storage, most usually in the form of electrolytic capacitors. Considering the required capacitances, very low profile and flexible construction would not be possible. Workarounds by using high voltage film capacitors coupled with complex transformers would not be feasible for the previous reason.

For this reason only the DC DMPPT approach will be considered in the following. Furthermore, two architecture variants will be considered in Chapter 4, each with its own type of converter:

1. Low output voltage, step-down/step-up converter where the outputs of the converters are connected in serial/parallel configurations to a low or high voltage DC bus, much like in traditional PV systems,
2. High output voltage, high step-up converter where the outputs of the converters are connected in parallel to a high voltage DC bus.

Looking at the number of physical layers that the converter and the PV module can share, one can consider different levels of integration. On the lowest level, the converter with its own enclosure can simply be attached to the back side of the PV module [3-1]. On the highest level, the converter could be directly assembled on the PV module which would act as a PCB. The former does not offer any cost benefits compared to the existing solutions for DMPPT, while still introducing design constraints due to thermal coupling. The later could achieve lowest cost, but would require using back contact layer which would limit the number of conductive layers for circuit tracks, while not offering significant design advantages.

In this thesis an intermediate approach is considered, where a converter assembled on a flexible PCB is mounted inside the PV module, using its encapsulant layer as an enclosure. As it will be shown in the following chapters, from the design point of view this will not differ much from the highest level of integration, but will enable cost savings when compared to the lowest level of integration.

3.4 Design Areas for PV Module Integration

Integration of the converter into the PV module will impose harsh environmental conditions on the converter operation with elevated temperatures and large temperature swings. PV modules are relatively simple and robust devices and it is a challenge to design a converter that can meet the reliability and lifetime of PV modules. Furthermore, a tight thermal coupling between the converter and the PV module and requirements for low profile and flexible construction introduces interdependence between different areas of the design process. Three main groups of specifications can be identified in the design process of the module integrated converter, each with its own goals:

1. **Electrical design** with the goal of maximizing the conversion efficiency,
2. **Technological design** with the goal of achieving low profile and flexible construction, while minimizing volume,
3. **Thermal design** with the goal of keeping the operating temperatures safe.

The first requirement with its spatial constraints and the third with its operating conditions will directly impact the technological and the thermal design. The electrical design becomes the victim, with limited options for possible topologies and component values. However, as in the case when designing a conventional converter, some parameters from the electrical design will directly affect the thermal and technological design. In conclusion, the integration of the converter into the PV module will introduce tight interdependences between the design areas. This will be discussed in the following sections.

3.4.1 Electrical Design

The main goal of the electrical design is to meet the input/output electrical specifications and the efficiency requirements, while keeping the losses and reached temperatures within the safe limits. All this has to be achievable within the available volume.

The converter ratings are predetermined by the used PV module. In the following, the available module has the maximum power point voltage in the range of 30 V, for the power range from 5 W to 120 W. The output voltage will depend on the DMPPT architecture, and will be up to 100 V and 380 V for the low and high output voltage converter respectively. There are numerous converter topologies capable of satisfying the required voltage gain, and the most suitable one for enabling PV module integration will be chosen.

For the sake of simplicity, the design procedure and optimization of the converter will be carried out for the fixed input and output voltages. However, for the component ratings, all possible conditions will be considered. For the chosen switching frequency, the inductance value is calculated under condition that a certain current ripple is obtained. Afterwards, the values of input and output filter capacitors are calculated to achieve required voltage ripple. With all circuit parameters known, the next step will be estimating power losses in active devices. Since the active devices in general have smaller volume, we can expect higher power loss density and higher operating temperatures than those found in passive components. Therefore it is important to select efficient active devices.

3.4.2 Thermal Design

The main goal of the thermal design is to keep the operating temperatures of all components in the converter and the PV module within the safe limits. Again, all this has to be achievable within the available volume.

The PV module can operate at higher temperatures, therefore it is important to estimate the temperature profile of the system, with special attention paid on the hot-spot location on the PV module where the converter is integrated, since this is the place with the highest power loss density. PV modules are relatively inefficient devices with usually more than 80% of the absorbed light energy transformed into heat. Under high irradiation and poor ventilation, the PV module operating temperature can easily reach 70°C or more. With its presence, the integrated converter may block the heat flow from the PV module and add additional heat through power losses in its components, creating a hot-spot in the PV module. It is the purpose of the converter’s thermal management to remove the excess heat without causing negative effects on the reliability of the PV module.

To achieve safe operation, suitable thermal management strategies have to be identified and examined. This is achieved by using a thermal model which takes the heat losses (from the electrical design) and loss distribution (from the spatial design and thermal management) as input variables and gives the estimate of the system temperature behavior. It can be shown that, with a proper thermal management and efficient heat spreading, the temperature of the components of the integrated converter, on one side, and that of the PV module hot-spot, on the other side, will reach similar levels. The fact that the maximum operating temperature of the PV module, which is in the range of 90-100°C, is much lower than that of the converter components (usually 125°C or more), means that the PV module hot-spot temperature will set the critical design limit.

3.4.3 Technological Design

The main goal of the technological design is to meet the desired volume and mechanical requirements. This means that, in case of the PV module integration, special technologies are necessary to achieve very low profile and flexible design of the converter. In this thesis, the goal will be to realize the flexible construction with the total thickness less than 2 mm.

Using the newly developed gallium-nitride (GaN) and silicon-carbide (SiC) devices with very fast switching speed, a breakthrough in switching performance can be achieved. Multi-megahertz switching frequency capability can significantly reduce the size of passive components, adding the cost benefits and increasing the integration level and power density [3-2]. The most important requirements for a PV converter, efficiency and cost effectiveness, can both be addressed with improved switching devices. In this thesis, the first generation of commercially available GaN transistors will be used. In Chapter 5 it will be shown that they already offer significantly improved figures of merit (FOM) compared to the currently available Si technology, which brings a disruptive improvement in switching performance.

A major barrier to meet the low profile and flexible requirements are magnetic components. Recent achievements show that this can also be addressed by using special core materials [3-3]. While it is possible to use polymer-like laminates filled with ferrite powder, their permeability is rather low, which limits the inductance values that can be achieved. On the other hand, large inductance is needed in order to decrease the current ripple and the associated core losses, since the aforementioned materials are rather lossy. However, the upper limit for the inductance value is determined by volumetric constraints. Large inductance results in higher number of turns which, considering the minimum wire cross-section area determined by inductor current capacity and conduction losses, increases the size of the inductor. This will lead to larger parasitic components, decreasing the inductor resonant frequency and suitability for high switching frequency operation. This introduces an additional design limit parameter, the maximum allowed inductance value.

Considering the filter capacitors, their values are determined by the maximum allowed voltage ripple. Later on it will be shown that, for the considered range of inductance and required voltage ripple, values of input and output capacitors are not critical, and can be easily achieved on a small surface area by paralleling low profile ceramic chip capacitors. As for the rest of the converter, double-sided flexible PCB has been employed, with all other components being available in small footprint low profile packaging.

3.5 Design Areas Interdependences

A properly designed PV module integrated converter should fulfill all the requirements from the electrical, thermal and technological design areas. From the discussion above, it can be seen that improvements in one design area can lead to making compromises in another. When designing a conventional converter, different design areas are usually loosely coupled, and the procedure is sometimes straightforward. When one of the design areas imposes strict limitations on others, we can expect tight design area interdependencies [3-4]. The following section summarizes the relations between the electrical, thermal and technological design, and the main trade-off parameters affecting these relations.

Technological-Electrical Design Interdependency

Power conversion involves converting electrical energy from one form to another, such as converting between AC and DC, changing the voltage or frequency, or combinations of these. This is accomplished using intermediary components for **energy storage**, such as capacitors and inductors, where the input energy is temporarily stored in the formed electrical or magnetic fields. For the field to be formed, a certain volume is required, depending on the amount of energy. With the thickness of the converter fixed to a certain value, we can further consider the area required for a component to change depending on the required volume.

The surface area for the components is, in principle, not limited, given that there is enough surface area of the PV module. However, to achieve low cost, it is important to aim for small volume, and therefore small converter surface area, which will minimize the amount of used material for the components, packaging and interconnections. Furthermore, the losses are not always independent of the components shape, which will be the case for the inductors as it will be shown later in this thesis. Increased area required for the components also increases the area required for the interconnections, which can introduce parasitic elements and associated losses.

Cost can be further reduced by selecting topologies with low component count. However the main parameter affecting the required volume will be the switching frequency of the converter. In general, increasing the switching frequency decreases the required volume for the inductors and capacitors, facilitating technological design by reducing the size of the components. There are limits to the maximum switching frequency, as it will come out in interdependencies between other design areas.

Technological-Thermal Design Interdependency

To decrease the cost of the PV module integrated converter, the total volume of the converter should be as small as possible. On the other hand, there are always power losses in the components during the process of energy conversion. These sources of heat will increase the operating temperature of the components. The increase over ambient temperature depends on thermal properties and the geometry of the converter parts, from the heat source to the converter surrounding. The thermal property and a measurement of a temperature difference by which an object or material resists a heat flow is referred to as the **thermal resistance**.

The thermal resistance is proportional to the thermal conductivity and the heat path length, and inversely proportional to the heat path cross-section. These are all parameters coming from the technological design, depending on the materials being used and the geometry of the converter. Decreasing the size of the converter in general leads to higher thermal resistances imposing higher stress on the converter components. This imposes burden on the thermal management, since efficient heat spreading has to be implemented in order to extract the heat from components and spread it over a large area.

Specifically in case of the PV module integrated converter, with a low profile, large surface structure, we can make a distinction between the orthogonal thermal resistance and the in-plane thermal resistance. Owing to the low converter profile and short heat path, the orthogonal thermal resistance is expected to be low. This will be the dominant thermal resistance for parts where the losses are distributed over a larger area, such as inductors and the PV module. The lateral thermal resistance will be critical for parts were losses are concentrated in small volume, such as active devices. These losses should be efficiently spread over a large area via lateral thermal resistance and dissipated into ambient via orthogonal thermal resistance. Very low profile will put limit on the achievable thermal resistance, and the trade-offs will be made by using different heat extraction strategies.

Electrical-Thermal Design Interdependency

In reality, power conversion is always associated with **power losses** due to components’ non-idealities. These losses are caused by finite conductivity of materials, directly through conductive or indirectly through switching losses, and due to losses in materials when the electrical and magnetic fields are formed. The losses increase the components temperature, requiring appropriate thermal management to dissipate the heat.

Keeping the same volume of the converter, increasing conversion efficiency decreases the losses and requirements for the thermal management. The amount of losses is determined by the parasitic components and material non-idealities. Switching and material losses depend in the first place on switching frequency, which is a parameter in the electrical design.

Using lower switching frequencies and more distributed topologies, the requirements for the thermal design can be lowered, at the expense of the required volume and cost, while by increasing the switching frequency the size of passive components can be reduced at the expense of the heat loss density. Therefore, for a chosen topology, the switching frequency will represent the main trade-off parameter to create balance between the converter efficiency and the temperature behavior.

3.6 Conclusions

This chapter presented the concept of the PV module integrated converter as the next step in DMPPT systems. In the previous discussion, the main areas in the design of the converter were defined, with their limitations and the main design parameters. Moreover, the links that make the design areas interact with each other were identified, forming the design area interdependence. This interdependence is summarized in Figure 3.2, showing the main design areas with their requirements, and the mechanisms and processes over which they interact.

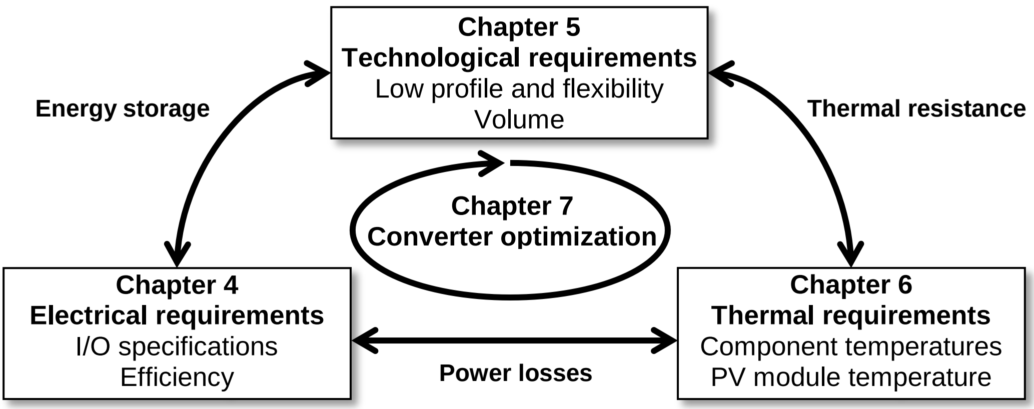

Figure 3.2: Design areas interdependences

The main design areas will be covered in their respective chapters. Chapter 4 will deal with the electrical design of the converter, selecting topologies and defining equations for component values. Chapter 5 will deal with the technological design of the converter, selecting technology platforms to enable low profile and flexible construction, and equations for spatial parameters. Chapter 6 will deal with the thermal design of the converter, identifying suitable thermal management strategies, and modeling the system to predict the thermal behavior.

In the end, an optimization procedure is needed to between all the design requirements. The switching frequency, being the dominant design parameter, will be used to make trade-offs in the design between efficiency, losses and the size of passive components, and the required thermal management. As the result, taking into account these limitations and interdependences, the unified converter design and optimization will be covered in Chapter 7.

3.7 References

[3-1] M, Acanski, J. Popovic-Gerber, J. Ferreira, “Thermal Modeling of the Module Integrated DC-DC Converter for Thin-Film PV Modules,” International Power Electronics and Motion Control Conference (EPE-PEMC), 2010

[3-2] M. Acanski, J. Popovic-Gerber, J. Ferreira, “Comparison of Si and GaN power devices used in PV module integrated converters,” Energy Conversion Congress and Exposition (ECCE), 2011

[3-3] J. Popovic, “Improving Packaging and Increasing the Level of Integration in Power Electronics,” PhD thesis, Delft University of Technology, 2005

[3-4] Mark Gerber, “The Electrical, Thermal and Spatial Integration of a Converter in a Power Electronic Module,” PhD thesis, Delft University of Technology, 2005

Chapter 4	*Electrical Design of the PV Module Integrated Converter*

4.1 Introduction

Electrical design is routinely the first and most important step when designing a power converter. The main goal of the electrical design is to satisfy the input and output electrical requirements. Indirectly, this will set the efficiency requirements, along with some others such as for thermal performance and EMI. The same is valid for the PV module integrated converter. However, based on the discussion in Chapter 3, requirement for a low profile, flexible construction and operation at elevated temperatures will set limits in the electrical design.

Electrical design should be therefore carefully done, starting from selection of a suitable topology for the PV module integrated converter. Furthermore, when designing the converter, there could be several iterations in order to meet all the converter requirements. On one hand it is important to achieve low enough power losses not to compromise the PV module. On the other hand, it is important to achieve low volume for energy storage components in order to avoid extremely large dimension ratios, considering that the converter thickness is limited. As it will be shown later in Chapter 7, the main parameter of the electrical design that will affect both objectives is the converter switching frequency.

Based on the previous discussion, the goals of this chapter are:

- Setting the input/output electrical requirements for the integrated converter based on the characteristics of the PV module and the DMMPT architecture.
- Ranking the existing converter topologies on the basis of suitability for integration into PV module and selecting the most suitable ones. Two selected topologies, with low and with high output voltage will be analyzed in details.
- Providing for input parameter, switching frequency, to be used in the final converter design in Chapter 7, in order to provide output parameters for the technological design in Chapter 5, via the required energy storage components, and for the thermal design in Chapter 6, via power loss models.

The chapter starts with a general description of the PV module integrated converter and its main parts. The following section specifies the input and output electrical specifications for the converter, determined by the used PV module and the selected system architectures. In the next section, possible topologies for the converter are listed and the most suitable ones are selected based on multiple criteria concerning the PV module integration. For the selected topologies, electrical designs for the power stage are presented together with key expressions that will determine the size of energy storage components. The chapter also presents in brief the supporting circuit in charge for control and MPPT.

4.2 Overview of the PV Module Integrated Converter

From the system level point of view, the converter can be divided into several functional parts, as shown in Figure 4.1. As noted, two versions of the converter will be considered, one with HV output and one with LV output. Both versions will have the most of the blocks shared. Only the main part in charge for power processing will differ, together with some minor differences in the signal measurement chain and the control algorithm.

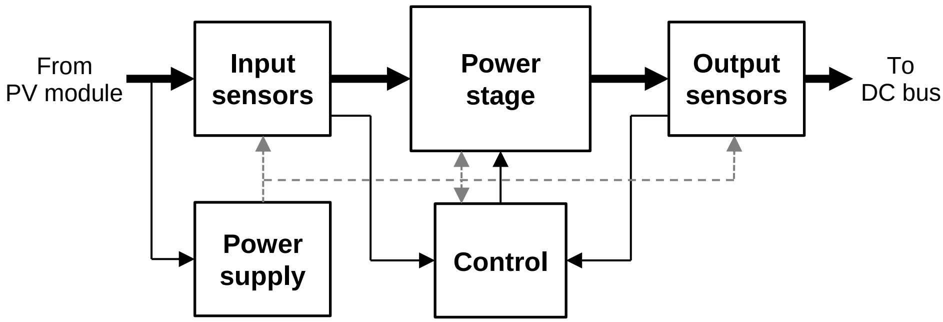

Figure 4.1: System level overview of the PV module integrated converter

The main functional parts of the converter are:

- **Power stage**, in charge of converting the power from the PV module and acting as an interface to the inverter.
- **Input/output voltage/current measurement stages**, in charge of measuring the relevant input and output voltages and currents. These measurements will be required for the MPPT algorithm, to control the output voltage if needed, and to protect the converter by detecting unsafe operating conditions.
- **Control stage**, in charge of generating the control signals for the power stage, performing MPPT algorithm, and providing signal monitoring and readouts, safe operation and diagnostic.
- **Auxiliary power supply**, in charge of providing power for the control stage, sensors and drivers in the power stage.

The main and most crucial part of the converter is the power stage. It consists of switching elements, accompanying driver electronics, and energy storage components. This is where the power processing occurs and where the majority of power loss will result in generated heat, affecting both the converter and PV module operation. This is also the largest part of the converter with its energy storage components which will have to be fit within the spatial constraint while retaining flexible construction.

Beside the power stage, other parts of the converter are not critical and are practically identical in both HV and LV version of the converter. They will be covered in more details at the end of this chapter. Since the power stage is the most important, it will be first addressed in the following section.

4.3 Converter Electrical Specifications

The fundamental step when designing a power converter is to choose an appropriate topology. However, before we start with the selection, we first need to determine the input and output electrical specifications. PV modules are variable, non-linear, temperature dependent power sources and depending on the output voltage, it might be required to increase and/or decrease the voltage during the normal operation. Depending on required input/output voltage ranges, this will narrow down the possible choices for the converter topologies.

In this section, the considered PV module will be modeled in order to predict possible voltage and current (and consequently power) ranges on the input side of the converter. Following that, the output voltage ranges will be determined based on the considered DMPPT architectures.

4.3.1 PV Cell Electrical Modeling

To determine the input electrical specification for the converter it is necessary to know the electrical characteristics of the PV module. In the following, a short description of the PV cell and module behavior will be presented, leading to their electrical models.

A typical structure of a PV cell, shown in Chapter 2 in Figure 2.1, contains of p-n junction where the light-induced voltage is generated. Therefore, a PV cell can, in a first-order model, be described as a superposition of the response of the device to two excitations: voltage and light. A simple equation that describes the current of the solar cell $\boldsymbol{I_{cell}}$ is given with Equation 4.1 [4-1]:

$$I_{cell} = I_{ph} - I_{dark} = I_{ph} - I_0(e^{\frac{V_{cell}}{V_T}} - 1) \tag{4.1}$$

where:

- $\boldsymbol{I_{ph}}$ is photovoltaic generated current,
- $\boldsymbol{I_{dark}}$ is the current of the intrinsic diode,
- $\boldsymbol{V_{cell}}$ is the cell voltage,
- $\boldsymbol{I_0}$ and $\boldsymbol{V_T}$ are the reverse bias saturation current and thermal voltage respectively, the parameters of the intrinsic diode. Moreover, the thermal voltage $\boldsymbol{V_T}$ is given with:

$$V_T = \frac{kT}{q} \tag{4.2}$$

where:

- k is the Boltzman constant,
- T is the absolute temperature in K,
- Q is the elementary charge.

All the parameters of the PV cell depend on temperature, however, the thermal voltage, the reverse saturation current and the photo generated current are dominant. The equation for the latter two is complicated and technology dependent, and for the further modeling the available temperature coefficients will be used after the model for a certain temperature is obtained.

The model described with Equation 4.1 is the simplest, but often used model of the PV cell and it can be easily represented with a current source and a diode (Figure 4.2a). It should be noted a junction capacitance should be added to the model if the dynamics of the PV module are being analyzed. However for our static considerations, the junction capacitance will not be taken into account. In some cases the simple model of Figure 4.2a is insufficient to accurately represent the maximum power delivered by the PV cell, because of the additional effects which have not been taken into account and which may affect the PV cell response:

- Series resistance: Losses in semiconductor material, front and back cell contacts and current collecting bus are represented as a lumped resistor $\boldsymbol{R_s}$, in series with the photocurrent generator.
- Shunt resistance: A number of shunt resistive losses can be identified, such as local shorts in the semiconductor layer or perimeter shunts along cell borders, represented as a lumped resistor $\boldsymbol{R_{sh}}$ in parallel with the photocurrent generator.
- Non-ideality of the diffusion diode: Real PV cells do not have ideal characteristics as described before, and it is common practice to add a parameter $\boldsymbol{n}$, diode ideality factor, to account for these non-idealities.
- Recombination effects: Non-ohmic current paths in parallel with the photocurrent generator can be represented with a second diode in the equivalent circuit, causing the current $\boldsymbol{I_{rec}}$.

Taking into account the abovementioned effects, a PV cell can be represented with a more detailed equivalent circuit shown in Figure 4.2b [4-2].

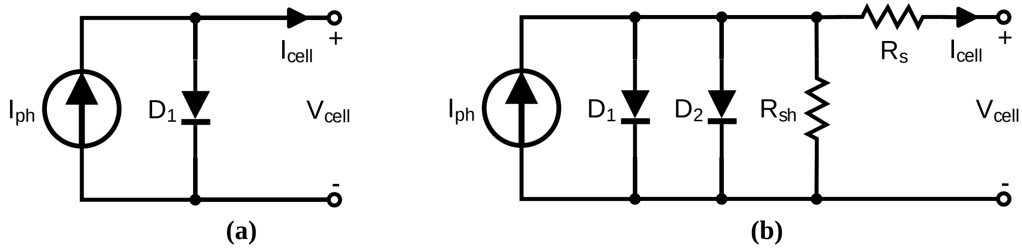

Figure 4.2: (a) Simple and (b) detailed model of a PV cell

From this above circuit, the relationship between the PV cell terminal current and voltage can be written as:

$$I_{cell} = I_{ph} - I_{01}\left(e^{\frac{V_{cell}+I_{cell}R_s}{n_1 V_T}} - 1\right) - I_{02}\left(e^{\frac{V_{cell}+I_{cell}R_s}{n_2 V_T}} - 1\right) - \frac{V_{cell} + I_{cell}R_s}{R_{sh,cell}} \quad (4.3)$$

Knowing the technological parameters of a PV cell, an electrical model can be made. The parameters can also be extracted from the measured I-V curves and fitted into the model. In general, both the short circuit current and the open circuit voltage of the PV cell depend on the specific technology, but while the voltage is more or less constant, the current can be scaled with the surface of the PV cell. Starting with the electrical model from Figure 4.2b, we can continue to make a model of the PV module.

4.3.2 PV Module Electrical Modeling

In most PV applications, voltages greater than a single PV cell voltage are required. It is therefore necessary to connect PV cells in series. A PV module consisting of ***N*** identical PV cells connected in series is shown in Figure 4.3.

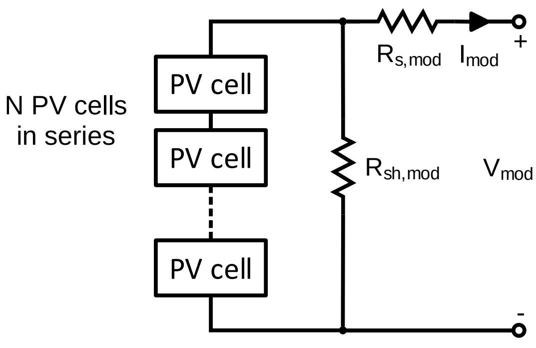

Figure 4.3: Model of a PV module

In the previous figure, $\boldsymbol{R_{s,mod}}$ is the series resistance of the PV module, while $\boldsymbol{R_{sh,mod}}$ is the shunt resistance of the module, added by interconnecting PV cells within the PV module. Usually, when modeling, the effect of $\boldsymbol{R_{sh,mod}}$ can be neglected.

For the following analysis a flexible thin-film PV module from Helianthos [4-3, 4-30], previously shown in Chapter 2 in Figure 2.7a, will be considered. This is a tandem junction (a-Si:H/μc-Si:H) PV module with close to 10% efficiency, normally consisting of 28 PV cells connected in series, each approximately 1 cm wide and having an arbitrarily length. The voltage can be scaled by changing the number of PV cells connected in series. The current, and hence the power, can be scaled by changing the surface area of the PV module. For the following analysis, the length of the PV module will be set to 1 m. The parameters of the model defined by Equation 4.3, not considering the effects of the secondary diode, are fitted to the stabilized PV cell data for standard test conditions (STC) provided by the manufacturer, and match well to the reported parameters [4-3]. The obtained model parameters corresponding to STC are presented in Table 4.1.

Table 4.1: Parameters of the considered PV cell

$\mathbf{I_{ph0}}$	$\mathbf{I_{01}}$	$\mathbf{n_1}$	$\mathbf{R_s}$	$\mathbf{R_{sh}}$
1.06 A	$1.4\text{x}10^{-5}$ A	4.6	18 mΩ	22.6 Ω

It should be noted that the fitted parameters of the model correspond to a single junction PV cell, even though the considered PV module is a double junction type. Nevertheless, the obtained I-V curve matches very well the measured I-V curve.

With the parameters being fitted, we can now obtain the electrical characteristic of the PV module. The I-V and P-V curves together with MPPs of the PV module for different irradiation levels $\boldsymbol{G}$ at 25°C are shown in Figure 4.4. We can see that the MPP voltage $\boldsymbol{V_{mpp}}$ does not change as much as MPP current $\boldsymbol{I_{mpp}}$ with irradiation level.

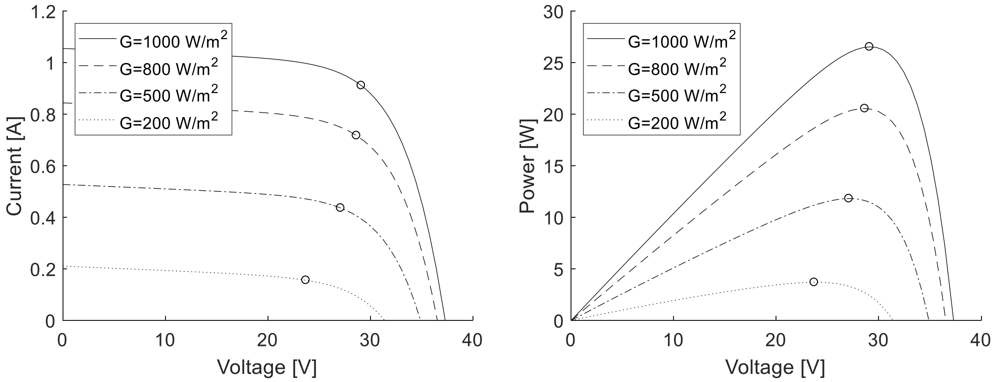

(a) **(b)**

Figure 4.4: (a) I-V and (b) P-V curves for a range of irradiation levels (T=25 °C)

As noted before, the operating temperature will affect the electrical response of the PV module via its temperature dependent parameters. This effect will be considered when determining the operating conditions. In general, as the temperature of the PV module increases, the open circuit voltage $\boldsymbol{V_{oc}}$ and the maximum power $\boldsymbol{P_{mpp}}$ decrease, while the $\boldsymbol{I_{sc}}$ slightly increase. The temperature coefficients for these parameters are usually given in datasheets for PV modules. Figure 4.5 shows the I-V and P-V characteristic for different operating temperatures $\boldsymbol{T}$.

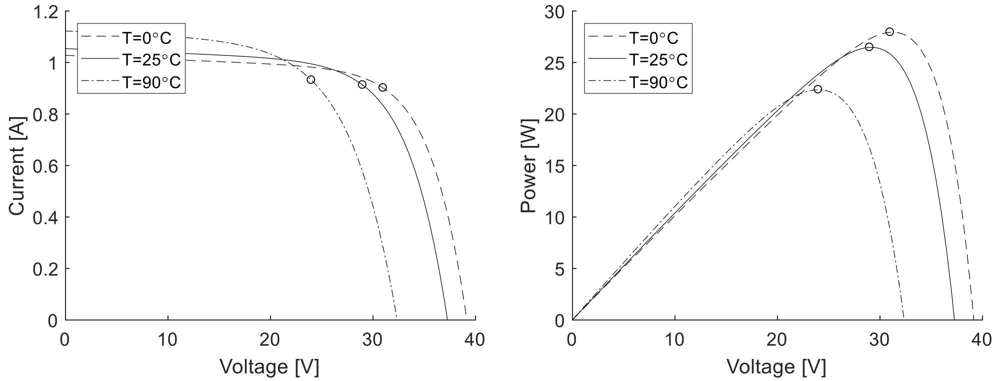

(a) **(b)**

Figure 4.5: (a) I-V and (b) P-V curves for a range of temperatures (G=1000 W/m²)

Looking at the Figure 4.5 we can see the range and maximum values of voltages and currents at the input of the converter. They can be anywhere within the area defined by I-V curves for all operating temperatures and irradiation levels. However, we normally expect the PV module to operate at maximum power point. It would be interesting to see the resulting normal operating area at the input of the converter. This is shown in Figure 4.6 where the shaded area shows the MPP positions for a range of temperature $\boldsymbol{T}$ and irradiation levels ($\boldsymbol{G}$=200-1000 W/m²).

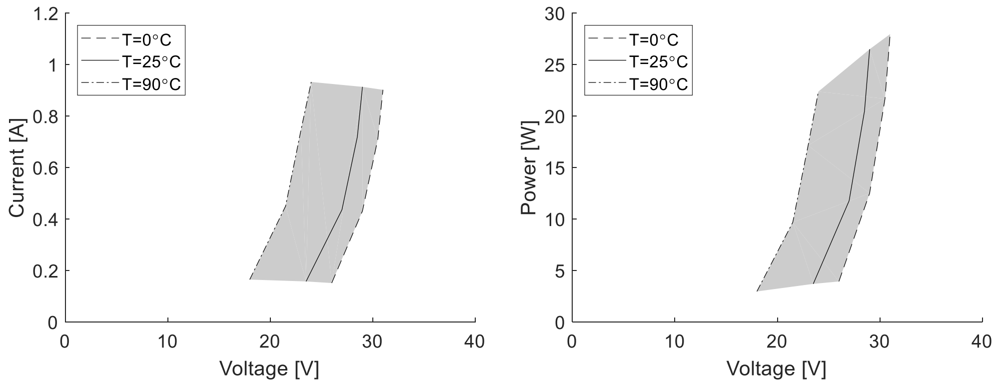

(a) **(b)**

Figure 4.6: Range of MPPs for a range of irradiation levels and temperatures

We can see that for the large range of temperature and irradiation levels, the operating voltage range of the PV module is rather narrow, assuming operation at MPP. Knowing the area in which the PV module is likely to operate, we can optimize the converter for the particular range of input voltages and currents.

Finally, let us consider the operation of a PV module with non-uniform temperature distribution. As it was discussed in Chapter 3, the integrated converter will introduce additional heat with its losses, and create a hot spot in the PV module, changing the electrical characteristic. The effect will depend on the shape of the hotspot. As an example, Figure 4.7 shows two possible orientations of a 10x5cm hotspot in the PV module. We can see that more PV sells are affected in Case A.

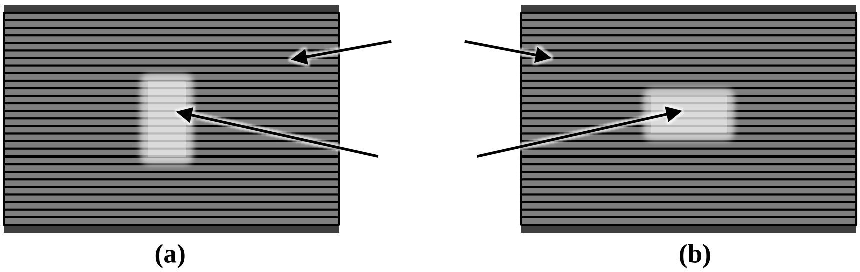

Figure 4.7: Considered orientations of the hotspot in PV module: (a) Case A, (b) Case B

As an example, let us assume the PV module temperature to be 25°C and the hotspot temperature to be 90°C. After testing our reference PV module, the resulting I-V curves are shown in Figure 4.8.

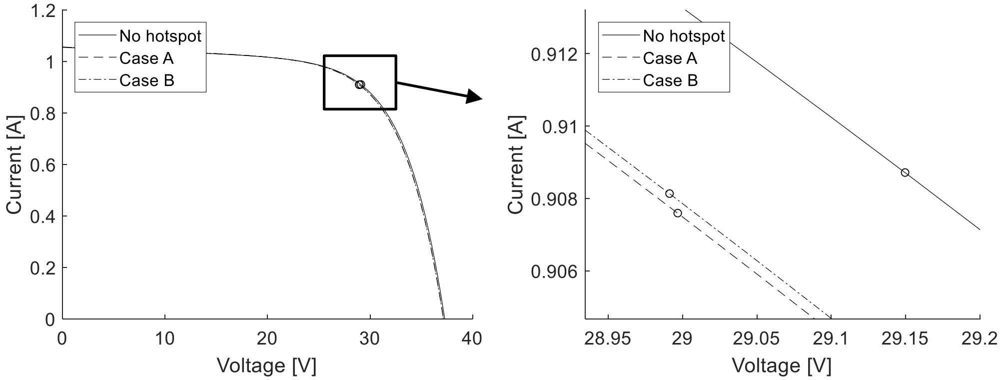

Figure 4.8: Effects of hotspot on PV module electrical characteristic

As it can be seen, the effect of the hotspot on the electrical characteristic is slightly smaller when less PV cells are affected, corresponding to the case B in Figure 4.7b. The output power of the PV module is in both cases reduces by approximately 0.5%. However, it should be noted that the temperature difference between the PV module and the hot spot will not have such a difference, as it will be shown in Chapter 6. In any case the effect of the hotspot on the electrical characteristic is extremely small and can be neglected in the electrical design. It will however affect the thermal design, as the (parts of the) cells with higher temperature operate with slightly higher losses.

4.3.3 PV System Electrical Modeling

The developed electrical model of the PV module can be used to make a PV system. The PV system model shown in Figure 4.9 is made of ***M*** parallel strings, each consisting of ***N*** parts connected in series and forming an array. Each module consists of a PV module and a converter. All strings are connected with each other over a common DC bus on the one side. On the other side of the DC bus is a central converter. Changing the number of strings ***M*** and number of converters in strings ***N***, it is possible to change the system configuration, from only parallel connected converters (***N***=1) to only serial connected converters (***M***=1). Resistance of the cables and connectors can also be modeled. Converters can be modeled as a simple power converter, with efficiency ***η*** dependent on the input power level or as a real circuit. It is also possible to change the operating conditions (temperature and irradiation) and characteristics of every module individually.

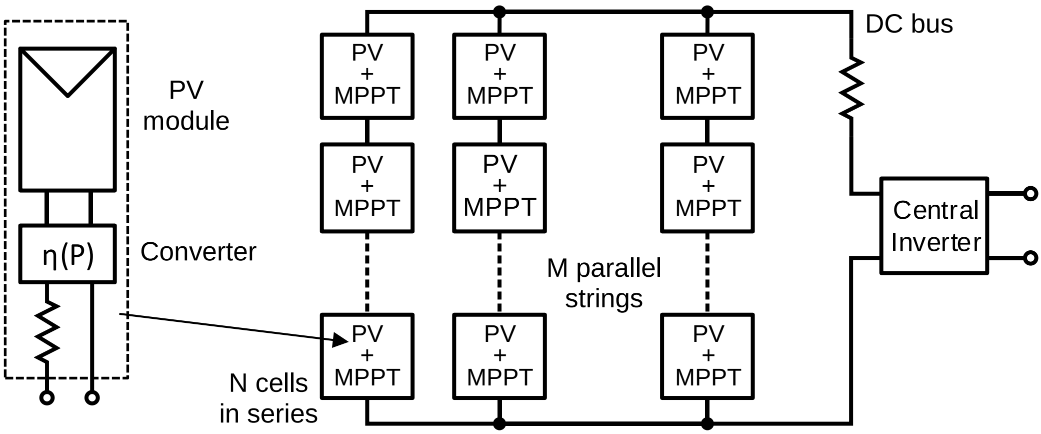

Figure 4.9: Electrical model of a DMPPT PV system

Using this model, different system configurations can be evaluated. By omitting the converters, it can be also used to test a traditional PV system. As an example, Figure 4.10a shows a shade distribution (caused by, for example, a nearby tree or building) over a PV array consisting of 20 of our reference PV modules defined by Figure 4.4 (with the total power of 530 W). When the shading occurs, the maximum output power in the traditional system is approximately 401 W assuming the operation at global maximum which cannot always be guaranteed (Figure 4.10b). In the (ideal) DMPPT system, the output power is around 472 W, an increase of 71 W or 18%.

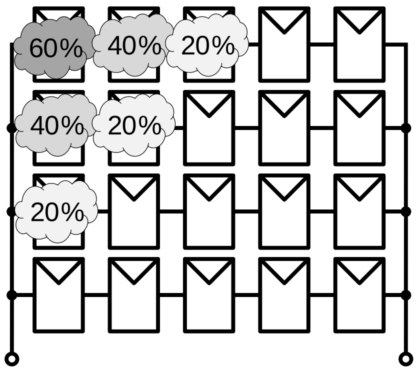

(a)

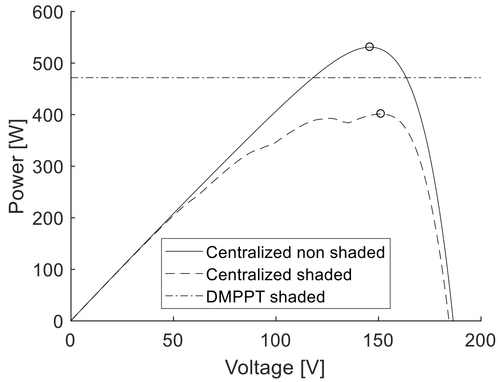

(b)

Figure 4.10: (a) Shaded PV array, (b) Power curves of the shaded PV array

4.3.4 Selecting DMPPT Architectures

In the following, two cases of the DMPPT system shown in Figure 4.9 will be considered:

- The array is formed with ***N*** converters connected in series, to form a string and then ***M*** strings connected in parallel,
- The array is formed with ***M*** converters connected in parallel only (***N***=1).

In both cases the converters are connected to a central inverter over a high voltage DC bus. In a typical small residential single-phase PV system, the rated input DC voltage for the inverter is 400 V.

In the first case, where we have array of ***N***x***M*** converters, the nominal output voltage of the converter is determined by the number of converters connected in series, ***N***. In the following, ***N*** will be set to 8, which will set the nominal output voltage to 50 V. This will be referred to as **low-output-voltage (LOV) converter**. Looking back at the typical operating range of the PV module, we can see that the LVO converter will normally have to boost the voltage. However, in case when one of the PV modules is shaded and operates at lower power, the adjoined converter will have to decrease the output voltage in order to keep the same string current, in some cases below the operating voltage of the PV module. Therefore the converter may also need to decrease the PV module voltage in this configuration.

In the second case, the output of the converter is directly connected to the DC bus, and that will set the specification for nominal output voltage to 400 V. This will be referred to as **high-output-voltage (HOV) converter**. Looking back again at the typical operating range of the PV module, we can see that the HVO converter will need to have high step-up ratio to boost the voltage to 400 V.

As discussed in Chapter 2, in the considered DMPPT systems the inverter does not perform MPPT as in traditional systems, but only sets the DC bus voltage by changing its input current. The converters on the other hand only perform MPPT without control of its output voltage. The output voltage will automatically change with the output current/load. This is illustrated in Figure 4.11 for the case of our reference electrical model of the PV module on Figure 4.4. The converter merely transforms the PV module from a non-linear power source (Figure 4.11a) to a constant power source (Figure 4.11b).

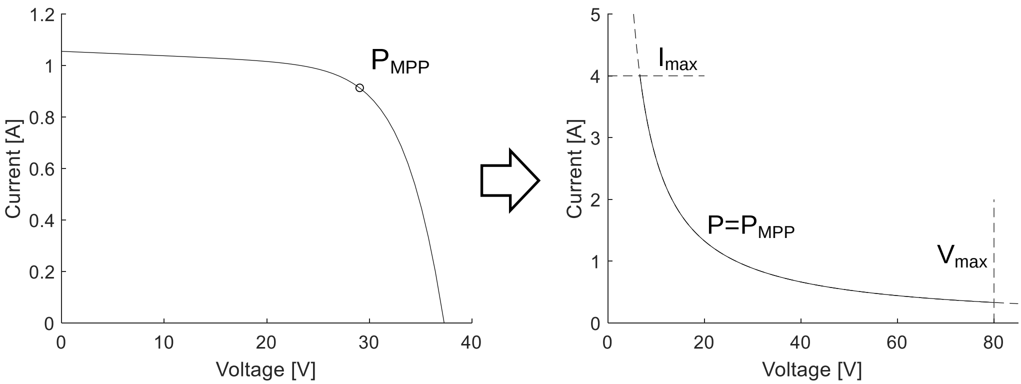

Figure 4.11: PV module integrated converter as a constant power source

However, although not controlling directly, the converter monitors its output voltage and current in order to keep them within the safe limits, as indicated in Figure 4.11b. The limits will depend on the used devices and components. The way the limiting is done will be presented in the later section when describing the converter control.

4.3.5 Converter Electrical Specifications

Based on the previous discussion, the selected electrical specifications for the LVO and HVO converter and our reference 1 m long PV module are shown in Table 4.2. Note that the current and power levels can be scaled and therefore fit within the limitations which will be set by thermal limits and the used components. Additionally, while the output of the HVO converter is set, the output of the LVO converter is variable, and will also be determined by the used devices.

Table 4.2: Converter Input/Output Electrical Specifications

V_{in_nom}	V_{in_max}	I_{in_max}	P_{in_max}	$V_{out\_nom\_LVO}$	$V_{out\_nom\_HVO}$
30 V	40 V	1 A	30 W	50 V	400 V

4.4 Converter Topology Selection

Knowing the electrical specifications for the PV module integrated converter, in the first place voltage, we can now continue with selecting the suitable topologies.

4.4.1 Topology Requirements

DMPPT is an efficient way to increase the PV system performance as long as the converters within the system meet certain requirements:

- If the components are to be integrated into the PCB, attention should be given to **components values and voltage/current ratings**. This usually implies small values of reactive components, which further implies high operating frequency. Additional level of integration can be achieved if several components can be integrated into one structure.
- **Efficiency** should be high enough or else the whole concept of DMPPT becomes pointless. Input and output voltage ranges of the converter will depend on the used system architecture, but in general they vary in broad ranges. Since the power from PV modules varies over the daytime, from 0% to 100%, it is important to maximize the efficiency over the whole range of input power.
- For the converters that will operate under harsh outdoor conditions, special attention should be given to the **reliability and fault tolerance**. For example certain topologies could be more sensitive to change in components values due to the temperature cycling or aging. PV modules are simple devices and to match their lifetime and reliability with a complicated device like a converter, robust topologies are required.
- System stability will be determined by the chosen **control** strategy. Using additional switches, variable operating frequency or special control strategies can complicate the converter design and increase the cost. Different control algorithms will have different effect on the overall system stability. This should be considered together with the design of the central inverter.
- **Cost** should be also considered. The additional elements added to improve the performance of the converter will increase the cost, although, this can be justified by increased efficiency and decreased payback time.
- Since the converter is indirectly connected to an AC grid, attention should be given to generation and susceptibility to **unwanted electromagnetic generation**. Industry standards and limits can prevent implementation of certain topologies and control techniques. Moreover, PV systems contain large area networks of PV modules and length of the interconnections is significant. This makes the PV systems susceptible to atmospheric discharges which can induce sufficiently high voltages that can damage or degrade the converters. Additional attention is required if transformerless designs are employed since strong ground currents might occur [4-4].

4.4.2 Topology Classification and Comparison

Depending on the DC bus voltage, one type of topologies can have advantages over the other, for example, for converters connected in parallel over a common high-voltage DC bus, high step-up topologies are required. If the DC bus voltage is not defined, all converters can be classified into two groups corresponding to already selected DMPPT architectures and the LOV and HOV converter respectively:

- Low step-up/step-down DC/DC converters suitable for parallel connected strings of series connected converters, for high voltage DC bus, or for parallel connected converters for low voltage DC bus,
- High step-up DC/DC converters suitable for the parallel connection to the common high voltage DC bus.

It is difficult, if not impossible, to find a topology which will achieve the best results concerning all the requirements mentioned before. Therefore, each topology should be evaluated on the number of desired properties. Different desired properties should be defined together with its weight factors. Different values should be assigned to weight factors, since some requirements could be more important than others, for example, possibility to use certain integration technology could be more important than the cost of implementation.

There are several solutions that consider converters that are not processing the whole power from the PV modules to achieve distributed MPP tracking, and using this approach, flat efficiency curve can be achieved over the whole range of input power. On the other side, this approach usually requires special architecture with additional power lines, can cause unstable string voltage or it does not fully isolate the PV module from the rest of the system from power processing point of view. Also, they are most effective in well positioned PV systems, when the PV modules are operating close to their normal operating conditions, but in the operating conditions of small residential PV systems where the whole PV module could easily be shaded completely, the converter should be designed to process the whole PV module power. Moreover, in some solutions the communication between the converters is mandatory.

Therefore, only conventional DMPPT approaches will be considered, with converters that process the whole power from the PV module. Since the efficiency is important, only transformerless topologies will be investigated. All considered topologies can be evaluated on the basis of multiple desired properties:

- Integrability:
  - Is there a possibility to use advanced integration technologies?
  - What are the required components values and voltage/current ratings?
  - Is there a possibility to integrate the components into PCB?
  - Is there a possibility to combine several components into one?

- Electrical performance:
  - What is the maximum possible efficiency, and does the topology has a flat efficiency curve?
  - What are the input/output voltage and current ranges and limits?
  - Is it suitable for high switching frequency?
  - Is the topology suitable for the low power level of a single PV module?
- Reliability:
  - What is the component count?
  - Is the topology fault tolerant and can it fail in a predictable manner?
  - What are the voltage and current stresses imposed on components?
  - Is the topology susceptible to effects such as overload, temperature changes, aging, or component tolerances?
  - Is the topology susceptible to generating unwanted signals?
  - Is the topology susceptible to interference?
- Cost:
  - Does the topology require special, expensive components?
  - Does the topology require additional input/output filtering and if so what are the values of the filter element?
  - Is there a large number of (energy storage) components?
- Control:
  - Is the complexity of the control circuit low?
  - Does the topology require low number of sensors?
  - Is the fixed-frequency operation possible?
  - Is it possible to implement fixed switching frequency operation?
  - Is the control algorithm simple?

In the following, several candidates for the converter topologies will be discussed based on abovementioned criteria, for both LOV and HOV converters.

4.4.3 Low Output Voltage Topologies

In order to change the PV module voltage from approximately 30 V around MPP to 50 V under normal operation, a step-up topology is required for the LOV converter. Although not absolutely required, ability to step-down the voltage might be useful in some situations. Otherwise, the converter should be bypassed, which is easy to achieve with an anti-parallel diode connected to its output. All topologies that can boost the input voltage from the PV module can be used, and in the following some high efficient non-isolated candidates will be considered.

ZCT Boost Converter

An ordinary boost converter is a proven topology, however large switching losses can prevent its use at high switching frequencies. Adding an auxiliary commutation circuit to the boost converter an active zero current transition (ZCT) boost converter is obtained [4-5]. The auxiliary commutation circuit consists of an additional switch, a capacitor and an inductor (Figure 4.12). Using this approach, turn-off losses of the main switch can be eliminated.

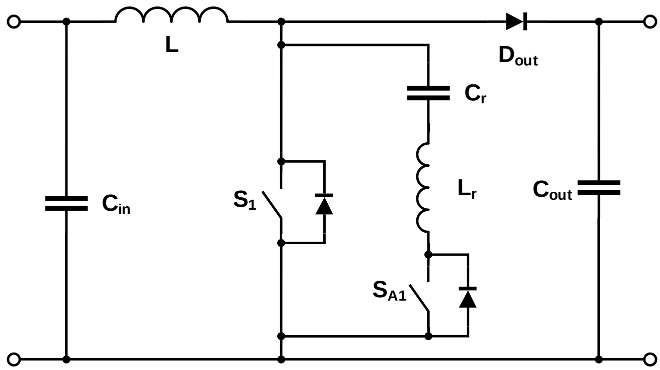

Figure 4.12: ZCT boost converter [4-5]

The turn-on of the main switch occurs at zero current and the output diode reverse-recovery problem is alleviated due to the boundary conduction mode (CDCM). The auxiliary commutation circuits provide ZCT when the main switch turns off. However, variable frequency control is mandatory for this converter. Summarized characteristics of this topology are as follows:

- Integrability: Large values of the resonant inductor, such as those reported, can prevent integration into PV module. However, increasing the switching frequency, values of the resonant capacitor and inductor can be reduced.
- Performance: Voltage and current levels are similar as for the conventional boost converter, but the efficiency is increased. As a result, the efficiency improvement reported in [4-5] is 1.7% (from 94.2% to 95.9%) compared to the conventional boost converter. However, for low output voltage, losses in the output diode will still be dominant.
- Reliability: This is a modified boost topology which has proven as a reliable and robust. Moreover, the auxiliary circuit is not in the signal path.
- Cost: The cost of added components is not high; the reactive components can have low values, while the power level of the auxiliary switch is several times lower than the power level of the main switch.
- Control: Additional control circuit is required for the generation of the auxiliary switch signals. Variable frequency control is mandatory for this converter, since CDCM mode was considered. It could be possible to implement fixed switching frequency operation with DCM, which would make the filter design and control easier.

ZVS Boost Converter

In some resonant converters with an auxiliary switch, the main switch can achieve soft-switching but the auxiliary switch is hard switched which can negate the benefits of soft-switching. A variant of a soft-switching boost converter with an auxiliary switch and a resonant circuit is proposed in [4-6]. The resonant circuit contains a resonant inductor, two resonant capacitors, two diodes and an auxiliary switch. The resonant circuit makes partial resonant path for the main switch to perform soft-switching at zero voltage. Moreover, the auxiliary switch achieves soft-switching. Figure 4.13 shows the proposed converter topology and the auxiliary circuit.

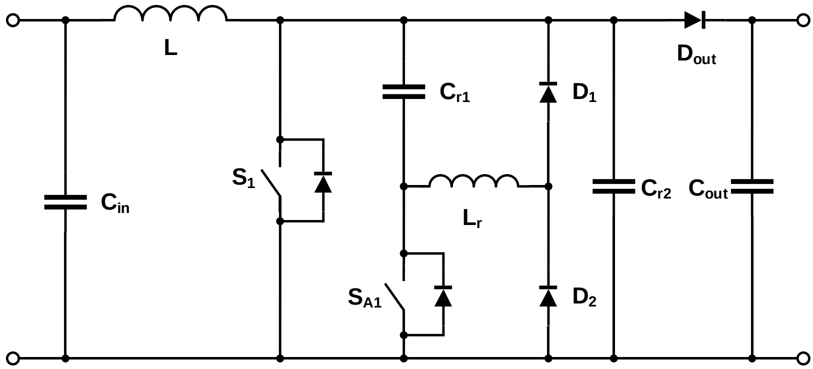

Figure 4.13: ZVS boost converter [4-6]

Summarized, the characteristics of this topology are:

- Integrability: The reactive components in the auxiliary circuit have low values. The rest of the components have the same values as in the case of a conventional converter.
- Performance: Compared with the conventional boost converter, the proposed topology achieves higher step-up ratio for the same duty cycle range. The achieved efficiency is flat from 20% of output load to the full load, with the maximum efficiency of over 96%, an increase of 5% in efficiency over the conventional hard switched boost, as reported in [4-6].
- Reliability: Again, a modified boost topology should be reliable and robust. Moreover, the auxiliary circuit is not in the signal path.
- Cost: The topology requires additional passive components and an additional switch when compared to the ordinary boost converter, which will increase the cost.
- Control: Additional control circuit is required for the generation of the auxiliary switch signal and to delay the main switch signal. Also, an additional sensor for the auxiliary circuit voltage is required. Constant switching frequency is used which makes the control and filtering easier.

Another soft-switching design for the boost converter is presented in [4-7] and shown in Figure 4.14. Within the main converter, we can see the auxiliary boost converter in charge of recycling the energy from the capacitor $\boldsymbol{C_r}$. Almost all designs with soft-switching techniques applied to the PWM converters are subject to either high voltage stresses or high current stresses, or both. In the proposed circuit, the switches are subject to same voltage and current stresses as those in conventional designs. Therefore, the advantages of the conventional PWM and the soft-switching resonant techniques are combined together.

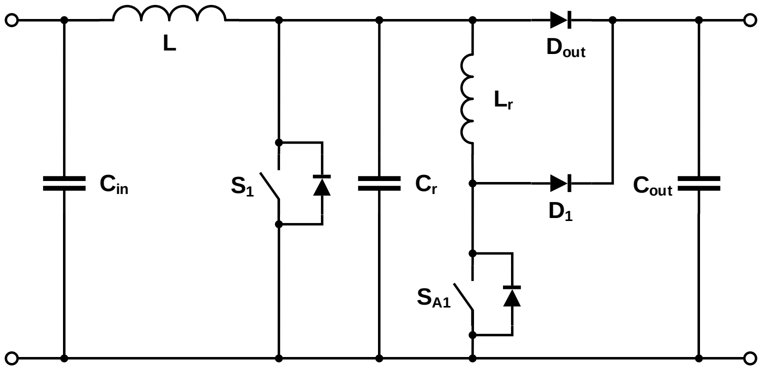

Figure 4.14: ZVS boost converter [4-7]

Summarized, the characteristics of this topology are:

- Performance: Both the active and passive switch operate with zero-voltage switching. Soft-switching operation can be easily maintained for wide Voltage and load range. The auxiliary resonant network only handles a small fraction (typically less than 10%) of the total output power.
- Integrability: Reactive components in the auxiliary circuit have low values. The rest of the components have the same values as in the case of conventional converter.
- Reliability: The basic boost circuit has remained almost the same, and the additional network is not directly on the signal path. Both switches are subject to same voltage and current stresses as those in their PWM counterparts. Voltage and current stresses are lower compared to other soft-switching solutions.
- Cost: The addition of an auxiliary switch, an inductor, and a diode can increase the cost of the converter.
- Control: Additional control circuit is required for the generation of the auxiliary switch signal and to delay the main switch signal. The additional sensor for the auxiliary circuit voltage is not required. The switching frequency is constant. As in the previous case, constant switching frequency PWM is used which makes the control easier.

Soft-Switching Boost Converter with SARC

A soft-switching boost converter using a simple auxiliary resonant circuit, which is composed of an auxiliary switch, diodes, a resonant inductor, and a resonant capacitor, is presented in [4-8] (Figure 4.15). The presented topology includes a simple auxiliary resonant circuit (SARC) and all of the switching devices perform soft-switching under zero-voltage and zero-current conditions eliminating turn-on and turn-off of losses.

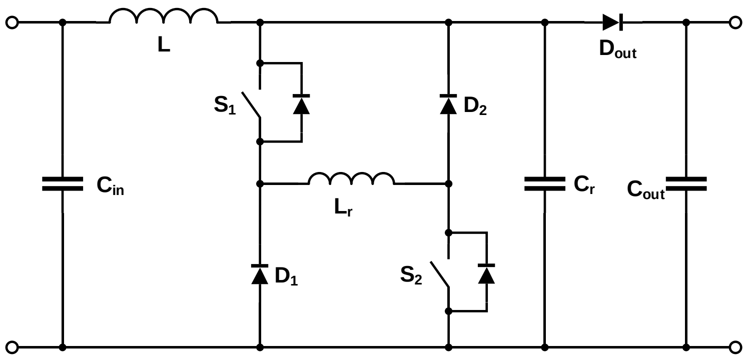

Figure 4.15: ZVS boost converter [4-8]

Summarized characteristics of this topology are:

- Performance: All of the switching devices in this topology achieved ZCS and ZVS with the resonant inductor and capacitor at turn/off, therefore, the switching losses were reduced. The reported efficiency exceeds 96%.
- Integrability: The resonant inductor and resonant capacitor have small values which can allow for them to be integrated into the PV module. Since the operating frequency is constant, filter design is simpler.
- Reliability: Since the voltage stress of the switches is reduced, the lifetime of the converter can be extended when compared to other topologies with resonant networks.
- Cost: Compared to the ordinary boost converter, and additional switching elements with similar ratings as the main switch are required, increasing the cost.
- Control: This topology is easy to control since both switches use the same PWM signal. No additional sensors have to be implemented, and for the MPPT control, input current and input/output voltage sensing is sufficient.

Tri-Mode Cascaded Buck-Boost Converter

A simple approach is presented in [4-9] based on previous results from a topology study presented in [4-10]. The designed converter presents a cascaded buck and boost topology sharing the same inductor, as shown in Figure 4.16. As it was shown in [4-10], among basic converter topologies, buck and boost converters are better solutions for MPPT realization, and this was used in the design presented in [4-9]. The main reason why this topology is preferred over the other simple one switch topologies, such as buckboost, Ćuk or zeta, are lower voltage and current stresses on components. Moreover, the topology can be used as a basis for high step-up conversion if the inductor is replaced with a transformer.

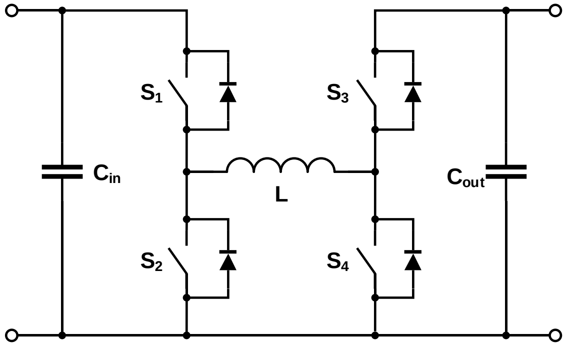

Figure 4.16: Three-mode cascaded buck-boost converter [4-9]

In this approach, depending on the input and output voltage, only one converter will operate at the time, while the switches in the other converter will be turned on or off to pass the current. If the PV module can operate close to its MPP without assistance of the converter, the circuit can operate in pass-through mode, directly connecting input and output port of the converter. Summarized, the characteristics of the topology are:

- Performance: The reported efficiency exceeds 95% for most of its operating range. Owing to synchronous rectification the achieved efficiency is relatively high considering that hard-switching was used.
- Integrability: The presented topology is based on simple buck and boost converters and with small reactive components the PV module integration should be viable at high switching frequencies. Since the input and output currents can be discontinuous, depending on the mode of operation, attention should be given to filtering.
- Reliability: High reliability can be expected since the simple boost and buck topologies are used. Also, at a time, only one half of the converter is active.
- Cost: High number of switches and their drivers could increase the cost. This can be offset by low number of magnetic components.
- Control: This topology is relatively easy to control since simple buck and boost topologies were used. However, in the synchronous design there are four switches, and four control signals with accompanying drivers are required, with dead-time control and DCM detection.

4.4.4 High Step-Up Topologies

If we want to connect a single PV module to a conventional central inverter, we need a high gain converter to boost the usually low voltage from the module to the high input voltage. Since the nominal PV module voltage is 30 V, and the required input voltage for the inverter is 400 V, a high-gain topology is required. Using the transformer and adjusting the transfer ratio, high gain can be achieved, but on the other hand, transformer can increase the cost and reduce the efficiency. Transformerless topologies can achieve higher efficiency, but additional problems arise when there is no galvanic isolation between the PV module and the grid [4-4], and additional measures have to be taken.

There is a large number of topologies which can achieve high gain, low cost and high efficiency performance in the PV grid-connected applications. All this requirements can be achieved in different ways, for example using coupled inductors, switched-capacitor, or their combinations [4-11]. An extensive list of step-up converters is given in [4-12]. In the following some high efficient non-isolated candidates will be considered.

High Step-Up Converter with Switched Capacitor

A capacitor can be used to act as an additional voltage source to achieve high step-up conversion. A switched-capacitor-based step-up resonant converter is proposed in [4-13] and shown in Figure 4.17. Using the switched-capacitor basic cell, input voltage can be increased and by adding a different number of switched-capacitor cells, different output voltage conversion ratios can be obtained. The voltage conversion ratio from 2 to any whole number can therefore be generated by these switching-capacitor techniques. A resonant tank is used to assist in zero-current switching and to reduce current spikes, which are typical for classical switched-capacitor topologies. Both high frequency operations and high efficiency are possible.

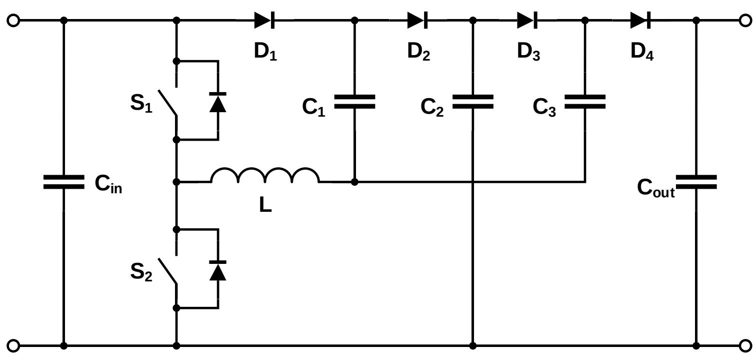

Figure 4.17: Triple-mode switched-capacitor resonant converter [4-13]

Summarized, the characteristics of the topology are:

- Integrability: Inductor and capacitor values are relatively small, especially inductance, and with the increase of switching frequency, reactive components can have low enough values to apply integration techniques. There is only one inductor to be integrated.
- Performance: All the switching devices inside the circuit are operated under zero-current switching condition by the resonance of the switched capacitors and a very small resonant inductor. An advantage is relatively fixed transfer ratio which varies little with the load changes. The reported efficiency is over 94%. Moreover, the waveforms are clean with no serious parasitic oscillations. The output current is discontinuous, therefore, attention should be given to filtering.
- Reliability: A large number of components in the power path is required for high step-up ratio, which can influence the converter reliability.
- Cost: Large number of switched capacitor cells required for high step-up ratio may increase the cost. Since the operating frequency is fixed, filter design is simpler.
- Control: The control is relatively simple, with fixed operating frequency, and there is no need for the additional control signals, since there are no additional switches in the resonant network. Because of the relatively fixed gain, control loop for the output voltage regulation is not necessary.

High Step-Up Converter with Inductor and Switched Capacitor

A switched-capacitor converter and a boost converter can be combined together to obtain a step-less voltage gain. A family of single-switch DC/DC converters with high voltage gain is proposed in [4-14]. High voltage gain converters from this group of topologies are based on the switched capacitor cell illustrated in Figure 4.18a. Figure 4.18b shows one example of this type of topology.

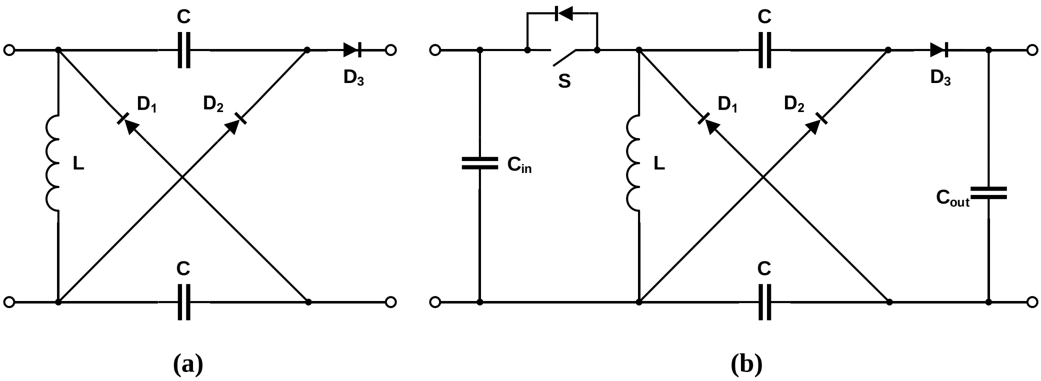

Figure 4.18: Zeta-derived converter with high voltage gain [4-14]

Other advantages of the proposed topology include lower voltage stress on the switching devices, simple structure and simple control. Moreover, the reduced voltage stress on the diodes allows using Schottky diodes for alleviating the reverse-recovery current problem, as well as decreasing the switching and conduction losses. Summarized, the characteristics of the topology are:

- Integrability: The values of reactive component will depend on the specific application. For the low power high frequency solutions, values can be sufficiently low, allowing the integration into PV module.
- Performance: Reduced voltage stress on the switching devices allows the use of low-voltage rated MOSFETs with lower R_{ds}, as well as enabling the use of Schottky diodes for alleviating the reverse-recovery current problem. Therefore, the circuit efficiency can be improved by reducing both the conduction and switching losses. The reported efficiencies are above 90%. The output current is discontinuous, therefore, attention should be given to filtering.
- Reliability: The topology contains a single switch structure with low stresses on the components, but large number of switched capacitor cell required for high step-up ratio may decrease reliability.
- Cost: Large number of switched capacitor cells required for high step-up ratio will significantly increase the cost.
- Control: This type of converter can be controlled with conventional PWM techniques at constant switching frequency. There is only one switching component to be controlled.

High Step-Up Converters with Coupled Inductors and Switched Capacitor

Coupled inductors and the switched-capacitors can be combined to derive converters with high voltage gain [4-15], [4-16]. An example is shown in Figure 4.19.

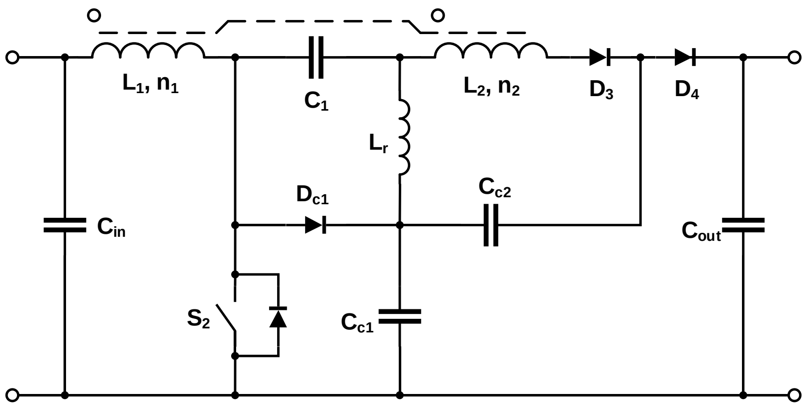

Figure 4.19: High step-up boost converter with coupled inductor and switched-capacitor [4-16]

A wide range of voltage transfer ratio can be obtained using these topologies. Additionally, in this particular approach, the output diode reverse-recovery problem is alleviated with the leakage inductance of the coupled inductor. ZCS turn-on of the switch is achieved to reduce the switching losses. The leakage energy is recycled and the voltage ringing on the MOSFET is suppressed by the additional clamping circuit. The energy stored in the clamp capacitor is transferred to the load by the resonance circuit. Summarized, the characteristics of the topology are:

- Integrability: The required capacitance and inductance values can be reduced at high switching frequencies, but large number of energy storage components may prevent integrability.
- Performance: The reported efficiency is relatively flat and reaches above 96%.
- Reliability: Owing to zero voltage switching and voltage and clamping, the stress on the devices is low.
- Cost: The topology is relatively simple, with addition of few components when compared to standard coupled inductors topologies.
- Control: There is only one switching element in the circuit and conventional PWM techniques can be used. The switching frequency can be constant.

Boost Converter with Coupled Inductors

A family of high-efficiency, high step-up, clamp-mode coupled inductor topologies is presented in [4-17]. A boost version of the converter is shown in Figure 4.20. The operation of the presented topology is similar to that of its active-clamp counterparts, but the new approach utilizes one additional diode instead of an active switch in order to realize the clamp function. By adding a small clamp capacitor, the leakage energy is recovered and the switch voltage stress is significantly reduced. Utilizing the leakage inductor to control the slew rate of the output current dramatically alleviates the reverse-recovery problem of the output rectifier. An improved version is shown in [4-18], implementing soft-switching, but with increased complexity. Another example of a high step-up ZVS boost converter with coupled inductors operating on the same principles is presented in [4-19].

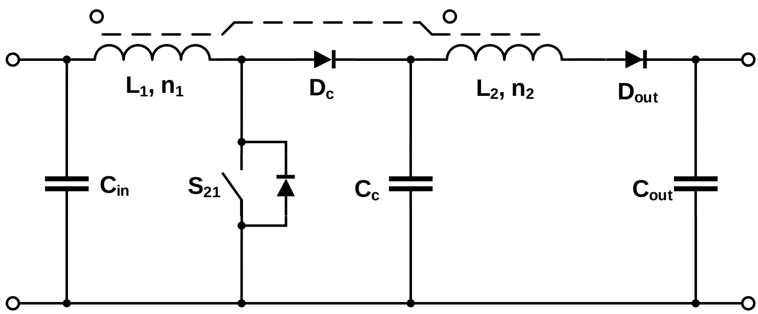

Figure 4.20: Boost converter with coupled inductors [4-17]

Summarized, the characteristics of the topology are:

- Integrability: There are only two inductors, and depending on the switching frequency, small values can be achieved. Large values for the output capacitors may be expected due to discontinuous diode current.
- Performance: The leakage energy is recycled and the reverse recovery effects are reduced leading to higher efficiencies. However the switch is hard-switched. The reported efficiency is above 93%. Control of the current slew rate of the output diode reduces reverse recovery problems.
- Reliability: Due to passive clamping, the stress on the switch is reduced, when compared to the ordinary boost converter with coupled inductors.
- Cost: Low cost is expected due to the minimum number of added components, when compared to the ordinary boost converter. Constant switching frequency control can be used, making the control and filter design easier.
- Control: The control is the same as for the ordinary boost converter, with a constant switching frequency PWM signal.

High Step-Up Interleaved Boost Converter

The previously described topologies have a single-phase design. The interleaved structures can be used to increase the power level, minimize the current ripple, reduce the passive component size and improve the transient response. Moreover, interleaving will distribute the losses over more components. A high step-up interleaved boost converter is proposed by inserting the switched-capacitors into the conventional boost converter [4-20] and is shown in Figure 4.21. High step-up ratio can be realized using the switched-capacitor cell. The main disadvantage is that the power devices operate under hard switching condition.

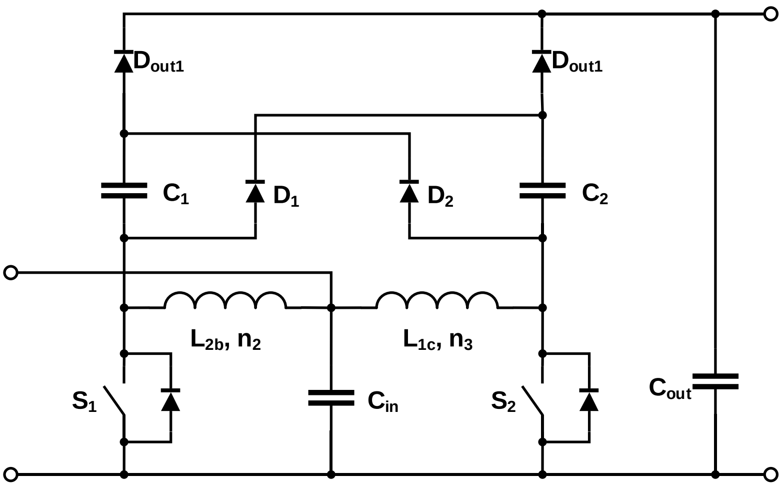

Figure 4.21: Interleaved boost converter with high step-up ratio [4-20]

Summarized, the characteristics of the topology are:

- Integrability: As with standard boost converter, only the inductors are critical. With high enough switching frequency, small values for the inductors can be achieved, allowing the PV module integration. Since interleaving is used, small values for the capacitors are expected.
- Performance: Two separate inductors can be coupled to optimize the magnetic core and to improve the magnetic behavior. The reported efficiency is above 95%.
- Reliability: Proposed topology allows operation with large step-up conversions ratio, while maintaining low voltage and current stress in the switches and diodes. Since interleaving is used, the power losses can be spread over more components and larger area.
- Cost: The topology is relatively simple and, compared with conventional interleaved boost, only two additional diodes and capacitors are required. Interleaving allows for smaller input and output filter components.
- Control: As in all interleaved topologies, phase shifted signals are required, usually achieved with digital control. Apart from that, an ordinary PWM control is required.

High Step-Up Converter with WCCIs

A high step-up interleaved DC/DC converter with winding-cross-coupled-inductors (WCCIs) is proposed in [4-21]. Compared to the ordinary boost converter with coupled inductors, a couple of third windings is added and inserted into the opposite phases, hence the name (Figure 4.22). In this approach the active clamp scheme was applied to recycle the leakage energy and to suppress voltage spikes.

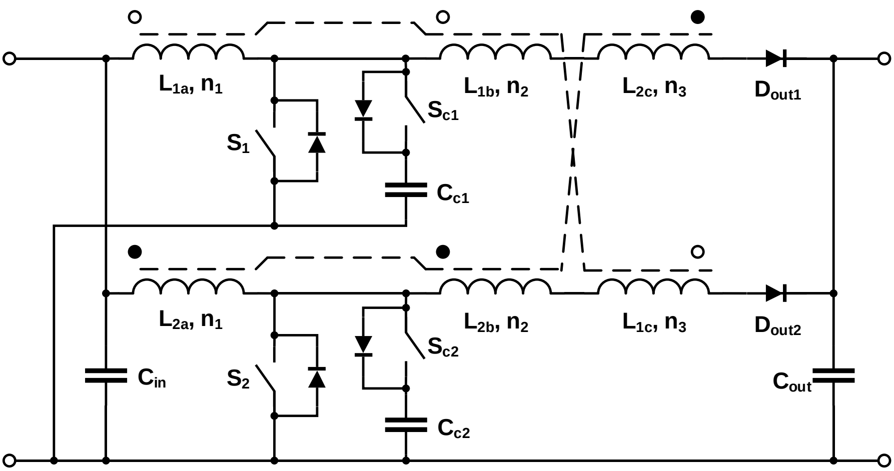

Figure 4.22: High step-up ZVS interleaved boost converter with WCCIs and active-clamp circuit [4-21]

With the active clamp circuits, ZVS performance of the main switches and the auxiliary switches are achieved during the whole switching transition. The output diode reverse-recovery problem is alleviated by the leakage inductance to minimize the reverse-recovery losses. The active clamp scheme can be replaced with a passive lossless clamp scheme [4-22]. The derived interleaved boost converter with passive-lossless clamp circuits is shown in Figure 4.23. ZCS turn-on can be realized and the clamp circuits are simple but effective to reduce the circuit complexity and the converter cost.

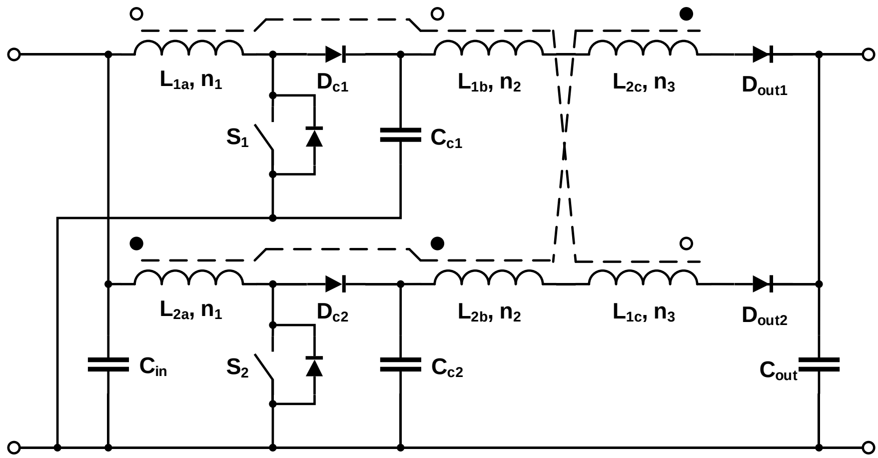

Figure 4.23: High step-up interleaved boost converter with WCCIs and passive-lossless clamp circuit [4-22]

Summarized, the characteristics of the topology are:

- Integrability: Relatively large number of coupled inductors could be difficult to implement using integration technologies. For low power applications, the required inductances can be made sufficiently small.
- Performance: Reported efficiency for the converter with WCCIs is above 95%. The transformer function of the WCCIs is employed to extend the voltage gain, minimize the power device peak current and reduce the switch voltage stresses. Interleaving allows for lower values for the input and output capacitors.
- Reliability: Proposed topology allows operation with large step-up conversions ratio, while maintaining low voltage and current stress in the switches and diodes. Interleaving allows for lower power loss density.
- Cost: Small number of switching components is required in case of the passive clamp.
- Control: Topologies with cross-coupled inductors require relatively complex control that can be achieved with DSPs, since complex computations have to be performed. On the other side, in the version with passive clamp circuit, there are only two low-side switches.

4.4.5 Topology Selection

The topologies listed and analyzed in the previous section can now be compared based on the previously mentioned criteria. When it comes to PV module integration, not all criteria have the same priority, and as a consequence, they will have different weight factors and will favor particular properties in different topologies:

- Integrability, or the possibility for PV module integration, has been given the highest importance. This will favor topologies with minimum number of energy storage components and possibility for their reduction by increasing the switching frequency. This criterion is the link between the technological and the electrical design. The maximum number of points in this category is 8.
- Performance, or the possibility for achieving high efficiency, is important to keep the DMPPT concept viable. With hindsight from Chapter 5, this will favor topologies suitable for novel switching devices and with low current ripple that will enable alternative magnetic materials. This criterion is the link between the technological and the thermal design. The maximum number of points in this category is 6.
- Reliability will favor proven robust topologies with small stress on switch components, and power loss distributed over more components, such as in interleaved designs. This criterion is the link between the electrical and thermal design. The maximum number of points in this category is 6.
- Cost is important but not critical considering that PV modules are significantly more expensive (per W) than power converters. It will favor simple topologies, with simple control and small component count. It is difficult to estimate, but with economies of scale and by removing pack layers, there is room for paying premium to achieve other goals such as high efficiency. The maximum number of points in this category is 4.
- Control is the least critical criterion, since with modern microcontrollers and DSPs with their powerful PWM peripherals, complicated control algorithms and high precision PWM can easily be implemented. The maximum number of points in this category is 2.

All the considered topologies are listed in Table 4.3 with their respective grades for each criterion. As the result, the selected topologies for the PV module integrated converter that will be analyzed in the following are:

- Cascaded buck-boost topology for LOV converter,
- Boost converter with coupled inductors and passive clamp for HOV converter.

Both topologies represent proven and robust designs, with minimum number of energy storage components. As for the potential drawbacks, LOV converter will require somewhat complicated control, while the main challenge with HOV converter will be maximizing the efficiency.

Table 4.3: Overview of the topologies

Converter topology	Ref.	Integrability (0-8)	Performance (0-6)	Reliability (0-6)	Cost (0-4)	Control (0-2)	TOTAL
ZCS boost converter	[4-5]	6	4	6	4	1	21
ZVS boost converter (1)	[4-6]	4	5	3	1	1	14
ZVS boost converter (2)	[4-7]	5	5	4	2	1	17
Soft-switching boost converter with SARC	[4-8]	4	5	4	2	2	17
Three-mode buck-boost converter	[4-9]	8	6	5	3	0	**22**
Boost converter with switched capacitor	[4-13]	7	4	4	2	1	18
Boost converter with inductor and switched capacitor	[4-14]	5	4	4	2	2	17
Boost converter with coupled inductors and switched capacitor	[4-15] [4-16]	6	5	4	3	2	20
Boost converter with coupled inductors and passive clamp	[4-17]	7	4	6	4	2	23
High step-up interleaved boost converter	[4-20]	7	5	5	2	1	20
Boost converter with WCCIs and active clamp	[4-22]	4	6	5	1	0	16
Boost converter with WCCIs and passive clamp	[4-21]	4	5	6	1	1	17

4.5 Electrical Design of the LOV and HOV Converter

In this section, a detailed design of the selected topologies will be conducted. As a result, a set of equations required to determine the values of the components will be defined. The majority of input parameters for the electrical design are already determined by the chosen PV module and DMPPT architecture. The remaining parameters, among which the switching frequency is most important, will come from Chapter 7, when we completely design the converter.

The main and unique part of the LOV and HOV converters is their power stage. But before we start analyzing the power stage, a few notes on the rest of the converter circuit. It was already defined in the beginning of the chapter and in Figure 4.1 noting that it stays the same for both LOV and HOV converter. The rest of the converter circuit is not critical for neither of the design areas, from the hardware point of view. The complete schematic with more details is presented in Appendix A. However, the control part and its software are important for proper converter operation and it will be described in this section.

4.5.1 Converter Control

The central part in charge for the operation of the converter is its control circuit. Here, the converter control is based on a microcontroller unit (MCU). Digital control in power management has slowly gained dominance over traditional analog control, inherently offering immense flexibility in design and consistence in operation [4-23]. Moreover, modern MCUs and digital signal processors (DSPs) have specialized stages for generating PWM driving signals, incorporating not only multi-phase PWM signal generation but also additional features such as protection, pattern generation, and duty cycle and dead time control with sub-ns precision. This is especially important for wide band gap devices which enable switching frequencies in MHz range which will be introduced in Chapter 5.

The converter control performs MPPT in order to keep the PV module at its maximum output power under all circumstances. To accomplish this, it is necessary and only possible to change the PV module load impedance. Therefore, MPPT is based on the load profile adjustment under varying environmental conditions. Many MPPT methods have been developed and implemented and they all vary in control strategy complexity, speed, implementation, cost and other respects [4-24].

For the PV module integrated converter here, an ordinary perturb-and-observe (P&O) MPPT was chosen [4-25], being one of the most commonly used method due to its ease of implementation. The method involves a perturbation in converter duty cycle ***D***, and observation of the PV module output power. Depending on the change in power caused by the perturbation, the decision is made for the next perturbation. This algorithm is illustrated in Figure 4.24. Two sensors are needed for this technique, one for voltage and one for current, since the power has to be computed.

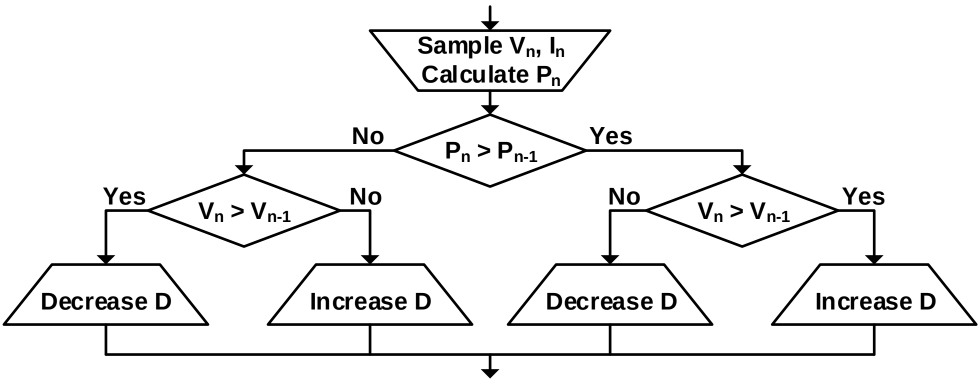

Figure 4.24: P&O MPPT algorithm

There is a trade-off between the tracking speed and the tracking accuracy, in the selection of the perturbation step size. A larger step will allow for faster tracking of the maximum power point, when sudden changes in operational conditions occur. But, when the MPP is reached, a large step size will increase oscillations around the MPP, decreasing the efficiency, as it will be shown. On the other hand, the speed at which the perturbation performed is limited by the transient response of the converter.

As previously noted, the control part is in charge only for the MPPT algorithm, there is no feedback loop for the output voltage. However, the input and output voltages and currents are monitored in order to implement protection by preventing operation outside of the safe area.

As for the PWM signal generation, there are some differences between the LOV and HOV converter. In case of the HOV converter, simple PWM signal is formed straightforward. In case of the LOV converter, four driving signals are generated depending on whether the converter operates in buck or boost mode. The detailed description of the implemented control is given in Appendix B.

4.5.2 MPPT Efficiency and Input Voltage Ripple

Any fluctuation of voltage around the MPP will cause a power loss, as evident from Figure 4.4b. The fluctuation of voltage can be caused by the MPPT algorithm, since the P&O method introduces perturbations into the PV module voltage. Fortunately for thin-film PV modules, their power curve is relatively flat at MPP when compared to crystalline PV modules with their sharp-knee I-V curve. To quantify the power loss due to shift from MPP, we can define MPPT efficiency as the ratio of the actual power extracted from the PV module and the MPP power available under the actual operating conditions (i.e. irradiance and temperature):

$$\eta_{MPPT} = \frac{P_{out}}{P_{MPPT}} \tag{4.4}$$

Moreover, the MPPT efficiency can be static and dynamic, depending on whether the environmental conditions are constant or variable [4-26]. We will here consider only static MPPT efficiency. To estimate the static MPPT we can linearize the I-V curve of the PV module in the vicinity of the MPP with a MPPT resistance $\boldsymbol{R_{MPPT}}$:

$$R_{MPPT} = -\left(\frac{di(v)}{dv}\right)^{-1}\Bigg|_{MPP} \tag{4.5}$$

As an example, Figure 4.25 shows the dependence of $\boldsymbol{R_{MPPT}}$ of our reference PV module for the range of operating conditions shown in Figure 4.6a. We can see that the $\boldsymbol{R_{MPPT}}$ decreases as both the operating temperature and irradiation increase.

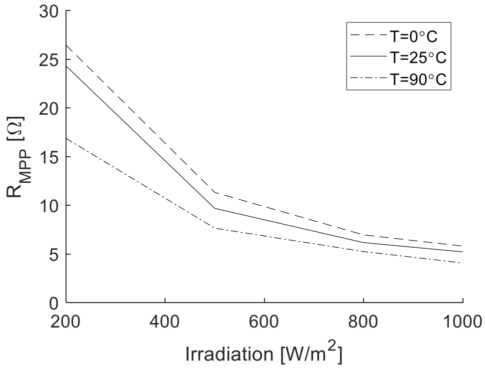

Figure 4.25: Dependence of R_{MPPT} on operating conditions

If we assume a triangle-like voltage ripple with a peak-to-peak voltage ΔV_{pp} present on the PV module, which is a typical response to MPP tracking or switching operation of the converter, it can be shown that the MPPT efficiency can be expressed as:

$$\eta_{MPPT} = \frac{P_{avg}}{P_{MPPT}} = 1 - \frac{\Delta V_{pp}^2}{12 R_{MPPT}} \tag{4.6}$$

Figure 4.26 shows the MPPT efficiency as a function of voltage ripple for our reference PV module at STC. Naturally, R_{MPPT} should also be scaled down/up when scaling the area of the PV module up/down.

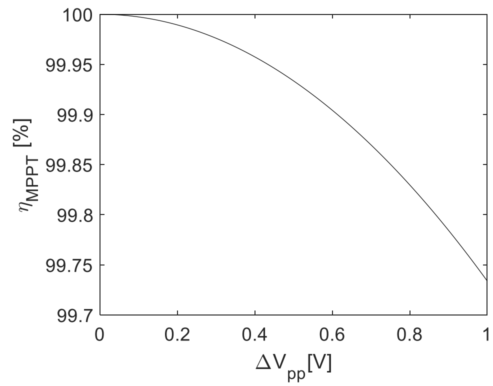

Figure 4.26: MPPT efficiency η_{MPPT} as a function of voltage ripple ΔV_{pp} for the reference PV module in Figure 4.4

As it can be seen, the MPPT efficiency stays very high even for larger voltage variations. Typically, in modern commercial converters MPPT efficiency is very high, well above 99%. Nevertheless it is important to stress that the overall efficiency of the system is the product of the MPPT efficiency and the conversion efficiency.

4.5.3 LOV Converter Design

The schematic of the LOV converter is shown again in Figure 4.27 with the relevant signals marked [4-9]. Considering the nominal operating conditions from Table 4.2, the converter will operate in boost mode. This means that Q_3 and Q_4 will be actively switched, whereas Q_1 will be always on and Q_2 always off. Moreover, the converter will operate in CCM. This is driven by requirements for the value L of the inductor, balancing between the size of the inductor and losses, as it will be shown in Chapter 5.

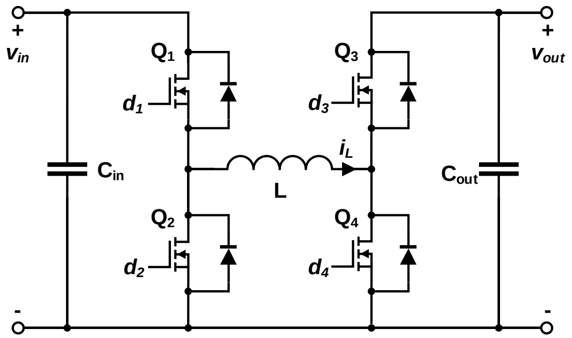

Figure 4.27: Schematic of the LOV converter

The waveforms, typical for a boost converter in CCM, are shown in Figure 4.28.

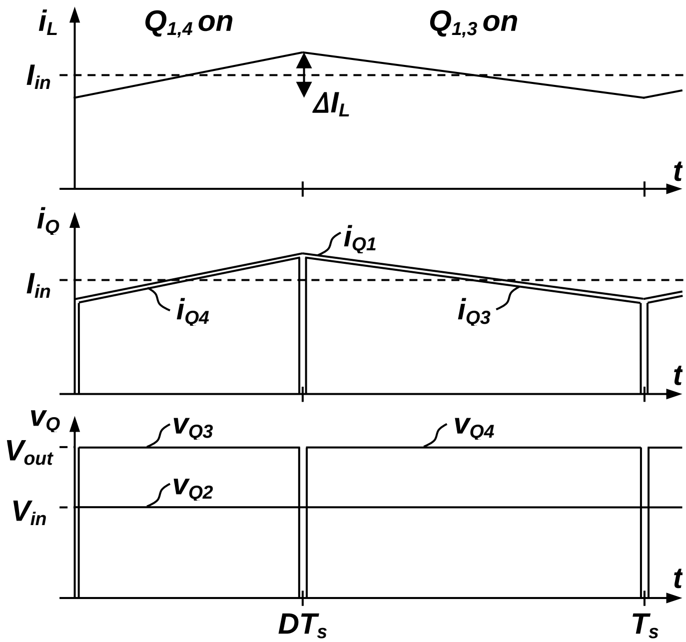

Figure 4.28: Relevant waveforms for the LOV converter operating in CCM

Based on the above waveforms and principles of converter operation [4-27], we can calculate the required values for energy storage components (i.e. inductances and capacitances). The following are expressions for inductance $\boldsymbol{L}$ as a function of switching frequency $\boldsymbol{f_{sw}}$ and inductor current ripple $\boldsymbol{\Delta I_L}$:

$$L = \frac{V_{in}D}{f_{sw}\Delta I_L} = \frac{V_{mppt}D}{f_{sw}\Delta I_L} \tag{4.7}$$

where:

$$D = 1 - \frac{V_{in}}{V_{out}} = 1 - \frac{V_{mppt}}{V_{out}} \tag{4.8}$$

The voltage gain of the converter is given with:

$$M = \frac{V_{out}}{V_{in}} = \frac{1}{1-D} \tag{4.9}$$

The values for the input and output capacitors $\boldsymbol{C_{in}}$ and $\boldsymbol{C_{out}}$ are determined by the desired peak-to-peak voltage ripple $\boldsymbol{\Delta V_{in,pp}}$ and $\boldsymbol{\Delta V_{out,pp}}$:

$$C_{in} = \frac{\Delta I_L}{8 f_s \Delta V_{in,pp}} \tag{4.10}$$

$$C_{out} = \frac{D I_{out}}{f_s \Delta V_{out,pp}} \tag{4.11}$$

In the equations above, the parameters $\boldsymbol{V_{in}}$, $\boldsymbol{V_{out}}$ and $\boldsymbol{D}$ are already known from Table 4.2. The remaining parameters $\boldsymbol{f_{sw}}$, $\boldsymbol{I_{out}}$ ($\boldsymbol{P_{out}}$), $\boldsymbol{\Delta I_L}$, $\boldsymbol{\Delta V_{in/out,pp}}$ will come as input when designing the converter in Chapter 7, where we will choose the power level (by resizing our reference PV module), the switching frequency, the inductor current ripple and the input/output voltage ripple.

Regarding the transistor rating, some come directly from Figure 4.28 and Figure 4.5. The rest of the ratings depend on the converter power level and the selected maximum output voltage (and the chosen devices), which will also be determined in Chapter 7. The current and voltage ratings for the transistors are given with:

$$\begin{aligned} &V_{Q12,max} = V_{in,max} = V_{oc,max} \\ &V_{Q34,max} = V_{out,max} \\ &I_{Q1,rms} = I_{in,max} = I_{sc,max} \\ &I_{Q3,rms} = (1-D)I_{out} \\ &I_{Q4,rms} = DI_{out} \end{aligned} \tag{4.12}$$

As for the control of the LOV converter, beside MPPT, it includes changing between boost and buck mode, detecting DCM operation, periodic switching of the $\boldsymbol{Q_2}$ ($\boldsymbol{Q_4}$ in buck mode) in order to keep $\boldsymbol{Q_1}$ ($\boldsymbol{Q_3}$ in buck mode) on, and voltage/current protection. More details about the implemented control are given in Appendix B.

4.5.4 HOV Converter Design

The HOV converter is shown in Figure 4.29 with the marked relevant signals [4-17, 4-28, 4-29]. For the same reasons as in the case of the LOV converter, we will assume operation in CCM.

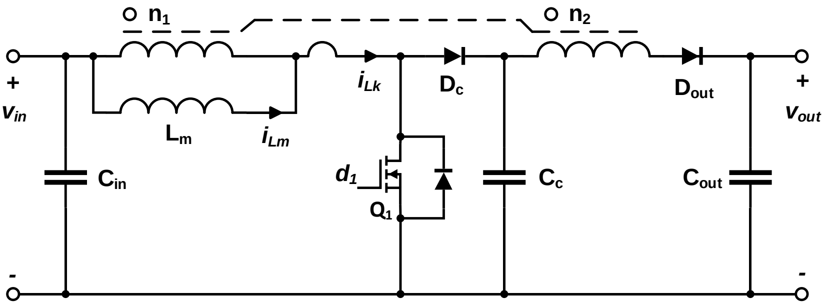

Figure 4.29: Schematic of the HOV converter

Here we have a passive voltage clamping with Cc, which recycles the energy stored in the leakage inductance $\boldsymbol{L_k}$. An additional role of $\boldsymbol{L_k}$ is to limit the slew rate of the output diode current, preventing reverse recovery losses. Contrary to the simple buck-boost topology of the LOV converter, in this case the derivation of the key equations is more complicated due to resonance between $\boldsymbol{L_k}$ and $\boldsymbol{C_c}$. A complete analysis of the converter operation is given in [4-17].

The relevant voltage and current waveforms are shown in Figure 4.30. The main goal is to find the expressions for the size of energy storage components. Analyzing the circuit and waveforms, we can obtain expressions for inductor $\boldsymbol{L}$ as a function of switching frequency $\boldsymbol{f_{sw}}$ and inductor current ripple $\boldsymbol{\Delta I_L}$, which happens to be the same as for the LOV converter:

$$L \cong \frac{V_{in}D}{f_{sw}\Delta I_L} = \frac{V_{mppt}D}{f_{sw}\Delta I_L} \tag{4.13}$$

where:

$$D \cong \frac{V_{out} - V_{in}}{V_{out} + nV_{in}} = \frac{V_{out} - V_{mppt}}{V_{out} + nV_{mppt}} \tag{4.14}$$

The approximate voltage gain of the converter is given with:

$$M = \frac{V_{out}}{V_{in}} = \frac{1 + nD}{1 - D} \tag{4.15}$$

The values for the input and output capacitors $\boldsymbol{C_{in}}$ and $\boldsymbol{C_{out}}$, and for the clamp capacitor $\boldsymbol{C_c}$ are determined by the their respective desired peak-to-peak voltage ripple $\boldsymbol{\Delta V_{in,pp}}$, $\boldsymbol{\Delta V_{out,pp}}$ and $\boldsymbol{\Delta V_{Cc,pp}}$:

$$C_{in} \cong \frac{(n-1)(1+nD)I_{out}}{(n+1)f_s \Delta V_{in,pp}} \tag{4.16}$$

$$C_{out} \cong \frac{2(1-D)I_{out}}{(n+1)f_s \Delta V_{out,pp}} \tag{4.17}$$

$$C_c \cong \frac{I_{out}}{f_s \Delta V_{c,pp}} \tag{4.18}$$

In the previous equations, the parameters $\boldsymbol{V_{in}}$, $\boldsymbol{V_{out}}$ and $\boldsymbol{D}$ are already known from Table 4.2. The remaining parameters $\boldsymbol{f_{sw}}$, $\boldsymbol{I_{out}}$ ($\boldsymbol{P_{out}}$), $\boldsymbol{\Delta V_{in/out,pp}}$ will come as input when designing the converter in Chapter 7.

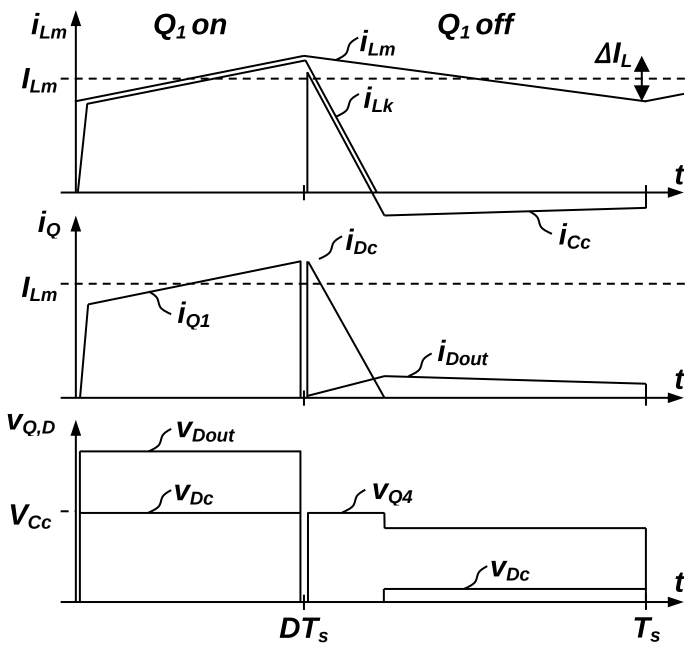

Figure 4.30: Relevant waveforms for the LOV converter operating in CCM

Regarding the transistor and diode ratings, some come directly from Figure 4.28 and Figure 4.5. The rest of the ratings depend on the converter power level, which will come in Chapter 7. The current and voltage ratings are given with:

$$
\begin{aligned}
&V_{Q1,max} = V_{Dc,max} = \frac{V_{in,max}}{1-D} = \frac{V_{oc,max}}{1-D} \\
&V_{Dout,max} = \frac{nV_{in,max}}{1-D} \\
&I_{Q1,rms} = I_{in,max} = I_{sc,max} \\
&I_{Dc,Dout,rms} = I_{out}
\end{aligned}
\tag{4.19}
$$

In the end, as for the control for HOV converter, beside the MPPT algorithm it includes only voltage/current protection. The description of the implemented control with is given in Appendix B.

4.6 Conclusions

In this chapter, an electrical design for a power converter was presented as the first step toward the PV module integrated converter. This step was done through three stages with the following results and conclusions:

- A reference electrical model of the considered thin-film flexible PV module was made. The electrical model is scalable in order to accommodate a range of voltage or power levels of the integrated converter. Moreover, the model takes into account environmental conditions, and can be used to test different DMPPT strategies, as well as the conventional PV systems. It was shown that the converter with its losses will not affect the module electrically. The model, together with two chosen DMPPT architectures set the input and output specifications for two versions – LOV and HOV converter.
- A list of simple non-isolated topologies was considered to find suitable platforms for electrical design of the PV module integrated converter. Based on multiple criteria relevant for PV module integration, namely integrability, performance, reliability, cost and control two candidate topologies were selected for further analysis.
- For the selected converter topologies, relevant expressions were derived, linking the size of the energy storage components (i.e. inductances and capacitances) and the voltage/current rating of the devices to the rest of the electrical parameters, in the first place converter switching frequency and the power level (i.e. PV module size).

The electrical design was the first step and will be revisited again in Chapter 7 when finally designing the converter. At this point some questions remain unanswered. Looking at the expressions for energy storage components, we can see that the switching frequency dictates their values without limits. Also, as it was shown, the heat generated by the converter does not affect the PV module electrically, but the thermal interaction is yet to be analyzed. These questions will be addressed in Chapter 5 by finding enabling technologies for PV module integration, such as new switching devices and magnetic materials to overcome technological constraints, and in Chapter 6, by analyzing thermal interactions and finding suitable thermal management strategies to handle the heat.

4.7 References

[4-1] J. Gow, C. Manning, "Development of a Photovoltaic Array Model for Use in Power-Electronics Simulation Studies," IEE Proceedings of Electric Power Applications, Vol. 146, No. 2, 1999

[4-2] L. Castaner, S. Silvestre, "Modeling Photovoltaic Systems Using PSpice," Wiley, 2002

[4-3] R. Bartl, R. Schlatmann, B. Stannowski, A. Gordijn, M.N. van den Donker, F. Finger, B. Rech, "TCO development for thin film silicon solar cells," European Photovoltaic Solar Energy Conference, 2006

[4-4] E. Gubia, P. Sanchis, A. Ursua, J. Lopez, L. Marroyo, "Ground Currents in Single-phase Transformerless Photovoltaic Systems," Wiley, 2007

[4-5] C. Stein, J. Pinheiro, H. Hey, "A ZCT Auxiliary Commutation Circuit for Interleaved Boost Converters Operating in Critical Conduction Mode," IEEE Transactions on Power Electronics, Vol. 17, No. 6, 2002

[4-6] S. R. Park, S. H. Park, C. Won, Y. Jung, "Low Loss Soft Switching Boost Converter," Power Electronics and Motion Control Conference (EPE-PEMC), 2008

[4-7] G. Hua, C. S. Leu, Y. Jiang, F. C. Lee, "Novel Zero-Voltage-Transition PWM Converters," IEEE Transactions on Power Electronics, Vol. 9, No. 2, 1994

[4-8] S. H. Park, G. R. Cha, Y. C. Jung, C. Y. Won, "Design and Application for PV Generation System Using a Soft-Switching Boost Converter With SARC," IEEE Transactions on Industrial Electronics, Vol. 57, No. 2, February 2010

[4-9] L. Linares, R. W. Erickson, S. MacAlpine, M. Brandemuehl, "Improved Energy Capture in Series String Photovoltaics via Smart Distributed Power Electronics," Applied Power Electronics Conference and Exposition (APEC), 2009

[4-10] G. R. Walker, J. C. Pierce, "Photovoltaic DC-DC Module Integrated Converter for Novel Cascaded and Bypass Grid Connection Topologies - Design and Optimization," Power Electronics Specialists Conference (PESC), 2006

[4-11] W. Li, X. He, "Review of Non-Isolated High Step-Up DC-DC Converters in Photovoltaic Grid-Connected Applications," IEEE Transactions on Industrial Electronics, Vol. 58, No. 4, 2011

[4-12] M. Forouzesh, Y. P. Siwakoti, S. A. Gorji, F. Blaabjerg, B. Lehman, "Step-Up DC-DC Converters: A Comprehensive Review of Voltage-Boosting Techniques, Topologies, and Applications," IEEE Transactions on Power Electronics, Vol. 32, No. 12, 2017

[4-13] K. K. Law, K. W. E. Cheng, Y. P. B. Yeung, "Design and Analysis of Switched-Capacitor-Based Step-Up Resonant Converters," IEEE Transactions on Circuits and Systems, Vol. 52, No. 5, May 2005

[4-14] E. H. Ismail, M. A. Al-Saffar, A. J. Sabzali, A. A. Fardoun, "A Family of Single-Switch PWM Converters With High Step-Up Conversion Ratio," IEEE Transactions on Circuits and Systems, Vol. 55, No. 4, 2008

[4-15] R. J. Wai, R. Y. Duan, "High-Efficiency DC/DC Converter with High Voltage Gain," IEE Proceedings - Electric Power Applications, Vol. 152, No. 4, 2005

[4-16] R. J. Wai, C. Y. Lin, R. Y. Duan, Y. R. Chang, "High-Efficiency DC-DC Converter With High Voltage Gain and Reduced Switch Stress," IEEE Transaction on Industrial Electronics, Vol. 54, No. 1, 2007

[4-17] Q. Zhao, F. C. Lee, "High-Efficiency, High Step-Up DC-DC Converters," IEEE Transactions on Power Electronics, Vol. 18, No. 1, 2003

[4-18] R. J. Wai, C. Y. Lin, C. C. Chu, "High Step-Up DC-DC Converter for Fuel-Cell Generation System," Conference of IEEE Industrial Electronics Society (IECON), 2004

[4-19] T. F. Wu, Y. S. Lai, J. C. Hung, Y. M. Chen, "Boost Converter with Coupled Inductors and Buck-Boost Type of Active Clamp," Power Electronics Specialists Conference (PESC), 2005

[4-20] R. Gules, L. L. Pfitscher, L. C. Franco, "An Interleaved Boost DC-DC Converter with Large Conversion Ratio," International Symposium on Industrial Electronics (ISIE), 2003

[4-21] W. Li, X. He, "ZVT Interleaved Boost Converters for High-Efficiency, High-Step-Up DC-DC Conversion," IET Electric Power Applications, Vol. 1, No. 2, 2007

[4-22] W. Li, X. He, “An Interleaved Winding-Coupled Boost Converter with Passive Lossless Clamp Circuits,” IEEE Transactions on Power Electronics, Vol. 22, No. 4, 2007

[4-23] L. Balogh, “A Practical Introduction to Digital Power Supply Control,” available online, *www.ti.com*

[4-24] B. Subudhi, R. Pradhan, “A Comparative Study on Maximum Power Point Tracking Techniques for Photovoltaic Power Systems,” IEEE Transactions on Sustainable Energy, Vol. 4, No. 1, 2013

[4-25] N. Femia, G. Petrone, G. Spagnuolo, M. Vitelli, “Optimization of Perturb and Observe Maximum Power Point Tracking Method,” IEEE Transactions on Power Electronics, Vol. 20, No. 4, 2005

[4-26] M. Valentini, A. Raducu, D. Sera, R. Teodorescu, “PV Inverter Test Setup for European Efficiency, Static and Dynamic MPPT Efficiency Evaluation,” Optimization of Electrical and Electronic Equipment (OPTIM), 2008

[4-27] R. W. Erickson, D. Maksimovic, “Fundamentals of Power Electronics, Second Edition,” 2001

[4-28] H. Liu, H. Hu, H. Wu, Y. Xing, I. Batarseh, “Overview of High-Step-Up Coupled-Inductor Boost Converters,” IEEE Journal of Emerging and Selected Topics in Power Electronics, Vol. 4, No. 2, 2016

[4-29] D. M. Van de Sype, K. De Gusseme, B. Renders, A. R. Van den Bossche, J. A. Melkebeek, “A Single Switch Boost Converter with a High Conversion Ratio,” Applied Power Electronics Conference and Exposition (APEC), 2005

[4-30] Hyet Solar PV Modules, available online: *https://www.hyetsolar.com/*

Chapter 5 Enabling Technologies for PV Module Integrated Converters

5.1 Introduction

In the previous chapter, the relations that link the electrical requirements and operating parameters of the converter with the required values for the energy storage components were set. In this chapter we will see how these requirements translate to the physical size of the components, given the spatial limitations of PV module integration.

When going from electrical design to the actual realization of a circuit in general, appropriate technologies need to be selected when choosing individual components. In conventional designs the choice of technologies is usually driven by cost or performance. In case of the PV module integration, Chapter 3 defined spatial requirements for the construction of the converter – very low profile and mechanical flexibility. These technological requirements will be the main drive when selecting appropriate technologies and at the same time the main limitation when designing the converter, affecting both electrical and thermal design.

The goal of this chapter is to identify possible and to select best suitable technology platforms that can enable PV module integration of power converters. To achieve this, the considered technology platforms are divided into three groups:

- Printed circuit board (PCB) technologies that can enable flexible construction with additional functionalities for thermal and magnetic design,
- Active devices that can enable efficient operation at high switching frequencies, and low volume for energy storage components,
- Materials and structures that can enable low profile magnetic components.

The chapter will start with identifying PCB technologies and technologies for standard and embedded active and passive components. In the following, through comparison with conventional Si devices, new wide bandgap devices are considered for high switching frequency operation. In the end, technologies for low profile inductors and transformers are identified and selected. Together with technologies for active and magnetic components, this chapter also considers the associated loss models. These models will be used for the unified design procedure in Chapter 7.

5.2 Enabling PCB Technologies

Chapter 3 presents the concept of the PV module integrated converter, and introduces and discusses the main design parameters that need to be met for successful integration of the converter. Regarding the selection of thin-film flexible PV module, one expects from the integrated converter to be flexible and to have low profile. Considering that the bending radius of the mounted PV module is not expected to be small, flexibility is not the problem for the majority of the components, as long as ther footprint is kept small. However, if the carrier for the connections and components, i.e. printed circuit board (PCB), is large, it needs to be flexible to some extent if the PV module is to be mounted on a curved surface. Moreover, the integrated converter should not add much to the thickness of the PV module. To keep the overall thickness low, both the PCB of the converter and the mounted components should have low profile.

5.2.1 PCB Technology Selection

There are several PCB technologies that could be a possible candidate to enable PV module integration. These technologies differ in the first place in type of insulating material that is used as a carrier for the components and conductive layers [5-1]. PCB technologies that will be considered further are:

- **Standard PCB technology** – This type of PCB is the most used one for conventional designs. It is based on various types of paper or fiberglass material compressed together with a binding epoxy resin and cladded with copper. Common substrate materials are FR-4 and FR-2, typically used in consumer and industrial products.
- **Direct bonded copper (DBC)** and **Insulated metal substrate (IMS)** – These PCB technologies are intended to provide interconnection together with thermal reinforcement for a circuit. Instead of the materials used for standard substrates, here a ceramic (in case of DBC) or aluminum combined with thin FR-4 layer (in case of IMS) are used in order to achieve low thermal conductivity.
- **Flexible PCB technology** – This PCB technology is based on using flexible plastic substrates such as polyimide of polyester as a carrier for conductive layers and components.
- **Rigid-Flex PCB technology** – This PCB technology is a combination of flexible and rigid substrates which are laminated together. The resulting structure is rigid where extra support is needed and flexible around corners and areas requiring extra space.
- **Thick film technology** – In this approach, the conductive layer(s) could be printed directly onto a PV module, using the PV module as a substrate and carrier. This would remove another physical layer in the construction and would correspond to the highest level of integration as described in Chapter 3.

Possible PCB technologies can be compared based on multiple criteria. The use of different substrate materials directly affects the electrical, mechanical and thermal properties of the converter and therefore has influence on all design areas. Concerning the PV module integration, we can consider several most important characteristics of the abovementioned PCB technologies:

- **Flexibility** – Flexible PCB technology or directly deposited copper layers have the highest degree of mechanical flexibility and have clear advantage here. If the PCB for the converter is sufficiently small and the bending radius of the PV module is not low, a rigid PCB could also be used. Moreover, if the substrate is sufficiently thin, some degree of flexibility can be achieved for all PCB technologies. In that case care should be taken to prevent stress induced effects caused by stiffness of the PCB which could lead to delamination of layers, for example.
- **Low profile** –a low profile PCB could be achieved with all PCB technologies. With thick film technology, the lowest thickness can be achieved since the PV module is used as a substrate. With flexible PCB technology, standard substrate thickness is below 0.1 mm. This could also be achieved with standard PCB and DBC/IMS technologies, although the standard thickness for the substrate is usually above 1 mm here.
- **Cost** – For low quantities, standard PCB technology has the lowest cost, followed by flexible and rigid-flex PCB. IMS/DBC and thick-film technologies are more expensive. However, scaling the production, the cost of the PCB could be decreased to the level where it could not significantly impact the cost of the converter.
- **Thermal performance** – The thermal performance of the PCB includes its thermal properties (thermal resistance) and the ability to sustain high temperatures and high number of thermal cycles. Here DBC/IMD technologies have the advantage, since they are purposely envisioned for high power level, high power density applications. Flexible PCB and thick film technologies also have excellent high temperature and thermal cycling properties, but the thermal resistance depends primarily on conductive layers. Standard PCB technology is on the last place regarding the thermal properties.
- **Compatibility with PV module** – With all PCB technologies, except for the thick film, the converter can be assembled separately and integrated into the PV module during one of the production stages. If the overall thickness of the converter is kept as low as possible, this should not impede the assembly of the PV module. In case of the thick film technology, the PV module substrate should be able to withstand the conditions during the depositions of the films and high temperatures during the soldering of the components which could make this technology least suitable for PV module integration, or at least dependable on the PV module technology.

The abovementioned criteria for the selection of the most suitable PCB technology are listed in Table 5.1. Based on the overall suitability for the PV module integration, flexible PCB technology was chosen. Clear advantages are intrinsic flexibility, low profile substrate and easy integration with the PV module, but the thermal performance will have to be examined, which will be performed in Chapter 6. In the following section a short overview of the flexible PCB technology will be given.

Table 5.1: Considered PCB technologies for PVMIC

	Flexibility	Profile	Cost	Thermal performance	Compatibility with PV module
Standard PCB	Low-Med	Low-Med	Low	Low	Med-High
DBC/IMS	Low	Med-High	High	High	Med
Flex PCB	High	Low	Med-High	Med-High	High
Rigid-Flex	Med-High	Low-Med	Med-High	Med	Med-High
Thick-Film	High	Low	Med	High	Low

5.2.2 Flexible Circuit Technology

Although not that widespread as the standard rigid PCB technology, flexible PCB can today be found in various electronics devices, from low cost consumer appliances to space and military applications. Its history is as long as the beginning of modern electronics technology. First traces of ideas for flexible interconnections were found in patents issued at the beginning of the 20th century and in some Edison's notes. After the World War II, with the strong growth of consumer electronics the use of flexible PCB started to grow. With specific applications come specific requirements for the PCB, and the flexibility is often required, for example for reliable connection, high density circuits or for rollable electronics (Figure 5.1).

(a) (b) (c)

Figure 5.1: Examples of circuits constructed with flexible PCB technology: (a) connector, (b) camera, (c) solar module on the ISS

Flexible PCB differs from other technologies in base material and adhesive layers used to bond the conductive layer to the substrate. For the base layer a polymer film is typically used. The adhesive layer is also formed using different polymer materials.

The conducting layer is typically created using rolled or annealed copper. The conducting layer is usually protected with coverlay, and if additional stiffness of the PCB is required a stiffener layer can be added. Table 5.2 lists the common materials used for constructing flexible PCB.

Table 5.2: Common materials used to build flexible PCB

Application	Typical materials
Base substrate	Polyimide, polyester, polyester terephthalate, thin glass-epoxy, fluorinated ethylene propylene, resin-coated paper
Conductor	Electrodeposited or annealed copper foil, stainless steel foil, aluminum foil.
Adhesive layer	Acrylic resin, epoxy resin, phenol resin, pressure-sensitive adhesives
Coverlay	Polyimide film, polyester terephthalate, flexible solder mask
Stiffener	Polyimide film, polyester terephthalate, glass-epoxy, metal boards, etc.

There are multiple variants of flexible PCB technologies, depending on the construction. The most common types are [5-2]:

- **Single sided flexible PCB** – This type consists of one conductive layer glued on a flexible film (Figure 5.2a). The copper layer is by definition accessible only from one side. Usually, a protective layer is applied on top of the conductive layer. Due to small number of layers, this is the cheapest type of flexible PCB.
- **Double access (back-barred) flexible PCB** – As in the previous case, here there is also a single conductive layer. To enable access to this layer from both sides, the base film is additionally processed (Figure 5.2b).
- **Sculptured flexible PCB** – This type of flexible PCB contains a conductive layer with varying thickness, manufactured by selective etching to different depths (Figure 5.2c). The thin parts can be used where increased flexibility is required, while the thick parts can be used for increased stiffness or for plug-in connections.
- **Double-sided flexible PCB** – This type of flexible PCB contains two conducting layers, usually interconnected with plated through holes. Terminations for components are provided on both sides of the PCB allowing them to be placed on either side (Figure 5.2d).
- **Multilayer flexible PCB** – In case when the complexity of electronic circuits requires more conductive layers, flexible PCB can have three or more conducting layers. Commonly, the conductive layers are interconnected by means of plated through holes, as in the case of double-sided flexible PCB (Figure 5.2e).
- **Rigid-flex PCB** – This type of PCB presents hybrid construction consisting of rigid and flexible substrates laminated together with conductive layers. The conductive layers are commonly interconnected by means of plated through holes (Figure 5.2f).

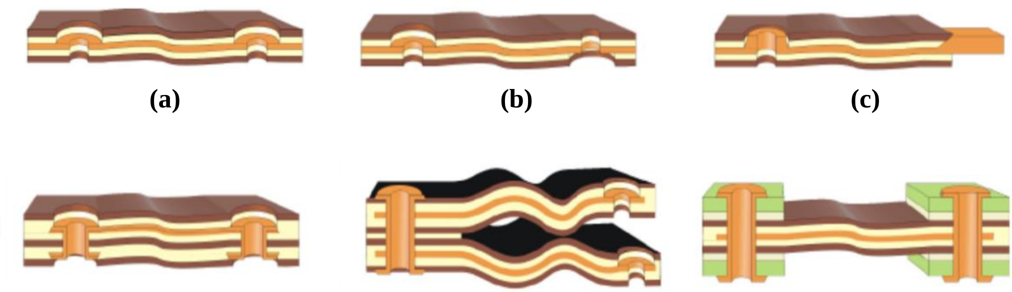

(a) (b) (c)

(d) (e) (f)

Figure 5.2: Common types of flexible PCB construction

Flexible PCBs are used in variety of electronic applications, such as consumer, automotive, computers, industrial control, military and aerospace to name a few. The main driver for their application is to solve difficult packaging problems, and compared with standard PCB technologies, flexible PCB possesses the following main advantages:

- **Static flexure of the circuitry** – Owing to the intrinsic formability, flexible PCBs are used to reduce the package size by replacing multiple rigid PCBs and corresponding board-to-board connections. This is beneficial in applications where the available space is limited, such as handheld devices. Moreover, flexible PCB is commonly several times thinner than conventional rigid PCB leading to further size reduction
- **Dynamic flexure of the circuitry** – The thinness of flexible PCB substrate, together with the ability to use thin copper layers, make flexible circuits the best candidate for dynamic flexing applications, making reliable interconnection between moving parts.
- **Point-to-point wire replacement** – Flexible PCB can replace wire harnesses between sub-assemblies, which are heavier and bulkier, which is especially used in tightly packaged devices such as in automotive and space aplications.
- **Reduction in weight** – Due to the thinness of the substrate, flexible PCB has lower weight when compared to other PCB technologies. This is the reason why flexible PCBs are popular in aerospace and portable electronics applications where weight is important.

The main disadvantage of flexible PCB is the cost, typically several times higher compared to the conventional rigid PCB. However, one has to take into account possibility to replace multiple rigid boards, connectors and wiring in the circuit by using flexible PCB, which can make the final price of the device lower.

In terms of mechanical and electrical properties, flexible PCB has additional advantages over standard PCB technology. The operating temperature can go above 200°C, but can be limited with adhesive materials. The dielectric strength of polyimide substrates, for example, can exceed 200 kV/mm, which is much higher than for FR4 material. This makes flexible PCB suitable for high voltage applications. Low dissipation factor, typically below 1%, makes the flexible PCB suitable for high-speed circuits and connections. Table 5.3 summarizes some properties of flexible PCB substrates compared FR4 material used for standard PCBs [5-1].

Table 5.3: Comparison of FR4 and common flexible PCB substrate materials

	FR4	Polyimide	Polyester
Standard thickness [mm]	0.4-1.6 mm	12.5-125 μm	25-188 μm
Flexibility	Low-None	High	High
Operating temperature [°C]	<130°C	>200°C	<70°C
Thermal conductivity [W/(m·K)]	0.3-1	0.1	0.2
Dielectric strength [kV/mm]	20	150-300	150-300
Dielectric constant	4.5	3.5	3
Dissipation factor [%]	0.018	0.002-0.003	0.005
Cost	Low	High	Low

5.2.3 Flexible PCB in Power Electronics

Regarding the use of flexible PCB technologies in power electronics, other PCB technologies still dominate. In consumer and industrial application, often the main driver is low cost, and standard rigid PCB has clear advantage here. In high power and high power density application, when thermal conductance of the PCB layers are of utmost importance, standard PCBs or DBC/IMS technologies are primarily used. Flexible PCB can be used in case when there are specific design requirements for a power converter, for example to further increase the power density or when there is a need for flexibility to conform to a surface.

An example where increased packaging level is accomplished using 3D construction with flexible PCB is given in [5-3], shown in Figure 5.3a. The concept is demonstrated on case of a 20W off-line LLC converter. Beside the role of achieving 3D construction, the flexible PCB is also used as a part of the thermal managements to handle the heat, and as a part of the magnetics providing windings for the transformer. When compared with the conventional construction, the presented converter offers increased functional, packaging integration level, better thermal management and power density of 250 W/l. Another example where flexible PCB is used to achieve high power density and physical flexibility is presented in [5-4]. Here, a multi-level 250W DC-DC converter is designed. Using high operating switching frequency, small values and size of the passive components are achieved. Combined with low profile

PCB, the resulting volumetric power density is very high – 6.6 kW/l. Moreover, GaN transistors are used as switching devices, an approach which will be also used here for the PV module integrated converter. A small 2 W boost converter fabricated using flexible PCB is presented in [5-5]. Here, the conducting layers of the PCB are also used to form the windings for the inductor. Other examples where flexible PCB is used in the construction of complete converters can also be found in the literature [5-6..8]. Other PCB technologies still prevail in power electronics, however for some components flexible PCB can be a good alternative, as it will be discussed further.

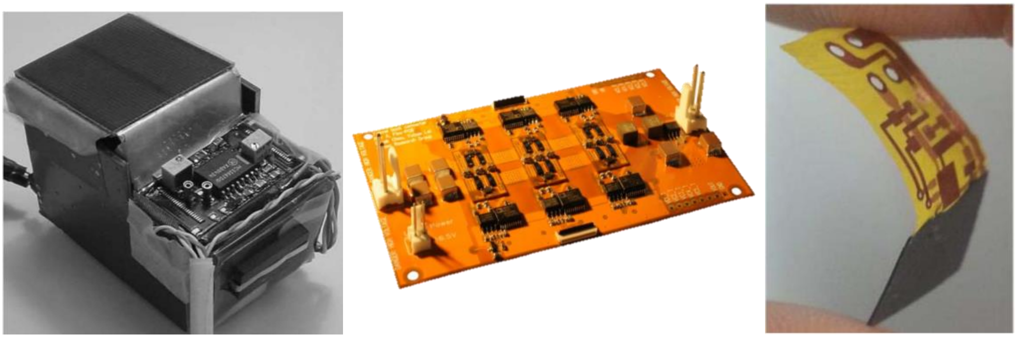

(a) **(b)** **(c)**

Figure 5.3: Examples of flexible PCB circuits in power electronics: (a) 3D off-line LLC converter [5-3], (b) Multi-level buck converter [5-4], (c) Boost converter [5-5]

Using flexible PCB technology is just one step in achieving flexible and low profile construction of the PV module integrated converter. The rest of the circuit which includes electronic components and any additional structures such as those for thermal management needs to have low profile as well. To achieve overall converter flexibility, the components need to be either flexible or to have small enough footprint. In the following section, suitable component technologies will be investigated.

5.3 Enabling Passive and Active Components

The concept of the PV module integrated converter presented in Chapter 3 shows the way the converter is integrated within the PV module. Whether using a PCB glued to the PV module or the PV module itself as the substrate for the circuit elements, the electronic components are arranged in a single layer. This means that the concept is not suitable for through-hole technology, instead, surface-mount technology (SMT) or PCB integrated components are needed. To achieve low thickness of the converter, the used components must have low profile construction. To achieve flexibility of the converter the components need to have either small footprint or to have flexible construction. In the following section, an overview of suitable technologies for passive and active components will be given.

5.3.1 Low Profile SMT Components

With the advancement of electronic circuits and their market, the need for lower cost was tackled by increasing the component density on a PCB. The first ideas for better component packaging appeared in 1950s [5-9]. Much of the pioneering work was done by IBM through the design of computers for space applications during the 1960s. Contrary to the leads used in through-hole technology, developed SMT components used tabs that could be directly soldered to the surface of the PCB. This gives the SMT numerous advantages over the through-hole technology, such as higher component density leading to smaller and lighter circuits, better EMC performance due to smaller of parasitics, faster automated assembly, and lower cost to name a few. By the end of the 20th century, surface mounted components dominated over their through-hole counterparts in majority of electronic circuits.

Regarding the PVMIC, almost all of its components can be found in SMT package with thickness under 1 mm, and with small footprint to enable flexibility of the complete assembly. Figure 5.4 shows the examples of SMT components that could be suitable for the integrated converter:

- **Resistors** – SMT resistors are commonly available in low profile and small footprint package, when they are needed for general use such as setting voltages and currents, or protection, but also for higher powers such as current shunts.
- **Capacitors** – Electrolytic capacitors can provide high capacity but their lifetime is limited, especially at higher temperatures. Moreover, they are not available in very low profile packaging. Multi-layer ceramic capacitors (MLCC) are a viable alternative, they are available in low profile small footprint packaging providing capacitances from pF to well above 1 µF, and voltages up to several hundreds of volts.
- **Inductors and transformers** – Inductors with height lower than 1mm are available in SMT, however their inductance and current ratings are quite limited. Considering the power level of the PV module integrated converter, alternative solutions are required, even when operating at high switching frequencies. This also applies for the transformers, which will be needed for HOV converter.
- **Integrated circuits** – SMT integrated circuits incorporating complete control and power stage are available in very low profile, requiring only few passive components to complete a converter. In case of the PVMIC, microcontrollers, gate drivers and sensor ICs are available in small footprint, low profile SMT packages.
- **Transistors and diodes** – Switching components for the power stage are also available in low profile, small footprint SMT packages. Since high switching frequency will be needed to decrease the size of energy storage components, new wide-bandgap devices will be used, which will be covered in separate section.

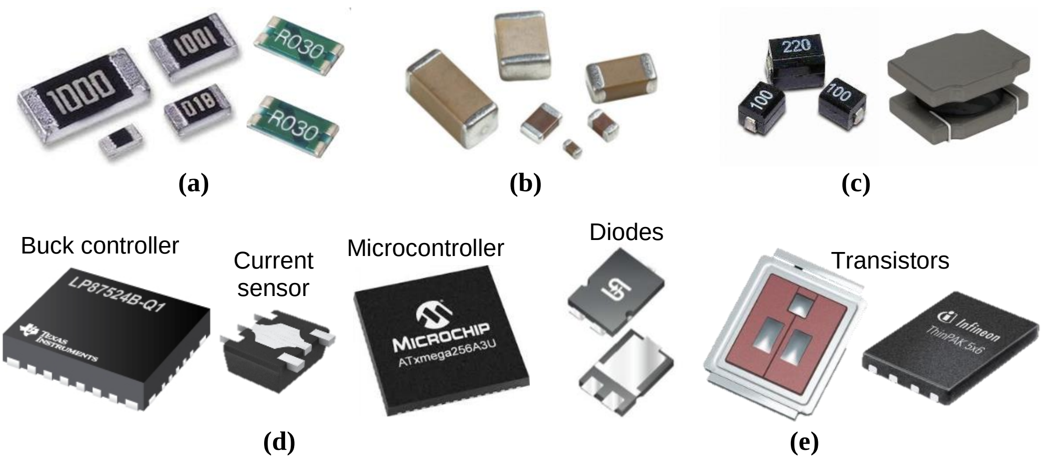

Figure 5.4: Low profile SMT passive and active components: (a) Resistors, (b) Capacitors, (c) Inductors, (d) Integrated circuits, (e) Transistors and diodes

As it will be shown later, standard SMT inductors will not be suitable for the PVMIC considering its power level. Alternative solutions in form of integrated or embedded components can be used, where the size is further reduced by increasing the level of integration. This does not have to be limited to magnetics only, since other components could also be found in integrated or embedded forms.

5.3.2 Integrated and Embedded Components

An integrated device presents a mean of integration where number of passive components, for example inductors, capacitors and transformers are integrated into one device. One example is electromagnetic integration of passives shown in Figure 5.5 [5-10]. The basic cell of this integrated device is the planar integrated L-C winding, which consists of a dielectric substrate with conductor windings directly deposited on both sides. With the appropriate connection of the structure's windings, series resonant, parallel resonant or low-pass filter circuits can be implemented.

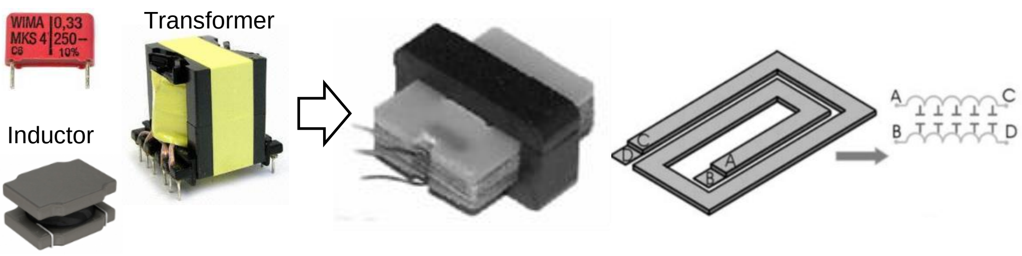

Figure 5.5: Electromagnetic integration of passives

Special materials have been developed to allow construction of passive components such as resistors, capacitors and inductors together with the PCB structure itself. These materials are used as an advanced substrate that enables increased functionality of the PCB, for example electromagnetic or thermal functionality. These substrates are laminated together with standard substrates in the same manufacturing process. Usage of embedded components can reduce the surface area of the PCB, allowing a smaller board to perform the same functions. Moreover, the performance of the circuit is expected to improve due to the shortened electrical path and minimized parasitic effects.

Embedded Resistors

Discrete resistors mounted on the surface of the PCB can be replaced with resistors buried inside the PCB [5-11], leaving more space available on the surface of the PCB decreasing the PCB size and improving the electrical performance of the circuit. Moreover, in some technologies resistors can be laser-trimmed to achieve high accuracy resistors.

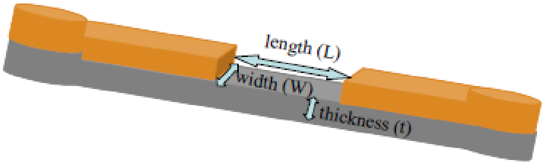

Figure 5.6: Thin film embedded resistor between copper traces

Corresponding to Figure 5.6, the resistance for the embedded resistor is defined with:

$$R = \rho \frac{W}{L \cdot t} = \frac{\rho}{t}\frac{W}{L} = R_S \frac{W}{L} \qquad (5.1)$$

where $\boldsymbol{\rho}$ is the specific resistivity of the material, $\boldsymbol{L}$ is the length of the resistor, $\boldsymbol{W}$ is the width and $\boldsymbol{t}$ is thickness of the resistor. $\boldsymbol{R_S}$ is the sheet resistance, defined as the ratio of the specific resistance of the resistor material and the resistor thickness. Commonly used technologies to fabricate embedded resistors are:

- **Thin film** – Here, embedded resistor is formed by plating a very thin layer of resistive film on a copper layer.
- **Ceramic thick film** – In this technology a ceramic thick film paste is used to form resistors by screen printing directly on the PCB.
- **Polymeric carbon paste** – Here, a carbon powder based thick film material is used to form resistors by screen printing.
- **Plating method** – In this approach, resistors are formed directly on the PCB by depositing resistive material by electroless plating process.

Embedded Capacitors

One or more capacitance layers can be included in the PCB of a circuit [5-12]. The conductors on top and bottom of this layer form the electrodes of the integrated capacitor. Since most of the capacitive layers has high breakdown voltages (1000 V or higher) they are suitable for power electronic circuits. In power electronic circuits, embedded capacitors can be used for decoupling, filtering, as snubber capacitors or as timing capacitors in control circuits. The capacitance is defined with:

$$C = \varepsilon_0 \varepsilon_r \frac{A}{d} \tag{5.2}$$

where $\boldsymbol{A}$ is the surface of the capacitor's electrode, $\boldsymbol{d}$ is the dielectric thickness, and $\boldsymbol{\varepsilon_r}$ and $\boldsymbol{\varepsilon_0}$ are the vacuum and relative permittivity of the dielectric respectively. Two major technologies used for embedded capacitive layers are (Figure 5.7) based on:

- Copper foils coated with dielectric layers,
- Composite laminates filled with high permittivity materials.

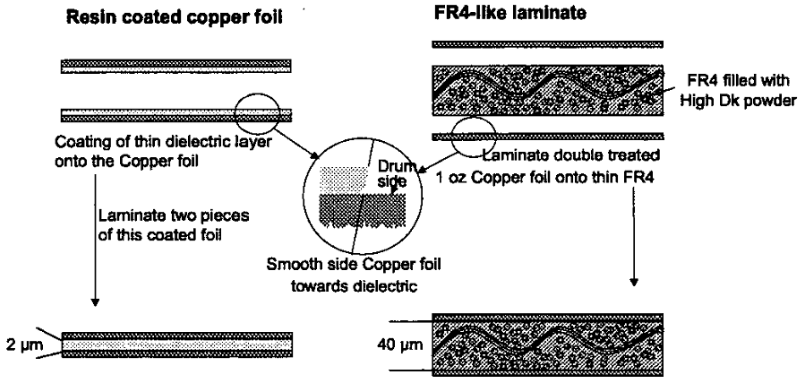

Figure 5.7: Manufacturing process of embedded capacitors

Embedded Magnetics

In the standard PCB technology, planar transformers have long been used as a mean of combining PCB layers with electromagnetic components in order to decrease the cost and improve the density of electronic circuits [5-13]. Taking this approach further, magnetic material can be integrated into the PCB to form the magnetic core. The resulting sandwich structure consisting of conductive, isolation and magnetic layers can form an inductor or a transformer (Figure 5.8) [5-14]. Depending on the type of the magnetic materials, integrated magnetics can be based on:

- Soft magnetic metal sheets,
- Ferrite-polymer compounds.

As an alternative to discrete power inductors for the PVMIC, integrated inductors will be investigated in more details in a separate section.

Figure 5.8: Embedded inductor using FPC [5-13]

Embedded Actives

Chip-on-board (COB) technology has been commonly used with standard PCB technologies to increase the component density and decrease the cost. Here, a bare die or IC is put directly on the PCB, interconnected with the rest of the circuit, and encapsulated for protection. Similar approach using flexible PCB is chip-on-flex (COF). Three common COF methods, shown in Figure 5.9, are [5-2]:

- **TAB** – In this method, the conductive traces from the flexible PCB are extended into free space or windows within the circuit. A bare integrated circuit is then attached to these “flying” leads.
- **Flip-chip** – In this approach a flipped chip is connected directly to the conductive layer by solder and appropriate reflow technology or by conductive adhesives. With flip-chip method enables maximum density and smallest parasitic effects to be achieved, providing maximum performance.
- **Chip-and-wire** – In this method, bare ICs are bonded to the flexible substrate using suitable die-attach materials and then interconnected to the PCB by means of gold or aluminum wire bonds.

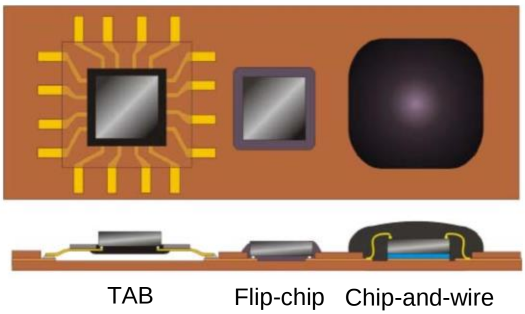

Figure 5.9: Embedding a die into flexible PCB [5-2]

5.4 Enabling Semiconductor Devices

The central functional elements of all switch-mode converters are switching devices. Their role is to periodically redirect voltages and currents in the circuit, enabling transformation of electric energy into energy of magnetic and electric fields of reactive components and vice versa, in order to obtain desirable voltages and currents. This is done by periodically turning the device on and off, either controlled or forced by external voltages and currents. In principle, as the switching frequency of the device increases, the required energy storage components (inductors and capacitors) become smaller, but the power losses caused by non-ideal switch behavior increase as well.

During the history of power electronics, the performance of switching devices was constantly improved, either by incremental technological improvements or by disruptive advances by changing the switching device completely [5-15]. Vacuum tubes used in early power converters were replaced by Si-based bipolar transistors and diodes by the middle of the 20th century. Shortly after, bipolar transistors were replaced by silicon MOSFETs which still dominate in modern power converters. Still, the constant need for cost reduction and increased performance pushed the modern silicon-based devices close to its theoretical performance limits.

5.4.1 Wide Bandgap Devices

Wide bandgap (WBG) materials, a group of materials with bandgap greater than 1.7 eV, present a suitable alternative to silicon for next generation power electronic devices. In many aspects, the properties of these materials, some of which are listed in Table 5.4, are superior to silicon when it comes to power electronics applications [5-16]. Translating the material properties to characteristics of switching devices, power transistors and diodes based on WBG materials bring improved conduction efficiency, breakdown voltage, switching performance, size and cost. This is primarily driven by superior relationship between on-resistance and breakdown voltage due to their higher electric field strength. This allows WBG devices to be smaller for the given requirements. Moreover, the possibility of operation at higher temperatures further reduces the cost by reducing the size of thermal management.

Table 5.4: Properties of semiconductor materials for power electronic devices [5-16]

	Si	**SiC**	**GaN**	**Diamond**
Bandgap [eV]	1.12	3.2	3.45	5.45
Dielectric constant	12	10	9	5.5
Electric strength [kV/cm]	300	2200	2000	10000
Electron mobility [cm^2/(V·s)]	1500	1000	1000-2000	2200
Hole mobility [cm^2/(V·s)]	600	115	850	850
Thermal conductivity [W/(m·K)]	150	490	130	2200

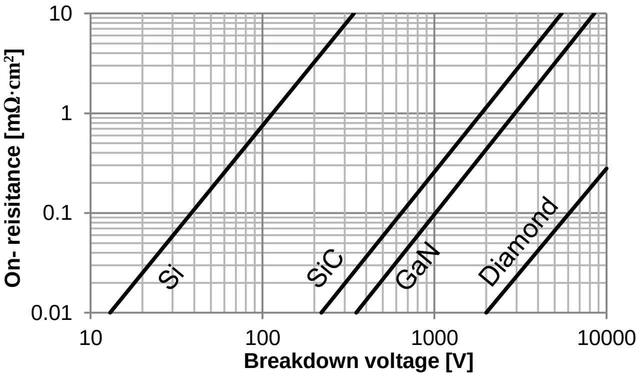

Figure 5.10: Limits of wide bandgap devices [5-17]

Although the potentials of WBG materials for power electronics were known for some time, it took considerable efforts and time to develop processes for manufacturing usable WBG power electronics devices. By the beginning of 2000s, first SiC schottky diodes became commercially available, followed by SiC JFETs and MOSFETS, primarily for 600-1200 V range. The development of GaN devices lagged behind, with first commercially available transistors becoming available around 2010 for 200 V range, and around 2015 for 600 V range.

Both GaN and SiC technologies are still in its infancy, the technology processes are yet to be perfected and their reliability is yet to be proven. Being more mature, as of 2017, the market share is dominated by SiC technology, dominating in medium and high voltage applications (Figure 5.11) [5-18].

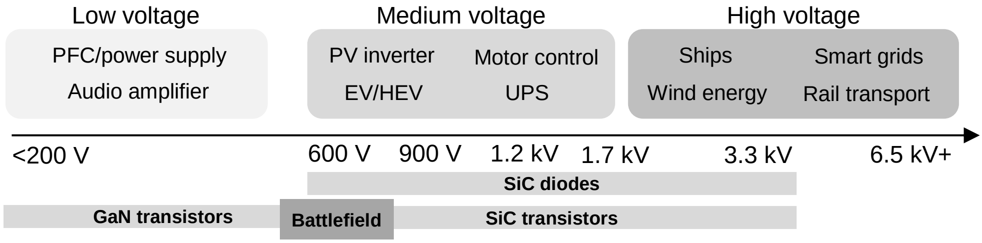

Figure 5.11: Market segmentation as a function of voltage range for GaN and SiC [5-18]

Considering the voltage range required for switching devices, defined in Chapter 4, GaN transistors and SiC diodes will be used for the LOV and the HOV PV module integrated converter. However, simple drop-in replacement of Si transistors with GaN/SiC transistors does not guarantee better performances of the converter. Due to the high switching speed combined with device limitations and parasitic circuit elements can even degrade the performance of a WBG device based converter. In the following, important design considerations for the GaN based converter will be covered.

5.4.2 GaN Power Transistors

GaN based power devices are a young technology with only a few manufacturers manufacturing them commercially as of 2017. Most of the available GaN devices are lateral heterojunction FETs, also known as high electron mobility transistors (HEMTs). HEMTs are inherently normally-on devices, which is inconvenient for power electronics, and the manufacturers are using different methods to fabricate normally-off GaN transistors. This is done either by using the cascode structure where GaN HEMT is combined with a MOSFET, or making enhancement-mode versions by modifying the gate structure. Table 5.5 lists some of the properties of the commercially/sample-available GaN devices. Considering the high speed operation and susceptibility to parasitics, small leadless packages are preferred for WBG devices in general. Figure 5.12 shows the packaging cases for some of the transistors listed in Table 5.5.

Table 5.5: Some of the commercially/sample-available GaN devices (2017)

Manufacturer	Type	Voltage [V]	Current [A]	R_{ds_on} [mΩ]	Package
EPC [20]	e-mode	100	48	4	LGA/BGA flip-chip
		200	22	25	
Texas Instruments [21]	cascode	600	12	70	VQFN
	e-mode	80	10	15	QFM
Transphorm [22]	cascode	600	17	150	PQFN/TO-220
MicroGaN [23]	cascode	600	30	170	die/TO-220
VisIC [24]	cascode	650	14	150	PQFN
		1200	50	40	
GaN Systems [25]	e-mode	100	45	15	PCB embedded flip-chip
		650	15	110	
Panasonic [26]	e-mode	600	10	155	DFN

Figure 5.12: Packages used for GaN devices

Takin into account the required ratings for transistors given in Chapter 4, and the availability of the devices at the time, EPC GaN transistors were considered for the design of the PV module integrated converter. In the following, a short overview of the properties and design recommendations for EPC GaN devices will be given.

A cross-section of the EPC enhancement mode GaN (eGaN) transistor is shown in Figure 5.13 [5-27]. A thin isolation layer is deposited on the silicon to isolate the device structure from the substrate. For current devices (<200 V) this layer provides isolation up to 300V. On top of the isolation layer, a thick layer of highly resistive GaN is deposited, which will serve as a foundation for the GaN transistor. An electron generating material is applied to the GaN layer making a highly conductive layer just on the surface. Next process forms a depletion region under the gate. After that, gate, source and drain contacts are formed.

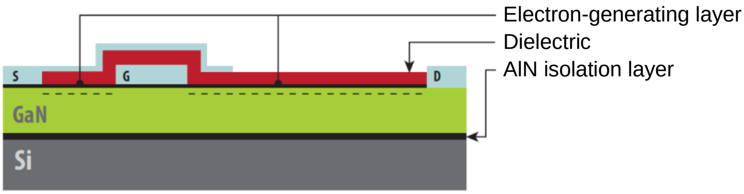

Figure 5.13: EPC eGaN transistor structure

eGaNs operates similarly to silicon power MOSFETs. With a positive bias on the gate relative to the source, a field effect will attract electrons from the GaN layer, forming the low resistance channel. When the bias is removed, the electrons from the channel are dispersed back into the GaN layer. Because of the lateral structure these devices are fundamentally different from MOSFETS and have some unique properties.

- **Gate threshold** – The threshold of eGaN transistors is lower than of Si MOSFETS. The negative relationship between threshold and temperature can is present, and this provides for excellent sharing in the linear region and diode conduction. However, since the device starts to conduct at voltages around 1.6V, care must be taken to ensure low impedance path from the gate to source when the device needs to be held off during high dV/dt transitions.
- **On Resistance** – $\boldsymbol{R_{ds,\ on}}$ versus $\boldsymbol{V_{gs}}$ curves are similar to MOSFETs and the channel resistance decreases as the maximum gate voltage is approached. Since there is negligible gate drive penalty, gate should be driven with 5V. Temperature dependence is lower compared to the Si devices (1.4 versus 1.7 times, for the temperature change from 25ºC to 125ºC).
- **Capacitance** – Because of the lateral structure, GaN transistors are very low charge device. Extreme small $\boldsymbol{C_{gd}}$ leads to very high switching speeds. They have the capability of switching hundreds of volts in nanoseconds which leads to a multi-megahertz operation possibility. $\boldsymbol{C_{gs}}$ is large compared to the $\boldsymbol{C_{gd}}$, which brings excellent dV/dt immunity. On the other side, $\boldsymbol{C_{gs}}$ is smaller compared to the Si devices, which brings very short delays and better controllability in extreme duty cycle applications.
- **Body diode** – Compared to the Si MOSFET, reverse bias or diode operation has different mechanism but similar function. Because of the structure, there are no reverse recovery losses. For the device with similar $\boldsymbol{R_{ds,on}}$ eGaN devices have

significantly lower C_{oss} than silicon MOSFETs. The forward voltage of the eGaN diode is somewhat higher than the forward voltage of the Si diodes.

EPC eGaN devices are isolated from the substrate which allows monolithic fabrication of transistors in any configurations and common heatsink without the need for an insulating layer between the device and the heatsink. Both the drain and source current are collected on the one side of the device. To accomplish low resistance in the metal layers that collect the source and drain current, wafer level line grid arrays are used where drain and source lines are alternated. Figure 5.14a shows the size comparison of GaN and Si transistors with similar electrical characteristics. Figure 5.14b shows the 200V, 12A, 25mΩ device with marked terminals which are in form of solder bumps.

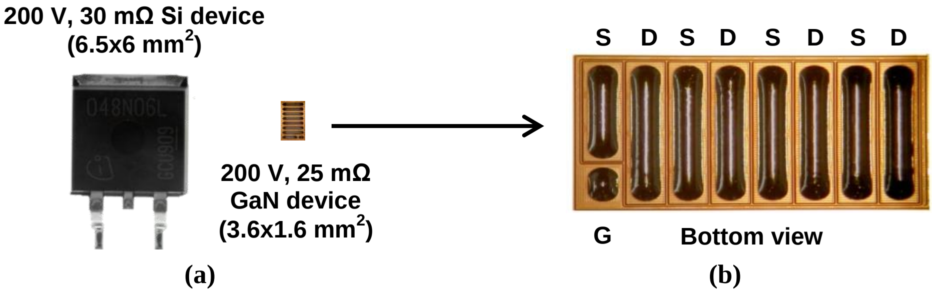

Figure 5.14: (a) Size comparison between EPC eGaN and Si device with similar ratings, (b) 200 V, 25mΩ eGaN transistor with marked terminals,

The equivalent circuit of the eGaN gate circuit is shown in Figure 5.15a. The gate consists of a small resistor R_g (~0.5 Ω) and a capacitor C_{gs}. Full enhancement can be done with 5 V but the gate voltage bellow the maximum voltage (~6 V), leaving little headroom for oscillations that can be caused by parasitic inductances. To keep the gate drive inductance on a PCB layout low, precautions have to be taken, such as keeping the traces short and using small SMT gate drivers with short leads. Some manufacturers have recognized the importance of proper driving of GaN devices and have integrated gate drivers with the GaN transistor in the same package [6-21].

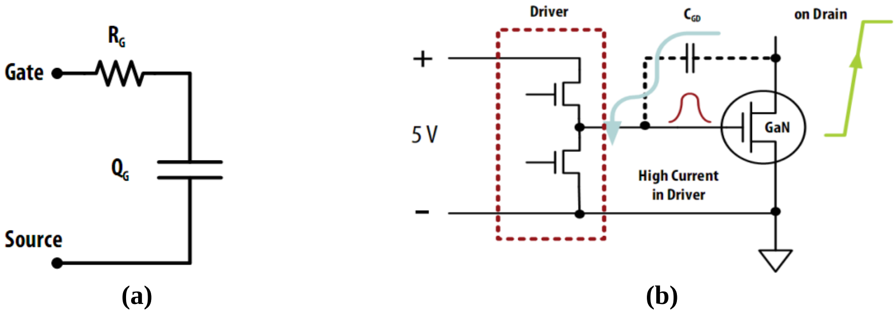

Figure 5.15: (a) eGaN gate circuit, (b) effect of dV/dt on off state of the device

5.4.3 Case Study – GaN vs. Si Transistors

In this section, a performance comparison between GaN and Si transistors is presented through a design process for a converter that can be used in a DMPPT system [5-28]. For the analysis, an interleaved boost converter with output voltage of up to 100 V and the power level of 100 W will be designed. The converter circuit diagram is illustrated in Figure 5.16. Since the main goal is to compare the switching performances, the converter was made using standard technology, i.e. using a standard PCB and ferrite core inductors.

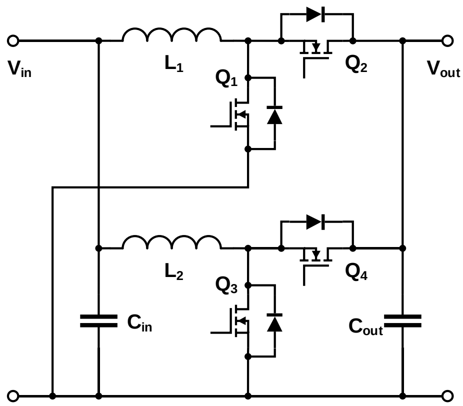

Figure 5.16: Interleaved boost converter used to compare GaN and SiC transistors

A range of available 100 V GaN and Si transistors were considered for the converter. According to the loss analysis, the main contributors to the losses are the device gate charge $\boldsymbol{Q_g}$, the on-resistance $\boldsymbol{R_{on}}$ and the output capacitance $\boldsymbol{C_{oss}}$. It is interesting to see the relation between the considered devices in terms of figures of merit (FOM) [5-29]. This is illustrated in Figure 5.17 where the comparison between the considered 100 V devices is based on two FOMs, $\boldsymbol{Q_g \cdot R_{on}}$ and $\boldsymbol{C_{oss} \cdot R_{on}}$.

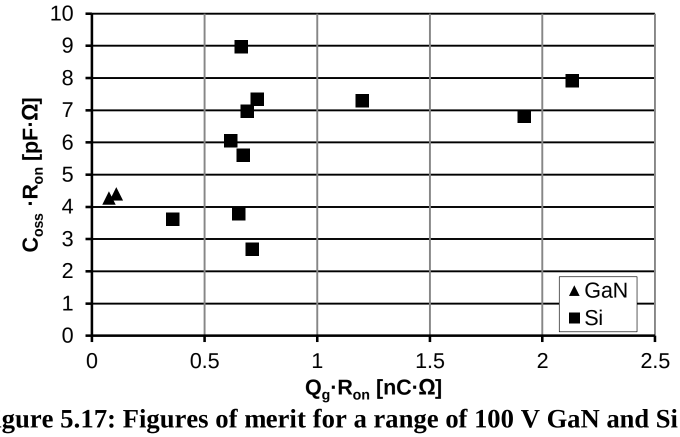

Figure 5.17: Figures of merit for a range of 100 V GaN and Si devices

It should be noted however that low figures of merit will not necessarily guarantee the lowest possible losses, since the gate drive circuit and the mode of operation can have influence on the final efficiency.

For the GaN based converter two devices were considered – EPC2001 and EPC1007 [5-30]. The performed analysis shows that, despite having increased on-resistance, the later device can allow lower losses at higher operating frequencies due to the lower $\boldsymbol{Q_g}$ and $\boldsymbol{C_{oss}}$. The former device is more suitable for lower operating frequencies and higher power levels. For this design, the boundary between aforementioned devices is in the vicinity of 400 kHz. The final design was, due to the practical limitations of hand soldering, based on EPC2001.

Concerning the Si based converter, the most suitable device was found to be IPI26CN10 [5-31]. It should be noted that, due to the available packaging (TO-263), this device would not be suitable for low profile designs.

Both versions of the converter were designed with the goal to achieve the same amount of losses in the transistors. This limit would be normally set by the available thermal management strategy, and mounting position of the converter, according to the thermal model. The results of the design process for both GaN and Si device are presented in Table 5.6.

Table 5.6: Converter specifications

	f_{sw} [Hz]	L [μH]	C_{in} [μF]	C_{out} [μF]	$P_{loss,act}$ [W]
Si converter	300	8.3	2.8	5.7	3.4
GaN converter	600	4.2	1.5	3	3.3

As expected, the higher operating switching frequency of the GaN based converter results in two times smaller values of the boost inductor and filter capacitors, which can significantly reduce the size and cost of the converter. Moreover, the minimum required capacitances for both versions of the converter can be easily achieved by paralleling small low-profile ceramic capacitors, making the filter capacitors not so critical components as the boost inductor.

To validate the results of the previous analysis, two prototype converters, shown in Figure 5.18, were built according to the specifications from Table 5.6. The 8.3μH inductor for the Si based converter was made using E/PLT22 core (using 3F3 ferrite material) with four turns of litz wire. On the other side, the smaller 4.2μH inductance for the GaN based converter was made using smaller E/PLT18 core (also 3F3 ferrite material) and also using four turns of litz wire. The same gate drivers were used for both versions of the converter (EL7158 [5-32]).

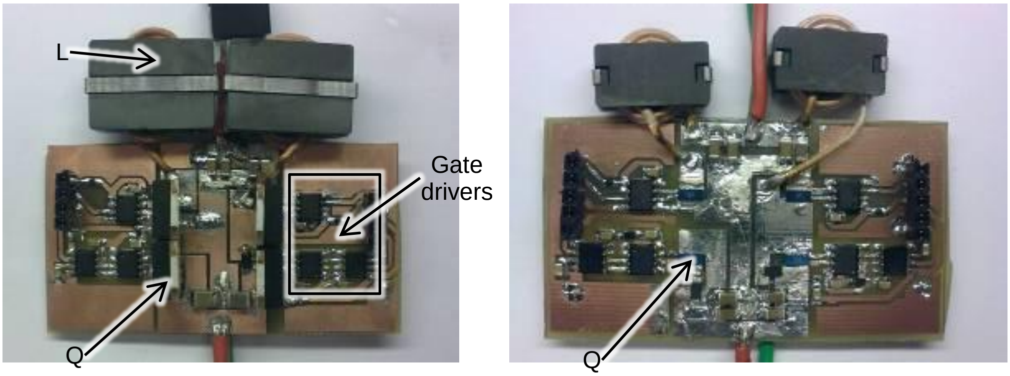

(a) (b)

Figure 5.18: Converter prototypes: (a) Si based converter, (b) GaN based converter

To obtain the losses in active components, first the overall efficiency of the converter was measured, not including the gate drive circuit consumption. After that, the inductor losses were obtained using the calorimetric measurements. Subtracting the inductor losses from total losses results in power losses in active devices, with assumption of small power losses in input and output capacitors.

Table 5.7 shows the breakdown of power losses and the measured efficiency for both versions of the converter operating at full input power level. Comparing the results from Table 5.7 and Table 5.6, it can be seen that the loss analysis underestimates the losses in active devices. The switching loss estimation in the design process is based on the piecewise linear model where device capacitances completely determine its switching behavior. However, in practice when using high-speed devices, parasitic inductances of the device leads and the PCB layout limit the switching process. This is especially the case with through-hole packaging such as TO-263. This calls for improved analytical loss models for power devices that include all relevant parasitic elements.

Table 5.7: Breakdowns of converter losses: total, inductor and transistor losses

	$P_{loss,total}$ [W]	$P_{loss,ind}$ [W]	$P_{loss,act}$ [W]	η [%]
Si converter	6.2	0.96	5.24	94.7
GaN converter	4.9	1.1	3.8	95.9

Figure 5.19 compares the conversion efficiencies as a function of input power. According to the efficiency curves, both converters perform similar in terms of power losses and maximum reached efficiency. However, for the same performance, higher operating frequency of the GaN based converter allows for smaller passives and increased power density.

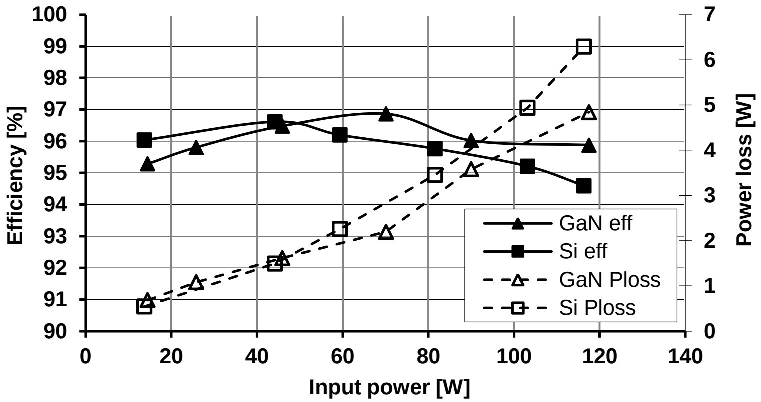

Figure 5.19: Measured conversion efficiencies and total power losses as a function of input power

It is also interesting to see the performance of the GaN based converter when the switching frequency is further increased. Figure 5.20 shows the efficiency curve for the operation under maximum power level, for switching frequencies increased up to 1MHz. As expected, the efficiency is reduced, although the high frequency performance can be improved using better cores, for example based on 3F4 material which is more suitable for higher switching frequencies. Therefore further reduction in size of passive components is possible if higher power losses are allowed.

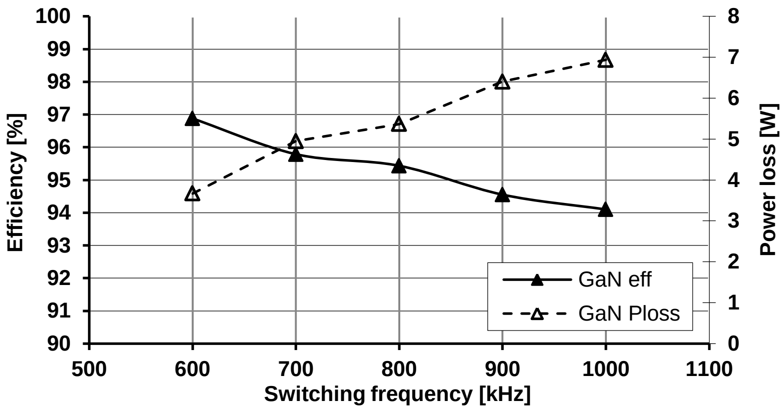

Figure 5.20: Measured conversion efficiency as a function of switching frequency for the GaN converter

The presented analysis shows that GaN based converter is capable of operating at two times higher switching frequency while achieving the same performances as the Si based converter. This allows for substantial reduction in size of passive components and can lead toward effective integration of the power electronic converter into the flexible PV module.

5.5 Low-Profile Flexible Magnetics

In order to achieve low profile and flexible construction all the components of the PVMIC should be low profile and in addition either flexible or with sufficiently small footprint. This is not an issue for all components except for power inductors. A typical SMT power inductor was shown before in Figure 5.4c. While it is possible to obtain a ferrite core inductors with thickness below 1 mm, their inductance and current rating are limited. For example, a typical low profile inductor can be rated for 0.47 µH and 4 A, having a footprint of 4 mm^2 and thickness of 1 mm [5-33]. Going back to Eq. 4.7 and 4.13, in Chapter 7 it will be shown that the usable inductance range lies in the range of at least couple of µH. Therefore, if standard SMT ferrite core inductors are used, a series-parallel arrangement of large numbers of inductors would be needed to scale the inductance and current rating, increasing the price of the converter. Moreover, attention should be given to achieve equal current sharing.

Alternatively, inductor windings can be realized in copper layers of the PCB, in the same way as windings for planar magnetic components. Several simple expressions for inductance of square or circularly shaped turns can be found in [5-34]. For example, according to modified Wheeler's expressions, the inductance of a square shaped spiral air inductor is given with:

$$L = 16\mu_0 n^2 D \quad \text{[nH]} \tag{5.3}$$

where $\boldsymbol{n}$ is the number of turns and $\boldsymbol{D}$ is the outer diameter of the coil in mm, assuming that the winding area is fully filled with turns. For example, to achieve inductance of 1 µH, assuming the turn width of 5 mm, the resulting diameter of the coil is 10 cm, which is large. Additionally, since there is no core, the magnetic field can induce losses in surrounding conducting bodies. Therefore, we need to add a core to increase the inductance and to contain the field.

5.5.1 Flexible Magnetic Structures

Adding a suitable magnetic material, the inductance of our previously mentioned air inductor can be increased. A structure where one or more spiral windings are sandwiched between two sheets of magnetic material is shown in Figure 5.21. The turns in different copper layers can either belong to the same winding or to different couple windings. In our case, we will use double sided flexible PCB and therefore 2 copper layers available for inductor windings.

Considering the size of the inductor windings, which is dictated by copper thickness of the PCB and the required current capacity of the copper traces, we can expect that the windings can occupy at least a few cm^2. To achieve flexible construction, the magnetic material should be also flexible, which rules out the standard ferrite used for cores.

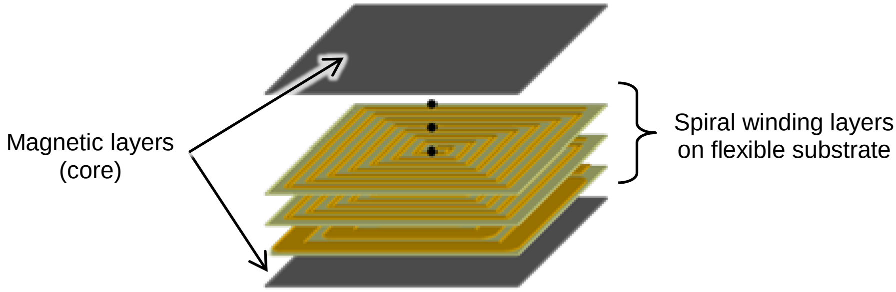

Figure 5.21: Spiral (coupled) inductors sandwich structure

Fortunately, two alternatives can be considered instead of standard rigid ferrite:

- Soft ferromagnetic materials, based on annealed high permeability alloys,
- Ferrite-polymer compounds (FPC), based on plastic material impregnated with ferrite powder.

Both alternatives come with its distinctive properties. The soft magnetic metal material, such as mu-metal, possesses very high permeability and comes in thin sheets which can be stacked together to form a core. One such example is presented in [5-35] where such material was used to realize and optimize a flyback transformer. However, since the material is conductive, large eddy current losses can occur if high switching frequencies are used, limiting its application far into sub-MHz range.

FPC material on the other hand possesses similar properties in terms of losses as standard ferrite materials which are the first choice when designing inductors for high switching frequencies. The main disadvantage is very low permeability when compared to other materials. However, as it will be shown, the permeability can still be high enough to increase the inductance of the corresponding air core inductor by several times.

Some properties of the considered magnetic materials are summarized in Table 5.8. For the final design of the PVMIC, FPC material will be used, primarily due to its low core losses at high switching frequencies.

Table 5.8: Some properties of the magnetic materials

	Metal-based	**FPC**	**Standard ferrite**
μ_r	5000..100000	10..400	1000..500000
B_{sat} [T]	~1	<0.5	~0.5
T_{max} [°C]	>400	<100	>200
Sp. Losses	High	Low	Low

5.5.2 Design Considerations for Single Inductors

FPC materials have been traditionally used for RF shielding and RFID applications. Lately, they have found its place in wireless charging applications as well. As of 2016, there are numerous manufacturers offering a range of materials making tradeoffs between the permeability, losses and optimum frequency range. The most important parameter for FPC materials is complex permeability $\underline{\mu}=\mu'+j\mu''$, where the real part μ' corresponds to relative permeability and the imaginary part μ'' corresponds to core losses. Figure 5.22 shows these parameters for IRJ04 material from TDK [5-36], which will be used as the core material for PVMIC.

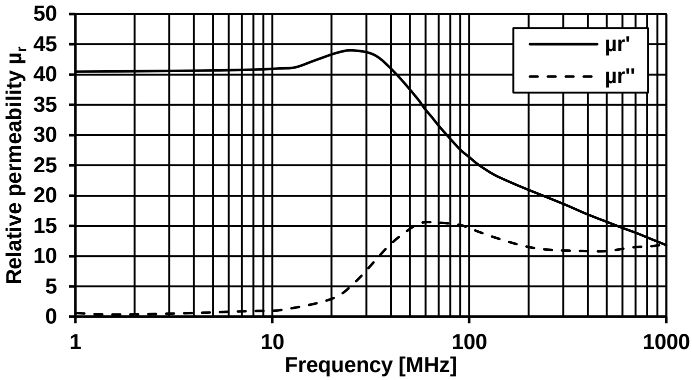

Figure 5.22: Permeability vs. frequency characteristic for IRJ04 FPC [5-36]

Rather low permeability of the used material will have strong implications on the inductor design. As it can be shown, the magnetic field will not be completely contained in the core. This will cause the field to have complex distribution with loosely coupled turns. Analytical methods to determine the inductor parameters can be found in [5-7], leading to complex equations not easily usable if needed for iteration during optimization procedure. Instead, in the following analysis we will use FEM analysis to determine the dependence of inductance on winding and core dimensional and material parameters.

The structure of the spiral, axis-symmetrical inductor with its dimensional parameters is shown in Figure 5.23. For the following, it was assumed that the 70 µm copper layers are laminated on the 70 µm polyimide layer and covered with 0.5 mm IRJ04 sheets. The turn width ***w*** is set to 5 mm and the turn spacing ***s*** is 0.5 mm. Figure 5.24 shows the single-layer inductance as a function of number of turns. While there can be seen exponential curve, it can be shown that the ratio of the inductance and the total winding length is almost constant, confirming that the turns are loosely coupled, and that the inductance primarily depends on the length of the winding. For larger number of turns, the curve becomes a linear one. This also implies that the inductance does not depend significantly on the shape of the inductor, or the way the winding is routed.

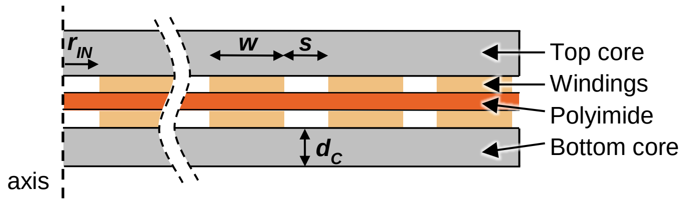

Figure 5.23: Structure of the spiral inductor

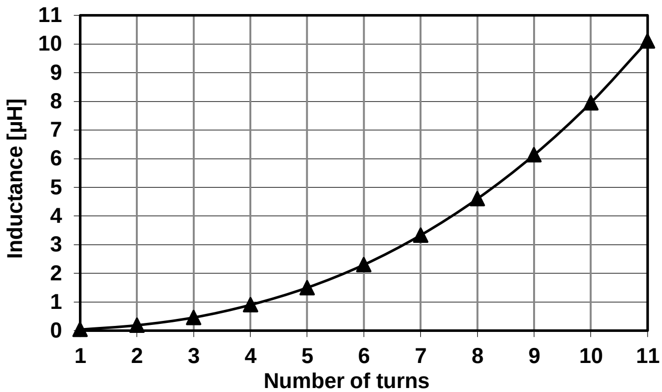

Figure 5.24: Inductance as a function of number of turns

Using FEM analysis, losses in the inductor can be determined as well, both for the windings, consisting of DC and AC losses, and for the core using μ'' as the loss parameter. Figure 5.25 shows the distribution of core and winding losses as a function of number of turns. In the analysis, the current was assumed to be 4 A with ripple ΔI_{pp}=4 A or 150%. As was the case with the inductance, it can also be shown that the losses are proportional to the winding length. For a given set of material properties and dimensional parameters, the inductance and loss curves can be fitted used as a part of optimization procedure for the LOV converter.

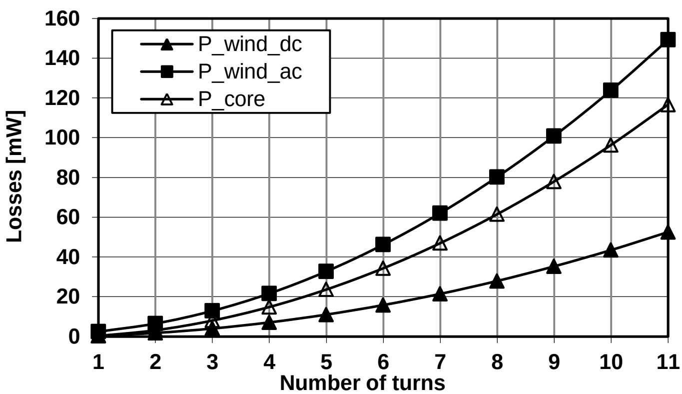

Figure 5.25: Inductor losses as a function of number of turns

5.5.3 Design Considerations for Coupled Inductors

For the purpose of designing HOV converter, as shown in Chapter 4, coupled inductors are required to achieve high voltage step-up ratio. The same concept as in the case of LOV inductor can be applied here, with multiple windings arranged in multiple copper layers, as shown in Figure 5.26. In addition to self-inductance, loosely coupled windings will result in leakage inductance and sub-optimal coupling. This will not have significant implications on the operation of the HOV converter, as the leakage inductance mainly limits the slew rate of the output diode. For other topologies where leakage inductances are actively used, such as LLC, the design can be adapted to meet the required specifications.

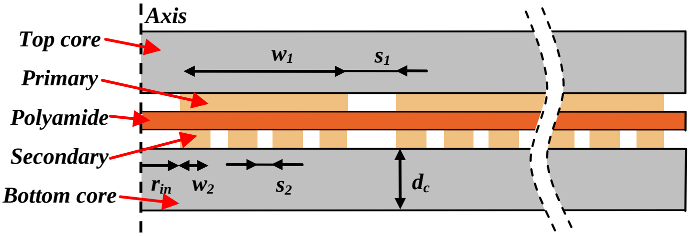

Figure 5.26: Structure of the spiral coupled inductors

A low profile coupled inductors were constructed using the same parameter as for the single inductor in the previous section. The number of turns for the primary winding is set to 5, whereas the number of turns for the secondary is set to 25, forming the turn ration of 1:5. Again, the structural and material parameters can be altered in order to see the influence on the key inductor parameters.

In Figure 5.27a the self-inductance of the primary is plotted as a function of relative permeability of the core [5.37]. As expected, the increased permeability or core thickness can significantly enhance the value of self-inductance. In Figure 5.27b, the primary leakage inductance is plotted as a function of core permeability for different core plate thicknesses $\boldsymbol{d_c}$. The leakage inductance increases with higher permeability. However, the increased leakage inductance does not introduce a worse coupling effect. In fact, better coupling effect is achieved since more flux concentrate in the core.

As the frequency increases, the current density becomes non-uniform due to the formation of eddy currents. Regarding the planar sandwich structure, the conductors between the two core plates form an airgap and almost all of the flux flows throughout the conductors. With increased core permeability, this effect will be strongly pronounced. It can be shown that the ratio of AC resistance to DC resistance reaches 65 at 1 MHz when the relative permeability is 150. The AC resistance can be decreased by using a narrower turn while increasing copper thickness, however, this is limited by PCB the available technology. One additional measure, not covered in this thesis, is to implement longitudinal slits in coper traces, which would keep eddy current flows within smaller areas.

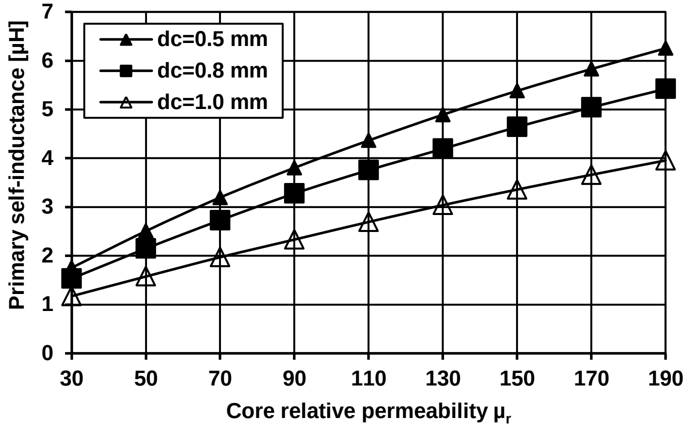

(a)

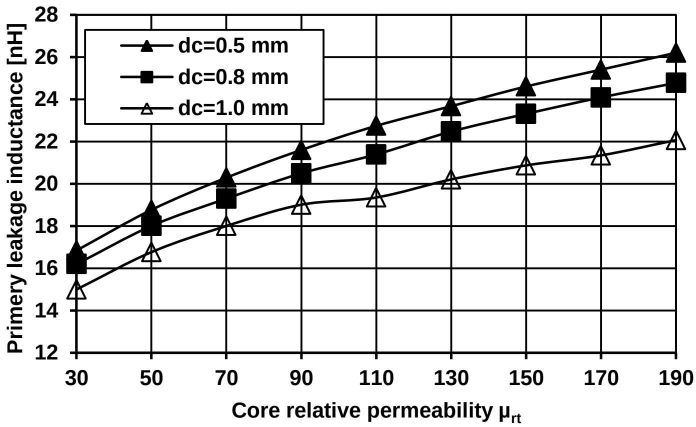

(b)

Figure 5.27: (a) Primary self-inductance and (b) primary leakage inductance as a function of core relative permeability μ_r and core thickness d_c

5.6 Conclusions

The technologies required to enable PV module integration are addressed in this chapter. Three groups are identified: PCB technologies and passives, power inductors and associated magnetic materials, and active semiconductor devices.

Flexible PCB technology was chosen to enable flexibility and low profile. Apart from having the interconnection function, the conductive layers can be utilized in the magnetic and thermal design as well. Flexible PCB technology is well known and mature technology, used especially in thermally demanding applications, enabling high temperature operation and intensive thermal cycling. It is more expensive than the standard PCB technology, but the cost can be kept low if low number or conductive layers is used. To decrease the number of required layers, the converter circuit should have high level of integration and small component count.

Standard SMT components can be used for almost all components of the converter. Due to their small size, low profile and flexibility are not a problem. To decrease the cost further, flexible PCB is compatible with screen-printed technologies which can produce a range of passives. As for the energy storage components, ceramic capacitors can provide enough required capacitance for filtering in a low profile, small footprint package. The inductors on the other hand are not available in such forms for the considered power levels. An alternative is considered in the form of PCB integrated windings coupled with flexible magnetic sheets. This may increase the cost of the converter, since inferior magnetic materials require large area for the inductor. The improvements are expected with new materials, such as those developed for wireless charging. Otherwise, the size of the energy storage components can be also decreased by increasing the switching frequency owing to novel active devices.

GaN devices were chosen as the main switching elements for the integrated converter. Although a new technology, it is making advances in low voltage applications, already outperforming Si counterpart, as was shown in the presented case study. However, the technology is immature and expensive with still to be proved reliability. The selected GaN devices are available in small package, enabling low profile design and flexibility. On the other hand, extracting the heat from such small devices can be challenging, and this will be covered in Chapter 6.

5.7 References

[5-1] C. F. Coombs, “Printed Circuits Handbook,” Sixth edition, McGraw Hills, 2008

[5-2] J. Fjelstad, “Flexible Circuit Technology,” Third edition, 2007

[5-3] E.C.W. de Jong, E.C.W. de Jong, J.A. Ferreira, P. Bauer, “Toward the Next Level of PCB Usage in Power Electronic Converters,” IEEE Transactions on Power Electronics, Vol. 23, No. 6, 2008

[5-4] D. Chou, Y. Lei, R. Pilawa-Podgurski, “A Zero-Voltage Switching, Physically Flexible Multilevel Gan DC-DC Converter,” Energy Conversion Congress and Exposition (ECCE), 2017

[5-5] G. Cao1, H. Kim, S. Lim, and G. Han, “An Embedded Inductor Using Sendust Powder Composite Films for Step-Up DC–DC Converter,” IEEE Transactions on Magnetics, Vol. 50, No. 11, 2014

[5-6] J.W. Lim, H.J. Kim, Y.S. Oh, H.S. Kim, S.T. Lim, “Embedded Flexible Fe–Si–Al Powder Composite Film Inductor for Low Power DC–DC Converters,” IEEE Transactions on Applied Superconductivity, Vol. 28, No. 3, 2018

[5-7] E. Waffenschmidt, B. Ackermann, M. Wille, “Integrated Ultra Thin Flexible Inductors for Low Power Converters,” Power Electronics Specialists Conference (PESC), 2005

[5-8] A. Ostfeld, “Printed and Flexible Systems for Solar Energy Harvesting,” PhD dissertation, University of California, Berkeley, 2017

[5-9] R. Strauss, “SMT Soldering Handbook,” Second edition, Newness, 1998

[5-10] J. Strydom, J. van Wyk, “Electromagnetic modeling for Design and Loss Estimation of Resonant Integrated Spiral Planar Power Passives,” IEEE Transactions on Power Electronics, Vol. 19, No. 3, 2004

[5-11] K. Perala, “Embedded Resistors in Printed Wiring Boards,” Advanced Packaging Materials: Processes, Properties and Interfaces, 2004

[5-12] J. Ferreira, E. Waffenschmidt, J. Strydom, J. van Wyk, “Embedded Capacitance in the PCB of Switchmode Converters,” IEEE, 2002

[5-13] Z. Ouyang, M. Andersen, “Overview of Planar Magnetic Technology - Fundamental Properties,” IEEE Transactions on Power Electronics, Vol. 29, No. 9, 2014

[5-14] E. Waffenschmidt, J. Ferreira, “Embedded passives integrated circuits for power converters,” Power Electronics Specialists Conference (PESC), 2002

[5-15] T. Wilson, “The Evolution of Power Electronics,” IEEE Transactions On Power Electronics, Vol. 15, No. 3, 2000

[5-16] J. Everts, J. Das, J. Van den Keybus, M. Germain, J. Driesen, “GaN-based power transistors for future power electronic converters,” IEEE Benelux Young Researchers Symposium, 2010

[5-17] P. Gammon, “Silicon and the wide bandgap semiconductors, shaping the future power electronic device market,” Ultimate Integration on Silicon (ULIS), 2013

[5-18] “SiC, Saphire, GaN…: What Is the Business Evolution of the Non-Silicon Based Semiconductor Industry?” Yole Development, 2016

[5-19] E. Jones, F Wang, D. Costinett, “Review of Commercial GaN Power Devices and GaN-Based Converter Design Challenges,” IEEE Journal of Emerging and Selected Topics in Power Electronics, Vol. 4, No. 3, 2016

[5-20] EPC-CO GaN devices, available online at *www.epc-co.com*

[5-21] Texas Instruments GaN devices , available online at *www.ti.com*

[5-22] Transphorm GaN devices, available online at *www.transphormusa.com*

[5-24] MicroGaN Gan devices, available online at *www.microgan.com*

[5-23] VisIC GaN devices, available online at *www.visic-tech.com*

[5-25] GaN Systems, available online at *https://gansystems.com/*

[5-26] Panasonic GaN devices, available online at *https://industrial.panasonic.com*

[5-27] A. Lidow, J. Strydom, M. de Rooij, and D. Reusch, “GaN Transistors for Efficient Power Conversion,” Second edition, Wiley, 2015

[5-28] M. Acanski, J. Popovic-Gerber, J. A. Ferreira, “Comparison of Si and Gan Power Devices Used in PV Module Integrated Converters” Energy Conversion Congress and Exposition (ECCE), 2011

[5-29] B. Baliga, “Power Semiconductor Device Figure of Merit for High-Frequency Applications,” IEEE Electron Device Letters, Vol. 10, No. 10, 1989

[5-30] EPC2001 and EPC1007 datasheet, available online at *www.epc-co.com*

[5-31] IPI26CN10 datasheet, available online at *www.infineon.com*

[5-32] EL7158 datasheet, available online at *www.intersil.com*

[5-33] PA4330 series inductors, available online at *www.pulseelectronic.com*

[5-34] S. Mohan, M. del Mar Hershenson, S. Boyd, T. Lee, “Simple Accurate Expressions for Planar Spiral Inductances,” IEEE Journal of Solid-State Circuits, Vol. 34, No. 10, 1999

[5-35] C. Marxgut, J. Muhlethaler, F. Krismer, J. Kolar, “Multiobjective Optimization of Ultraflat Magnetic Components with PCB-Integrated Core,” IEEE Transactions on Power Electronics, Vol. 28, No. 7, 2013

[5-36] Flexield series EM shield materials, available online at *www.tdk.com*

[5-37] Z. Ouyang, M. Acanski, J. Popovic, J. Ferreira, O. Thomsen, M. Andersen, “Design Considerations of Very Low Profile Coupled Inductors for Flexible Photovoltaic Module,” International Conference on Integrated Power Electronics Systems (CIPS), 2012

Chapter 6 Thermal Management for PV Module Integrated Converters

6.1 Introduction

Due to losses, every electrical device generates some amount of power in the form of heat. If the amount of heat is too large or too concentrated, and the heat paths for its dissipation are obstructed, it can cause excessive temperatures leading to degradation, shorter lifetime, or failure of the device. It is up to thermal design of the device to determine how to deal with losses in those cases. To a layman, thermal design of an electronic device is not immediately visible, especially when looking at the schematic of the circuit alone. This is not strange, traditionally thermal design would usually be the last step when designing a circuit, or often completely omitted. When needed, it would usually end in selecting a large enough heatsink in order to satisfy the requirements for operating conditions.

As the power electronics technology improves and the market evolves leading toward devices with lower cost and higher performance, there is a trend toward miniaturization. This confines losses into smaller volumes, increasing the power loss density, and putting additional constraints on thermal design. This is especially the case with our converter integrated in the PV module. The environmental conditions, coupled with the electrical, spatial and technological limitations will impose significant restrictions when dealing with heat losses in the converter. For example, requirement for a low profile design prevents the use of conventional heatsinks cool the semiconductor devices and alternative paths for heat extraction and dissipation have to be found.

Moreover, with its presence and losses, the converter will change the temperature profile of the PV module, creating a hotspot on the place where it is mounted. While the converter may operate within its temperature limits, the operation and reliability of the PV module should not be compromised.

Based on abovementioned, the goals of this chapter are as follows:

- Modeling the thermal behavior of the PV module and the integrated converter in order to estimate the operating temperature and to test the effectiveness of the selected thermal management strategies,

- Identifying and selecting thermal management methods for the PV module integrated converter in order to efficiently extract and dissipate the losses from its active and passive components,
- Providing input for parameters from Chapter 4 and Chapter 5, power losses from the converter components, in order to provide output parameter for the final design of the converter in Chapter 7, the reached operating temperatures.

In this chapter, the thermal design and modeling of the PV module, the integrated converter, and their assembly will be presented. It will start with analyzing the PV module, to determine baseline temperature conditions for the module alone and any devices that should be added to the module. It will be followed by including the integrated converter with its loses to assess the impact of the converter on the PV module and vice versa. In the end, the converter will be analyzed on a PCB and component level, identifying thermal management methods to extract and dissipate the heat from its high power loss density parts.

6.2 Energy Balance and Heat Flows in PV Modules

Summarized from Chapter 4, we can say that the electrical output power of a PV module depends on:

- Solar radiation energy (irradiation) $\boldsymbol{G}$ [W/m^2] being absorbed in the PV module and transformed to electricity,
- Operating temperature $\boldsymbol{T}$ of the PV module, determined by environmental conditions, mounting configuration and PV module structure,
- Properties of the PV module, in the first place efficiency, dictated by the used technology.

The Sun's energy that reaches the PV module is only partially converted into electrical energy. One part of the module reaching irradiance is reflected back from the surface of the PV module and the remaining part continues its way through the front layers of the module until it reaches the active semiconductor layer. If the module is transparent, a transmitted component of the radiation will be also present. Under realistic conditions, reflective losses are typically up to a few percent average of the incoming irradiance, considering that the incident angle of light varies during the day [6-1]. Large research and development efforts are being made to increase the absorption of the light in PV modules, for example by structuring the PV cell surface [6-2]. Furthermore, only one part of the absorbed radiation is converted to electrical energy, while the rest is converted into heat. The PV module output electrical power is determined by efficiency and load profile. For typical tandem a-Si/µ-Si thin-film modules, the stabilized efficiency is in the range of 10% [6-3]. The efficiency decreases with increasing temperature, with output power having typically a thermal coefficient in the range of -0.2..-0.5%/°C.

Looking at how high the absorption coefficient is, being close to 100%, versus the efficiency being around 10%, one expects large amount of heat generated in a PV module. If not used, this heat is wasted and contributes only to the increase of temperature of the PV module. Alternatively, this heat can be used in photovoltaic-thermal (PVT) applications where the heat is actively extracted from PV modules and used for heating purposes [6-4].

Moreover, if the PV module does not operate at its MPP, the electrical energy meant to be consumed by a load will also be dissipated internally. In any case, the absorbed component of the solar irradiance that is not converted into electrical energy will generate the heat. The PV module exchanges its heat with the environment through heat transfer processes, which will be described in following sections. Depending on the way the generated losses are exchanged with the environment, or what is the thermal resistance from the PV module to the environment, the temperature pf the PV module will increase.

As it will be show, there are three components of the heat flow. Determining single components is difficult since they depend significantly on surrounding environmental conditions and the way the module is mounted. Nevertheless, we can identify the main processes and parameters that determine the energy balance and the module temperature (Figure 6.1):

- Environmental conditions, that is, module reaching irradiance ambient temperature and wind,
- Properties of the PV module, that is, photovoltaic conversion efficiency and optical properties,
- Balance of heat flows, determined by thermal processes,
- Electrical characteristic of the load, or the power being extracted.

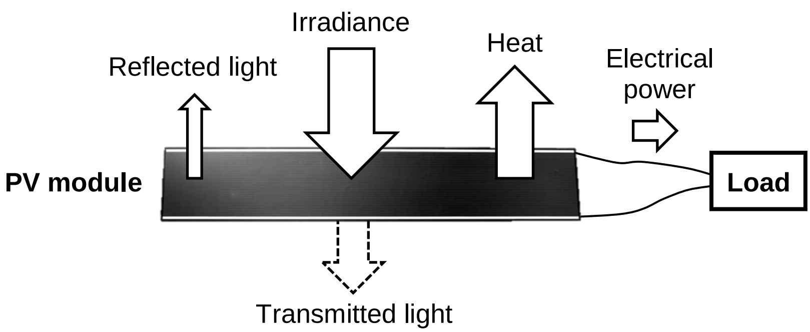

Figure 6.1: Energy balance in PV module

Except for the heat flows, the other parameters and processes are usually already known. The relation between the generated heat and the operating temperature will however depend on many factors, and needs to be determined. Moreover, if a converter is to be integrated into the PV module, it will introduce additional losses and disturb the heat exchange between the PV module and its surroundings, changing its temperature profile. Therefore, to predict the temperature profile of the PV module and the integrated converter, all individual heat flows have to be identified and estimated.

6.3 Thermal Modeling of a PV Module

Before modeling the whole system, including the PV module and the integrated converter, in this section we will first look into the thermal behavior of the PV module alone. This will give us a feeling of typical operating temperatures of the PV module, which would then be the "ambient" temperature for the integrated controller. The thermal behavior will first be modeled analytically, which gives simple relations between the environmental conditions and the PV module properties on one side and the reached temperatures on the other. The results will be confirmed by FEM analysis, which is, although not as quick and illuminating as analytical modeling, more accurate and can be used to verify the modeling approach.

In the literature, various thermal models for PV modules have been developed in order to predict the temperature and assess its impact on performance. In general, the thermal modules can be divided into two groups: explicit and implicit. Explicit mathematical models predict the PV module temperature directly from input data. Implicit models give a set of equations where certain parameters depend on the operating temperature. Therefore, iterations are required to solve those models.

A group of simple explicit thermal models are based on nominal operating cell temperature (NOTC) data, which are usually provided by manufacturers. NOCT is defined as the temperature reached by open circuited cells in a module under the solar irradiance of 800 W/m^2, ambient temperature of 20°C, wind speed of 1 m/s, and with PV modules mounted at 45° tilt with its back side open. These operating conditions are more realistic then those defined by standard test conditions (STC) for modules. As an example, Ross thermal model [6-1] predicts the temperature $\boldsymbol{T_{cell}}$ according to:

$$T_{cell} = T_a + G \cdot \frac{NOCT - 20}{800} \tag{6.1}$$

where $\boldsymbol{T_a}$ is the ambient temperature, and $\boldsymbol{G}$ is the solar irradiation [6-5]. A typical NOCT for conventional modules lies between 40°C and 50°C. Already here we can see that a PV module can operate at high temperatures under worst conditions, when the irradiation is high and there is no wind. Looking at the datasheets, the maximum operating temperature of PV modules is typically below 100°C, meaning that there is little thermal headroom left for any additional circuit integrated into the PV module.

Furthermore, we can distinguish between static and dynamic thermal models. Static, or steady state, thermal models assume instantaneous response of the PV module temperature to the changing conditions, neglecting the thermal masses. Dynamic models take into account PV module thermal masses. They require more detailed modeling of the PV module structure and layers, and are in general harder for computation. A comprehensive review of thermal models for PV modules is given in [6-6].

The choice of the model depends on needed accuracy. Some of the models in the literature are application specific, corresponding to fixed scenarios or locations. The majority of thermal models correspond to conventional PV modules, mounted on a rack with its back side open for ventilation (Figure 6.2a). In case of flexible PV modules, a supporting structure is needed, and the simplest way to mount them is directly on a free surface, such as walls or roofs (Figure 6.2b). In this case, the back side of the PV module is blocked, meaning that the majority of heat losses will have to be dissipated on the front surface of the PV module. Mounting the PV module on an additional supporting structure to provide backside cooling would defeat the advantage of lower installation cost.

(a) (b)

Figure 6.2: Typical mounting configuration for (a) conventional, (b) flexible PV module

Moreover, the integrated converter will make the temperature distribution of the PV module non-uniform with its presence and losses. The thermal model should correctly take this non-uniformity of heat losses into account. For our purposes, we will therefore make a new thermal model to take into account the presence of the integrated converter.

6.3.1 Analytical Model of the PV Module

A heat exchange takes place whenever there is a temperature difference between a PV module and its surroundings. The heat flows from a hotter to a colder body through three processes [6-7]:

- **Thermal conduction** is the transfer of heat by direct contact due to microscopic collisions of particles and movements of electrons within a solid, liquid or gaseous body.
- **Thermal convection** is the transfer of heat due to bulk movement of molecules within fluids, such as liquids and (in case of PV modules) gases. There are two types of convection flows:
    - Natural convection occurs due to temperature differences which affect the density which again affects buoyancy. As a consequence, the hot fluid, which gets less dense, is displaced by the cooler fluid. The flow can be:
        - Laminar, when fluids flow in parallel, with no disruption between layers,
        - Turbulent, when flow is characterized by chaotic changes in pressure.
    - Forced convection occurs when a fluid is forced to flow over the body surface. In case of PV modules this type of convection is caused by wind, or by forced air cooling in PVT systems.
- **Thermal radiation** is the transfer of heat by means of electromagnetic waves and occurs through a transparent medium or vacuum.

The distribution of heat flows from the PV module to its surrounding depends on the way the PV module is mounted. Some of the heat transfers mechanisms can also be neglected sometimes. For example, when mounting standard PV modules on frames, the conduction between the edges of the PV module and the frame can be neglected, since the PV module can be regarded as a thin plate.

The purpose of thermal modeling is to make a temperature prediction based on simple and usable set of equations. Instead of modeling the system down to molecular scale, we can lump together parts of the system with similar thermal properties into single elements. We can estimate the temperature distribution by dividing our system into finite number of lumped elements and setting the equations which describe heat flows between the elements and the environment. Different heat processes can be represented with an equivalent electrical circuit, where current sources represent heat flows, resistors represent thermal resistances and voltages represent temperatures, as shown in Figure 6.3. This electrical circuit can then be solved using conventional methods.

If we assume that our body of interest has uniform temperature distribution and thermal properties, we can represent it with only one point. This is a common practice in thermal design to get a simple yet sufficiently accurate thermal model of simple bodies, for example for a heatsink.

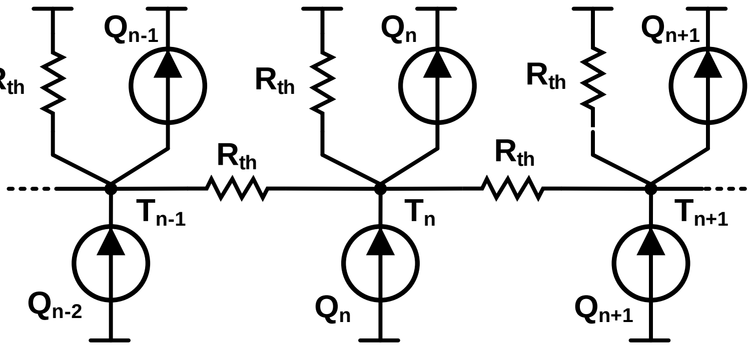

Figure 6.3: Equivalent electrical representation of thermal processes between lumped parts of a system

We will consider our reference PV module from Chapter 4, without the converter, and make the following assumptions:

- The PV module is attached to a vertical or horizontal supporting structure with certain thermal resistance and without air gap between them,
- We will regard the PV module as a two-dimensional body, considering that the thickness of the PV module of around 0.5 mm is much smaller than the surface area of 0.3x1 m.
- Assuming the uniform temperature distribution, we will represent the PV module as a single lumped element.

The first step in building the thermal model is to identify and model the individual heat flows.

Heat Losses

A large part of the absorbed irradiation, typically 80-90%, that is not converter to electricity will be dissipated as heat. If we assume that the PV module operates at MPP, the amount of heat losses $\boldsymbol{Q_{loss}}$ can be determined as:

$$Q_{loss} = G \cdot A_{mod} \cdot (1 - \eta_{mod}) \tag{6.2}$$

where:

- $\boldsymbol{G}$ is solar irradiation,
- $\boldsymbol{A}$ is the PV module surface,
- $\boldsymbol{\eta}$ is the efficiency of the PV module.

It should be noted that the efficiency depends on temperature, and to a lesser extent to irradiation $\boldsymbol{G}$. However, we will consider it to be constant, since the decrease of efficiency will not affect the amount of losses significantly.

Conduction Heat Flow

The conduction heat flow will occur between the PV module and the supporting structure. For the worst case conditions, we can assume a low thermal conductivity structure, so that the conduction heat losses can be neglected. In reality, there is a relatively thick layer of glue with relatively low thermal conductivity, used to attach the PV module to the surface. The equivalent thermal resistance will also largely depend on the thermal properties of the supporting structure. In general, the thermal resistance R_{cond} between two points can be expressed with:

$$R_{cond} = \frac{1}{k}\frac{l}{A} \tag{6.3}$$

where:

- k is the thermal conductivity of the materials along the heath path,
- l is the length of the heath path,
- A is the cross section area of the heath path.

Convection Heat Flow

The convection heat flow will, in case of our PV module, occur between the front surface of the PV module and the surrounding air. We will neglect the presence of wind and consider only natural convection. In the equivalent thermal model, convection heat flow on the surface with the area A is represented with the thermal resistance R_{conv}:

$$R_{conv} = \frac{1}{h \cdot A} \tag{6.4}$$

where h is the convective heat transfer coefficient which depends on temperature and geometry. As noted, we will consider two orientations of the PV module - vertical and horizontal. The heat transfer coefficient h for the surface can be expressed as:

$$h = \frac{Nu \cdot k}{\delta} \tag{6.5}$$

where:

- k is the thermal conductivity of air (0.026 W/(m·K)),
- δ is characteristic length of the surface,
- Nu is the Nusselt number given with:

$$Nu = CRa^{n} \tag{6.6}$$

where:

- C and n are coefficients that depend on the orientation of the surface,
- Ra is the Rayleigh number.

For an isothermal vertical surface the Nusselt number is given with:

$$Nu = \begin{cases} 0.59 \cdot Ra^{1/4}, & 10^4 < Ra < 10^9 \\ 0.1 \cdot Ra^{1/3}, & 10^9 < Ra < 10^{13} \end{cases} \tag{6.7}$$

and the characteristic length $\boldsymbol{\delta}$ is equal to the surface height $\boldsymbol{L}$.

$$\delta = L \tag{6.8}$$

For an isothermal horizontal upward-oriented surface the Nusselt number is given with:

$$Nu = \begin{cases} 0.54 \cdot Ra^{1/4}, & 10^4 < Ra < 10^7 \\ 0.15 \cdot Ra^{1/3}, & 10^7 < Ra < 10^{11} \end{cases} \tag{6.9}$$

and the characteristic length $\boldsymbol{\delta}$ is equal to the surface area divided by its perimeter:

$$\delta = \frac{L \cdot W}{2(L+W)} \tag{6.10}$$

where $\boldsymbol{L}$ and $\boldsymbol{W}$ are surface length and width respectively. The Rayleigh number $\boldsymbol{R_a}$ is given with:

$$Ra = \frac{g\beta(T_{mod} - T_a)\delta^3}{v^2} Pr \tag{6.11}$$

where:

- $\boldsymbol{g}$ is the gravitational acceleration (9.81 m/s^2),
- $\boldsymbol{\beta}$ is the coefficient of volume expansion given with:

$$\beta = \frac{1}{T_f} = \frac{2}{(T_{mod} + T_a)} \tag{6.12}$$

- $\boldsymbol{T_{mod}}$ and $\boldsymbol{T_a}$ are the PV module and ambient temperature respectively,
- $\boldsymbol{v}$ is the dynamic viscosity (16.5×10^{-6} m^2/s for air),
- $\boldsymbol{Pr}$ is the Prandtl number (0.7 for air).

Radiation Heat Flow

The radiation heat flow will occur between the front surface of the PV module and the environment, and should not be neglected since its share in heat transfer is in a similar range as the convection. In our case the heat flow occurs from the PV module on one side and the sky, ground and other structures on the other side. If we approximate the environment around the PV module with only sky and flat, featureless ground, the radiation heat flow can be expressed as:

$$Q_{rad} = \sigma A \varepsilon_s \left(\varphi_{sky}\left({T_{mod}}^4 - {T_{sky}}^4\right) + \varphi_{gr}\left({T_{mod}}^4 - {T_{gr}}^4\right)\right) \tag{6.13}$$

where:

- $\boldsymbol{\sigma}$ is Stefan-Boltzmann constant (5.67×10^{-8} W/(m^{2}K^4)),
- $\boldsymbol{A}$ is the PV module surface area,
- $\boldsymbol{\varepsilon}$ is emissivity of the PV module surface, typically assumed to be 0.9,
- $\boldsymbol{T_{mod}}$, $\boldsymbol{T_{sky}}$ and $\boldsymbol{T_{gr}}$ are the PV module, sky and ground temperature respectively,
- $\boldsymbol{\varphi_{sky}}$ and $\boldsymbol{\varphi_{gr}}$ are the view factors which depend on the PV module orientation:

$$\left(\varphi_{sky}, \varphi_{gr}\right) = \begin{cases} (0.5, 0.5) & \text{for vertical surfaces} \\ (1, 0) & \text{for horizontal surfaces} \end{cases} \tag{6.14}$$

The ground temperature $\boldsymbol{T_{gr}}$ can be assumed to be equal to the ambient temperature $\boldsymbol{T_a}$. The sky temperature $\boldsymbol{T_{sky}}$ is given with [6-8], and is shown in Figure 6.4 for a range of ambient temperatures. We can see that the sky is “colder” than the ambient, and the radiation heat exchange will be stronger between the PV module and the sky.

$$T_{sky} = 0.0552 \cdot {T_a}^{3/2} \tag{6.15}$$

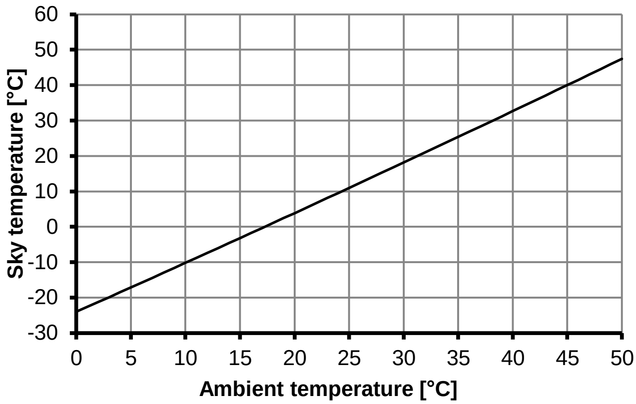

Figure 6.4: Relationship between the ambient and the sky temperature

PV Module Thermal Model

With all the heat transfers known, we can represent the thermal model of the PV module with an equivalent electrical circuit [6-7], as shown in Figure 6.5.

Solving for the circuit we can obtain the PV module temperature:

$$T_{mod} = T_a + (R_{conv} || R_{cond})(Q_{loss} - Q_{rad}) \tag{6.16}$$

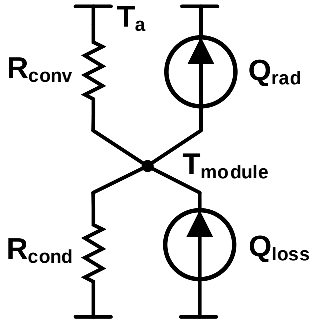

Figure 6.5: Simple thermal model of a flexible PV module

It should be noted that, according to the equations above, some of the circuit elements depend on temperature. Therefore, multiple iterations have to be performed when solving for the PV module temperature.

6.3.2 Evaluation of the Simple PV Module Thermal Model

Having the thermal model of the PV module, we can determine the operating temperature under various conditions. The goal here is to see how the losses generated in the PV module will set its temperature. Looking back at the thermal model of the PV module in Figure 6.5, all the parameters can be easily determined by the PV module orientation and its characteristics, in the first place power losses. However, the heat flow from the PV module to the supporting structure and beyond depend primarily on the thermal characteristics of the supporting structure, modeled with the thermal resistance R_{cond}. This is unknown a priori, however, we can consider some specific cases:

- **Worst case condition** – The PV module is mounted on a supporting structure with high thermal resistance, such that we can neglect the conduction heat flow and R_{cond}, and any dynamics due to the low mass of the PV module per surface area.
- **Best case condition** – The PV module is mounted on low thermal resistance, high thermal capacity structure with the temperature equal to ambient temperature, for example. This is a trivial case and the PV module temperature will be close to the temperature of the structure/ambient, and determined mostly by the thermal interface between the PV module and the supporting structure. To be completely accurate, the thermal dynamics might be also considered, taking into account the thermal capacities of the supporting structure and time dependence of the irradiation
- **Open back side** – The PV module is mounted on a thin supporting structure with open back side so that convection is present on the back side as well. In this case R_{cond} is equal to the R_{conv} in case of the vertical orientation and slightly lower in case of the horizontal orientation of the PV module.

In all previous conditions, it is assumed that there is no wind, otherwise, convective thermal resistance $\boldsymbol{R_{conv}}$ can be significantly lower. Figure 6.6 shows the PV module temperature $\boldsymbol{T_{mod}}$ as a function of irradiation $\boldsymbol{G}$ for different cases of conductive thermal resistance $\boldsymbol{R_{cond}}$ and different PV module orientations. On the same graphs, the temperatures obtained using computer simulations and FEM modeling are given. For our reference PV module from Chapter 4, it was assumed that there are no reflective losses and that the ambient temperature is 25°C.

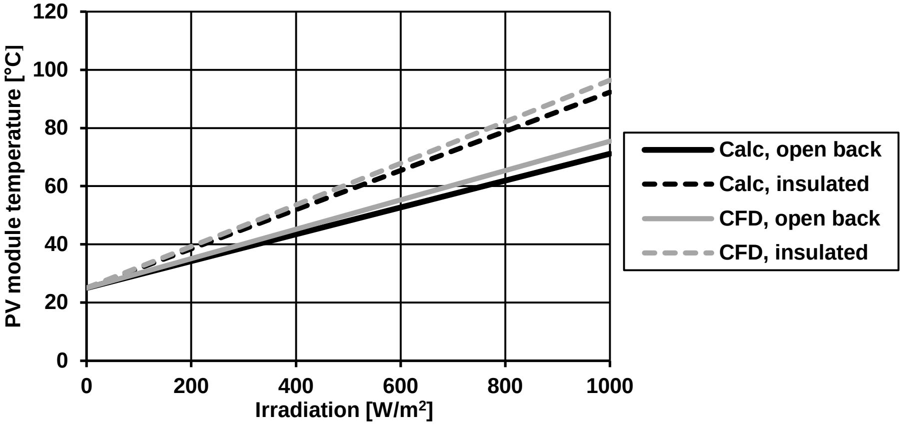

Figure 6.6: PV module temperature as a function of irradiance for vertical orientation

As we can see from Figure 6.6, when the supporting structure has high thermal resistivity, the PV module temperature can reach high temperatures, up to 50°C, leaving not much headroom for additional temperature rise. Having a heat path on the back side of the PV module, either by allowing airflow or by having thermally conductive supporting structure, lowers the temperature significantly. At the same time we can see that the analytical model agrees sufficiently well with the results obtained using FEM/CFD analysis, with slight overestimation of temperatures. It should be noted that the worst case conditions are not realistic for vertical orientation, since the maximum considered irradiance of 1000 W/m^2 will never happen on a vertically mounted PV module.

It is interesting to modify Figure 6.6 and see the dependence of the PV module temperature as a function of heat loss density present on the PV module. This can be used to get the feeling how much loss we can allow in total per certain area before reaching the maximum PV module operating temperature. In the previously considered cases, the source of heat losses was the PV module itself. If there is a converter in the PV module, it will also contribute to total losses with its own heat losses due to its limited efficiency. Figure 6.7 show the temperature curves for one abovementioned case, but now as a function of heat loss density.

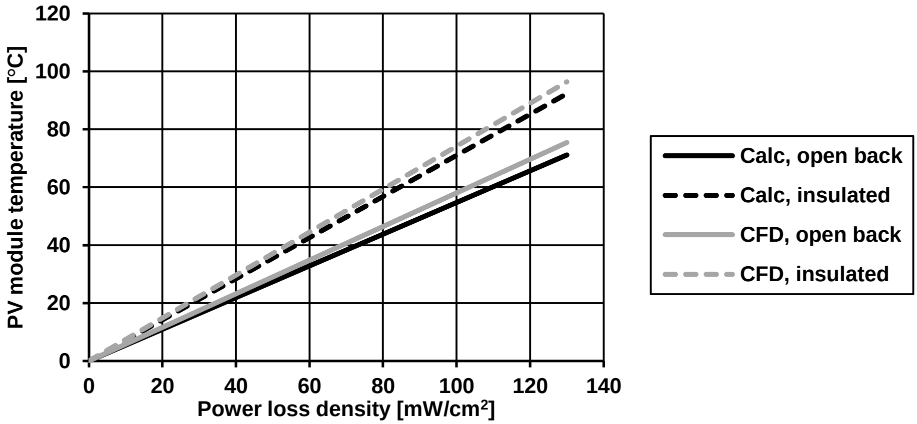

Figure 6.7: PV module temperature as a function of heat loss density for vertical orientation

From Figure 6.7 we can see that, at ambient temperature and under worst case mounting conditions, we can allow up to 130 mW/cm^2 before the PV module temperature reaches the maximum allowed 90°C. This translates to the additional 40 mW/cm^2 of heat losses external to the PV module, on top of the 90 mW/cm^2 coming from the PV module itself.

The above discussion assumes uniform losses over the whole surface of the PV module. In reality when adding a converter a local hotspot will be created, and to determine the reached temperatures, the thermal model should also take into account the dimensions, properties and position of the integrated converter within the PV module.

6.4 Thermal Modeling of the PV Module Integrated Converter

Looking at the overall efficiency of the PV module and the integrated converter, the converter efficiency is not very important, since the PV module efficiency is much lower. Change in PV module efficiency from 10% to 9%, caused for example by aging or shading, will be equivalent to the drop of converter efficiency from 95% to 85%. However, from the thermal point of view, every percent of the efficiency will bring savings through thermal management, and lessen the thermal influence of the converter on the PV module. Figure 6.8 shows again the concept of the integrated converter and the cross-section of the complete assembly. With its losses, the converter will contribute to the losses generated in the PV module, and create a hot-spot on the PV module surface. If the total heat loss density is large enough locally, it can lead to damage of the PV module or the converter components. It is therefore important to estimate the temperature distribution for all parts.

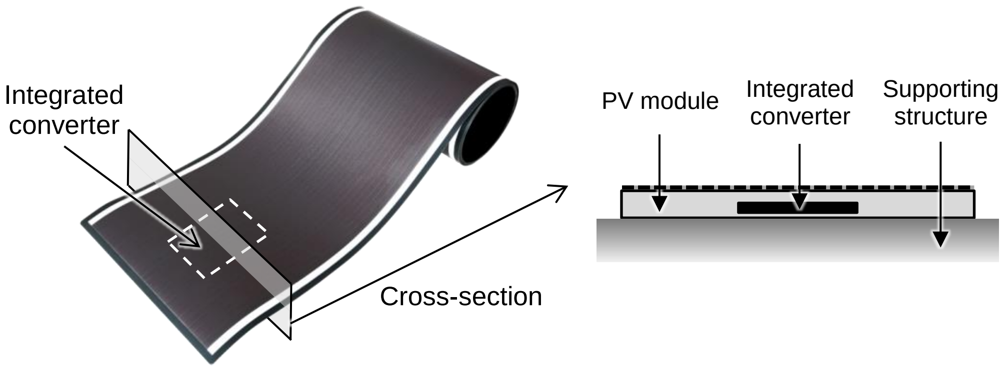

Figure 6.8: Thermal coupling between the PV module and the integrated converter

Since the height of the converter is limited to approximately 1 mm, the thermal management for the converter is limited vertically. Therefore, the heat should be spread laterally over a certain area until the total power loss density is within the safe limits. In principle, there are no limits in how much of the surface area of the PV module can be used for spreading the heat losses from the integrated converter. However, as it will be shown later, spreading the heat from small footprint components over a larger area requires lower lateral thermal resistance.

For a fixed power/area PV module, it is possible to replace a single converter with a multiple lower power converters. In that way we can spread the heat loss sources, instead of spreading the heat losses from a single source, as shown in Figure 6.9. This also increases the granularity of DMPPT. However, multiplying the number of converters per area of the PV module increases the cost, since we are multiplying the component count, and the cost of power devices do not scale down linearly with power ratings. Moreover, efficiency of a converter decreases in general with its power level. Another possibility is to mount the converter outside the active area of the PV module, where there are no losses due to photovoltaic conversion. That area can be

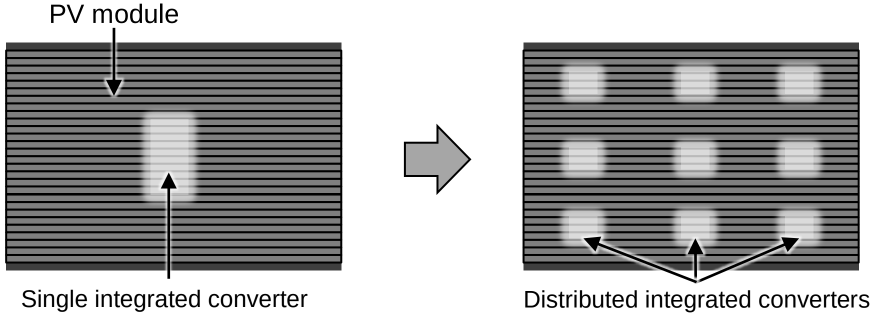

Figure 6.9: Distributing heat losses over a large area of the PV module with distributed converters

coated with a reflective film which prevents absorption of light, allowing only losses from the converter to be dissipated. In this thesis, we will consider a single converter with as large as possible power level, and see which conditions should be met in order to spread the heat losses sufficiently, in order to keep the temperatures within limits. Table 6.1 lists the maximum operating temperatures for the PV module and for different parts of the integrated converter.

Table 6.1: Maximum operating temperatures for different components and materials for the PV module and the integrated converter

	Maximum temperature
PV module	90°C
Flexible PCB	>200°C
Magnetic materials	90°C
Passives	125°C
Transistors/Diodes	125..150°C
Other actives	125°C

6.4.1 Analytical Model of the PV Module and the Integrated Converter

In the following analysis, a more detailed thermal model based on the prototype of the converter will be given [6-9]. Figure 10a shows the topology of the LOV converter from Chapter 4. Again, since the converter has a very low profile, the equivalent thermal model is represented as a single layer body, but with different thermal properties in different directions. Figure 10b shows the position of the main heat loss sources in the circuit and the amount of generated losses when the converter is operating under the maximum power level. As expected, the majority of losses come from the boost stage and the inductor. The marked areas are represented as nodes in the equivalent thermal resistance network shown in Figure 10c.

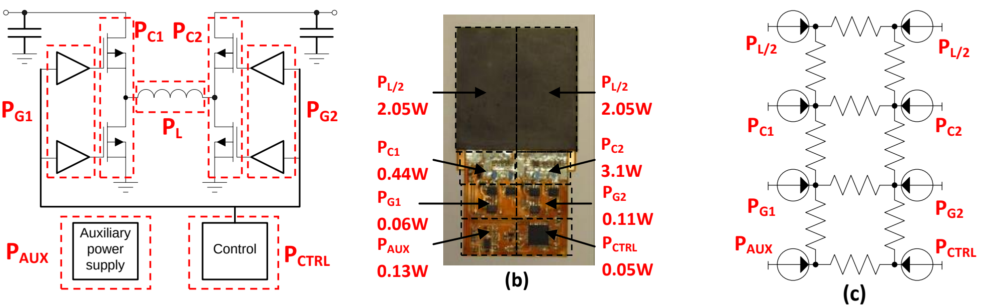

(a) (b) (c)

Figure 6.10: Converter thermal modeling: (a) Schematic, (b) Main heat sources, (c) Thermal model

A typical PV module consists of many layers with different thicknesses and thermal properties [6-10], but considering a very low profile of the PV module compared with its width and length, the whole module can be represented as a single layer body with different directional thermal conductivities. The obtained converter model is further used to model the thermal behavior of the PV module. For the area of the module where the converter is mounted the same nodes that were chosen for the converter thermal resistor network will determine the position of nodes in the PV module thermal network. As for the rest of the module, remaining areas are represented with only one node each, since their temperature will always be lower than the hot-spot temperature and therefore are not critical (Figure 6.11a). Since all PV module construction and material details can be entered as model parameters, it is also easy to adapt the thermal model to different PV modules.

Finally, the supporting structure for the flexible PV module has to be taken into account as well. In the following analysis two types of supporting surfaces are considered, one with a low thermal conductivity that corresponds to a worst case mounting conditions and one that allows the convection heat flow on the back side of the PV module. The supporting structure is modeled using the same nodes arrangement as for the PV module. To obtain the complete thermal model, first the PV module, converter and supporting structure thermal models are combined, and after that the heat sources that represent radiation heat transfer together with thermal resistors that represent convection heat flow have to be added. This is illustrated in Figure 6.11b, with the cross section of the complete thermal model.

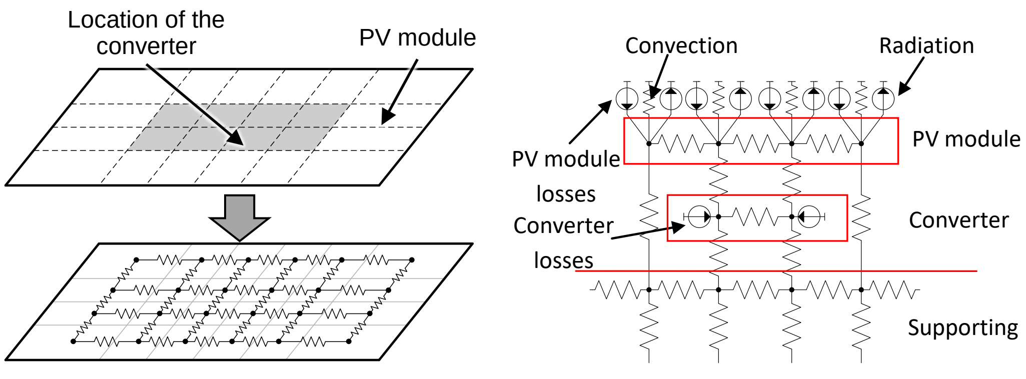

(a) (b)

Figure 6.11: (a) PV module thermal model, (b) Cross-section of the complete model

The complete thermal model that includes the PV module and converter thermal network, supporting structure and ambient conditions defines a set of linear equations with one equation for each node. This set of equations is formed and can be solved in the same way as the electrical circuits in nodal analysis. Translated into the linear matrix equation form this system can be represented with:

$$Q = G \cdot \Delta T, \quad Q = \begin{bmatrix} Q_1 \\ Q_2 \\ . \\ . \\ Q_n \end{bmatrix}, \quad \Delta T = \begin{bmatrix} \Delta T_1 \\ \Delta T_2 \\ . \\ . \\ \Delta T_n \end{bmatrix}, \quad G = \begin{bmatrix} \sum_k G_{1k} & G_{12} & . & . & G_{1n} \\ G_{21} & \sum_k G_{2k} & . & . & G_{2n} \\ . & . & . & . & . \\ . & . & . & . & . \\ G_{n1} & G_{n2} & . & . & \sum_k G_{nk} \end{bmatrix} \tag{6.17}$$

where Q is the vector of heat sources, ΔT is the temperature difference vector and G is the matrix of thermal conductivities. The previous matrix equation can be implemented as a spreadsheet in computational software programs such as Mathcad or represented as an electrical circuit, transforming the thermal values into their analog electrical values and using circuit solvers such as SPICE. In either case the resulting node temperatures can be obtained performing the matrix inversion:

$$\Delta T = G^{-1} \cdot Q \tag{6.18}$$

In the end, several iterations have to be performed until the node temperatures start to converge, since the convection heat transfer coefficients, radiation heat exchange and the PV module efficiency all depend on temperature.

6.4.2 Validation of the Complete PV Module Thermal Model

To validate the developed thermal models, the experimental setup shown in Figure 6.12a was used. In order to reach the full level of irradiance (1000W/m^2), the tilt angle of the setup was set to approximately 45°. This is also a typical mounting angle for roof mounted PV modules at the tested location. For practical reasons only a part of the PV module was tested (1 m by 0.3 m), but since the area of interest is around the converter and thus small in comparison to the PV module surface, it is not necessary to analyze the whole PV module.

The thermal behavior of the system depends significantly on the type of supporting structure, therefore two different scenarios were considered. In the first scenario the PV module and the converter were mounted on a surface with a very low thermal conductance (styrofoam k=0.06 W/(m·K)) which corresponds to the worst case mounting conditions such as well insulated walls. In this way almost all generated heat is transferred to the front side of the PV module. In the second scenario, the PV module and the converter are mounted on a thin plastic plate (2 mm, k=0.2 W/(m·K)), which allows the heat to flow and convection to take place on the back side of the plate. This scenario could correspond to the mounting conditions where the PV module is attached to the glass, for example a window. The respective thermal models for both scenarios are shown in Figure 6.12b and Figure 6.12c.

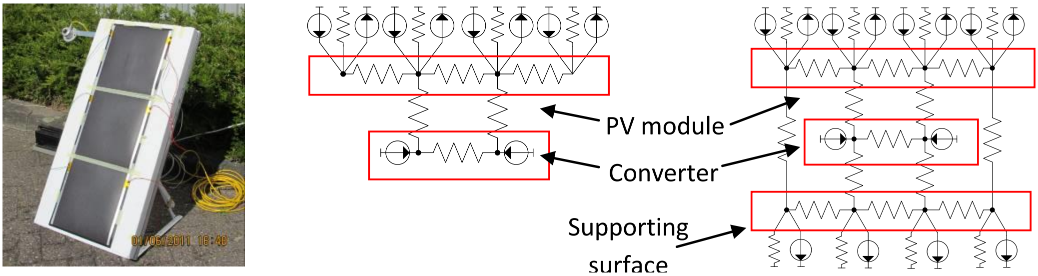

(a) **(b)** **(c)**

Figure 6.12: (a) Thermal models of the system with: (a) Low and (b) High thermal conductivity surface

The goal of the thermal models is to predict reached temperatures in the system for different mounting conditions. Furthermore, it is important to determine where the temperature will first reach its limits. In the following analysis the PV module operating temperature was limited to 100°C while the maximum operating temperature for the converter components (used integrated circuits, switches, passives and magnetic material for the inductor) is limited to 125°C. As already mentioned, the converter is operated at the full PV module power with heat losses shown in Figure 6.10b. Since only a part of the PV module is used, the converter is powered via external power supply, while the maximum power point tracking of the mounted PV module is performed by another DC-DC converter.

The results of thermal measurements for both types of supporting structures are shown in Figure 6.13. Obtained measurement results were also compared to the results obtained using FEM analysis. The ambient temperature was approximately 21°C while the irradiation level was slightly above 1000 W/m^2, which is very close to standard test conditions for PV modules. Under these conditions, the heat generated in the PV module is in the range of 80-85 mW/cm^2. On top of these losses the PV module has to deal with the additional 110 mW/cm^2 heat flux coming from the integrated converter when operated at full power level. It can be seen that in case of the low thermal conductivity supporting surface the maximum operating temperature for the PV module was already reached before reaching the maximum power level in the converter components (Figure 6.13a). The reason for this is relatively low converter efficiency of approximately 92% and thus high losses concentrated on a small area. In the case of a high thermal conductivity surface, the converter can still be operated under the maximum power level, since the maximum reached temperature is below the operating limits of the PV module (Figure 6.13b), but the reached temperature could be even higher if the ambient temperature increases. Meantime, the component temperatures are below their operating limits with the calculated maximum temperature of 112°C reached in the boost stage, which makes the hot-spot temperature on the PV module surface the limiting factor in the system design.

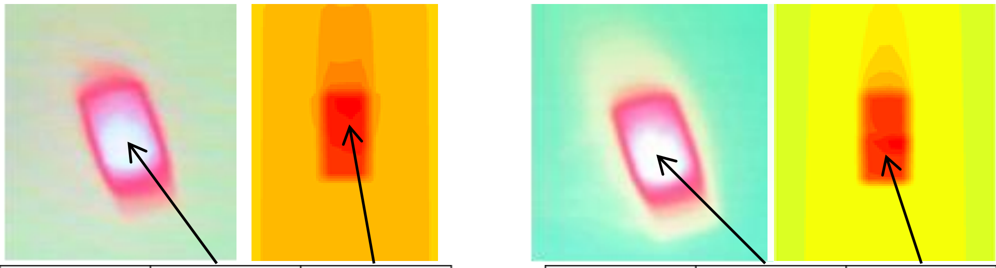

Analytical	Measured	FEM
103°C	97°C	105°C

(a)

Analytical	Measured	FEM
103°C	97°C	105°C

(b)

Figure 6.13: Analytical, experimental and CFD simulation results for the setup with supporting surface with: (a) Low and (b) High thermal conductance

In both cases, the results obtained using the analytical model coincide well with the measurement results and the results obtained using FEM simulations. From the previous results it can be concluded that the considered converter cannot be safely used for PV module integration without taking the additional measures. One obvious solution is to improve the converter efficiency which would decrease the heat flux density added to the PV module. Considering the case from Figure 6.13a, the efficiency should be improved from 92% to 97% in order to keep the hot-spot temperature in safe area. It can be shown that this would also further decrease the hot spot temperature for the scenario in Figure 6.13b by 12°C.

6.5 PCB and Component Level Thermal Modeling for PVMIC

The thermal model of the converter presented in the previous sections assumes that the heat losses are uniformly distributed over their respective areas. In order to make the model valid, the heat generated in the thermal nodes of the model has to be uniformly spread over their respective areas. For some model elements, additional measures have to be taken in order to spread the heat. In general, in case of the PVMIC we can divide the heat loss components into two types:

- **Area-like power loss sources** with the footprint area equal to their respective area in the thermal model. These are the power inductor and the PV module.
- **Point-like power loss sources** which are all the components with the footprint area smaller than their area in the thermal model. These are the power transistors and diodes, as well as the other small passive and active components.

For the area-like power loss sources, the heat is already spread over the area that is joined to them in the thermal model. Therefore, as for the thermal behavior, they are modelled correctly. For the point-like power loss sources we need to provide that the heat is extracted and spread as much as possible uniformly over the adjoined area considered in the thermal model.

6.5.1 Thermal Management Strategies for Heat Extraction

Spatial requirements for low profile and flexibility of the integrated converter rule out the use of conventional heatsinks to extract and dissipate the heat from power loss components. Instead, the existing parts and elements will have to provide the heat path or alternative thermal structures have to be considered. In general, we can identify three groups of structures used to extract and spread the heat:

- **Device packaging** provides heat path from the device junction to a metal pad which can then be connected thermally to a heatsink or the PCB.
- **PCB** can be used to spread the heat from the component pads over an area larger than the component’s footprint.
- **Additional thermally conducting layers** can be added to the converter to spread the heat outside of the PCB area.

Device Packaging

The first part of the path that heat has to cross is through the device package, from the device junction to the device case or leads. For high power components, a low thermal resistance is desirable to minimize the temperature rise caused by losses. However, low thermal resistance of the package alone does not guarantee efficient heat extraction under all conditions. As it will be discussed later, the size of the device, or more precise the device footprint, will affect the effectiveness of heat spreading.

Figure 6.14 shows a few examples of power transistors and their packages. The shown devices are similar in voltage and current ratings – 100 V and approximately 40-50 A. The first two examples are ubiquitous TO220 and DPak packages used for standard through-hole and SMD power components. The third example is the thermally enhanced DirectFET package which enables double sided cooling. The last two examples are GaN devices mentioned back in Chapter 5, with their specific packages which also can utilize double sided cooling. In Figure 6.14, typical thermal resistances are shown, with $\boldsymbol{R_{th\_jc}}$ being thermal resistance from junction to case, and $\boldsymbol{R_{th\_jpcb}}$ being thermal resistance from junction to pads or PCB.

In this thesis, GaN transistors from EPC were employed and will be used in the following section when considering the thermal model. Although having thermal resistances comparable to other packages, the very small size of LGA flip-chip package will severely limit the effectiveness of heat spreading, as it will be shown.

Package	TO 220	D-Pak	DirectFET	GaN*PX* (PCB)	LGA flip-chip
R_{th_jc} [K/W]	1	-	1.4	0.5	1
R_{th_jpcb} [K/W]	-	1	1	5	2

Figure 6.14: Some examples of packaging for power transistors with typical thermal resistances

PCB as Part of Thermal Management

When no additional space is available for the thermal management, the existing PCB can be used as a part of the thermal management. This also lowers the cost, especially if low power devices are used when the standard FR4 PCB can handle the amount of generated losses. Copper possesses excellent thermal properties, however only one or few thin layers are available to conduct the heat, which limits the amount of losses that can be handled, and spread parallel to the PCB. Moreover, standard PCB substrates have high thermal resistance, meaning that the heat flow will be prevented in normal direction to the PCB. Therefore, two effective thermal resistances can be identified in the PCB of our PVMIC, horizontal R_{th_h} parallel to the PCB and vertical R_{th_v} normal to the PCB, as shown in Figure 6.15. Two measures can be taken to thermally reinforce the PCB:

- **Increasing the number and thickness of Cu layers** in order to decrease R_{th_h},
- **Increasing the number and density of thermal vias** in order to decrease R_{th_v}.

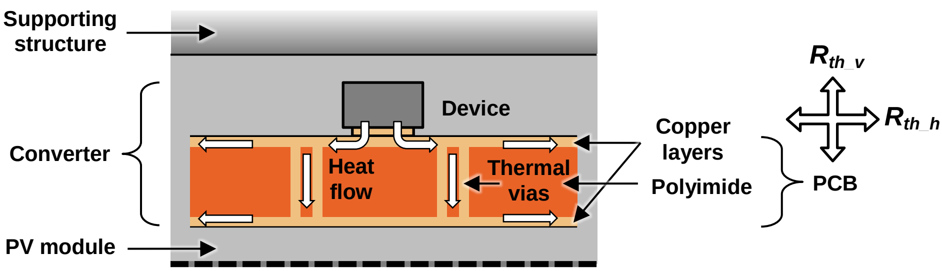

Figure 6.15: Heat extraction and spreading using PCB layers

Increasing the number of Cu layers will make the PCB design easier as well, but will increase the cost, especially in case of the flexible PCB. The thickness of the Cu layers is also limited by the technological constraints, since it becomes difficult to reliably make very small footprints for devices with very small pads. The number of vias on the other hand is not critical, and they can be applied only where needed.

Additional Thermally Conducting Layers

As previously noted, increasing the number and thickness of copper layers to increase the heat spreading capabilities of the PCB will increases the cost and may also affect manufacturability. Moreover, when dealing with small number of layers, thicker copper layers may not be effective solution since limited area may be free for use to spread the heat. Alternatively, additional copper layer external to the converter can be attached to the PCB, as shown in Figure 6.16. This copper layer would not have the limitations imposed by the used PCB technology, and would lead to a similar to the IMS PCB technology.

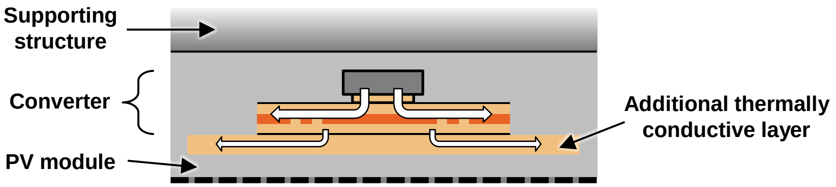

Figure 6.16: Heat extraction and spreading with additional thermally conductive layers

6.5.2 Analysis, Simulation and Test Results

In the following analysis, the EPC flip-chip package shown in Figure 6.15 will be considered, as these devices will be used when designing the converter power stage. The goal of the analysis is to determine the effective size of the PCB area used for heat spreading, depending on the parameters of the PCB such as copper thickness and number of layers.

Thermal Model

Changing the PCB parameters i.e. the number of copper layers, copper thickness, and the density of vias we can adjust the thermal resistance of the PCB and therefore its heat spreading abilities. However, as it will be shown, due to the low profile of the PCB and small footprint of the transistor tabs, there is a limit in minimum achievable horizontal thermal resistance R_{th_h} which will limit the usable size of the heat spreading area. Therefore, for fixed PCB construction parameters, we can find the maximum area that can be used for heat spreading, and vice versa, the PCB parameters needed to achieve a certain thermal resistance.

The considered structure of the transistor and the flexible PCB is shown in Figure 6.17, with n_{Cu} layers of copper with thickness d_{Cu}, creating a square heat spreading area with side a_{HS}. This arrangement will result in an effective thermal resistance R_{th_ja} from the device junction to the ambient.

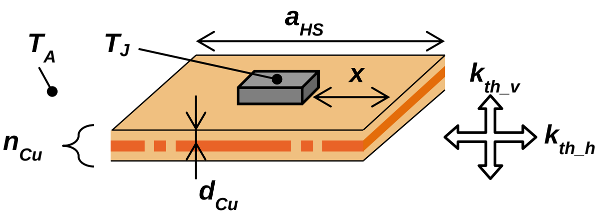

Figure 6.17: Parameters for PCB heat spreading

The above structure can also be modeled with thermal resistor network, but because the temperature profile throughout the PCB will have gradient we would need many elements. Therefore we will analyze this structure using FEM analysis. To make the analysis faster, it is possible to represent the PCB as a single body with heterogeneous thermal properties, with equivalent vertical and horizontal thermal conductivities k_{th_v} and k_{th_h}.

PCB as a Heat Spreader

In the following analysis, the PCB parameters will be changed to see their effect on the thermal resistance. As noted, the PCB is represented as a body with equivalent vertical and horizontal thermal conductivities k_{th_v} and k_{th_h} calculated from the PCB layer stack-up. It can be shown that the number of copper layer n_{Cu} will dominate in k_{th_h}, whereas the via density will dominate in k_{th_v}. As for the via density it is assumed that we have 100 vias/cm^2 with the following parameters: via diameter of 0.7 mm, with 35 µm copper plating and filled with solder. Considering that the copper and solder thermal conductivities are typically 380 W/(m·K) and 50 W/(m·K) which is much higher than the polyimide thermal conductivity of typically 0.5 W/(m·K), we can neglect the polyimide layers in flexible PCB when calculating equivalent PCB thermal conductivities k_{th_v} and k_{th_h}.

The equivalent thermal resistance for the structure shown in Figure 6.17 is obtained using FEM analysis. This thermal resistance is composed of two parts, the thermal resistance from the junction to the transistor pads R_{th_jp}, and the PCB thermal resistance R_{th_pa}. The former one is constant and depends on the device used. The later one is a function of PCB parameters. In our case for EPC2001C device, the junction to pad thermal resistance is R_{th_jp}=2 K/W.

Figure 6.18 shows the resulting equivalent junction-to-ambient thermal resistance R_{th_ja} for several scenarios with different number of copper layers and its thickness. Considering that the thermal conductivity of the polyimide layer is much lower than that of the copper layers and vias, in the end it is the total thickness of copper that determines the effectiveness of the PCB heat spreading.

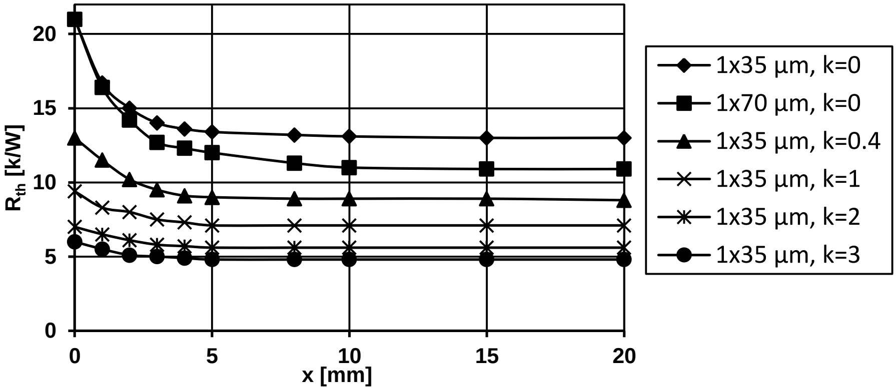

Figure 6.18: Equivalent junction-to-air thermal resistance as a function of the copper pad area for different scenarios of copper layers thickness and PCB thermal conductivities

Looking at the results, it can be seen that the thermal resistance from the device pad to the ambient $\boldsymbol{R_{th\_pa}}$ dominates in the total resistance $\boldsymbol{R_{th\_ja}}$, and can severely limit the thermal capabilities of the converter. And, as noted, the upper limit of total copper thickness in PCB is determined by cost and manufacturability of small pads required for the used GaN devices, at least for the component side layer. For the final design, double-sided flexible PCB with 70 µm copper layers was chosen for practical reasons and availability. For that case, the thermal profile of the PCB is shown in Figure 6.19, where the power dissipation was assumed to be 1 W.

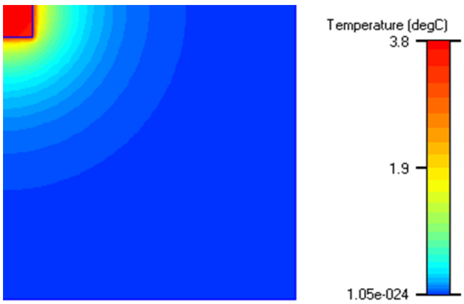

Figure 6.19: Temperature profile of the PCB heat spreader for the case of two 70 µm copper layers (symmetry was used for both dimensions)

The heat spreading effectiveness can further be enhanced by improving the thermal capabilities of the device packaging. The footprint of the device considered in the previous analysis measures approximately 6.5 mm^2, and the heat transfer from the junction to the PCB goes only in one direction through the package. If a metal can, for example in a form similar as used for DirectFET devices (shown in Figure 6.14), could be added to the package, this would improve the equivalent $\boldsymbol{R_{th\_ja}}$ both due to the lower resistance from the junction to PCB and due to the increased footprint area.

External Layers as a Heat Spreader

In the following analysis copper layers with two different thicknesses were attached between the PV module and the converter using the double sided adhesive thermal tape. By changing the in-plane thermal resistances in the analytical model as the consequence of the introduced conductive layers, it is possible to estimate the size of the heat spreading layer required to decrease the hot-spot temperature into the safer area. Figure 6.20b shows the calculated maximum reached hot-spot temperature versus the size of the heat spreading layer for two different heat spreading copper layer thicknesses (70µm and 140µm). Figure 6.20a illustrates the attached heat spreading layer.

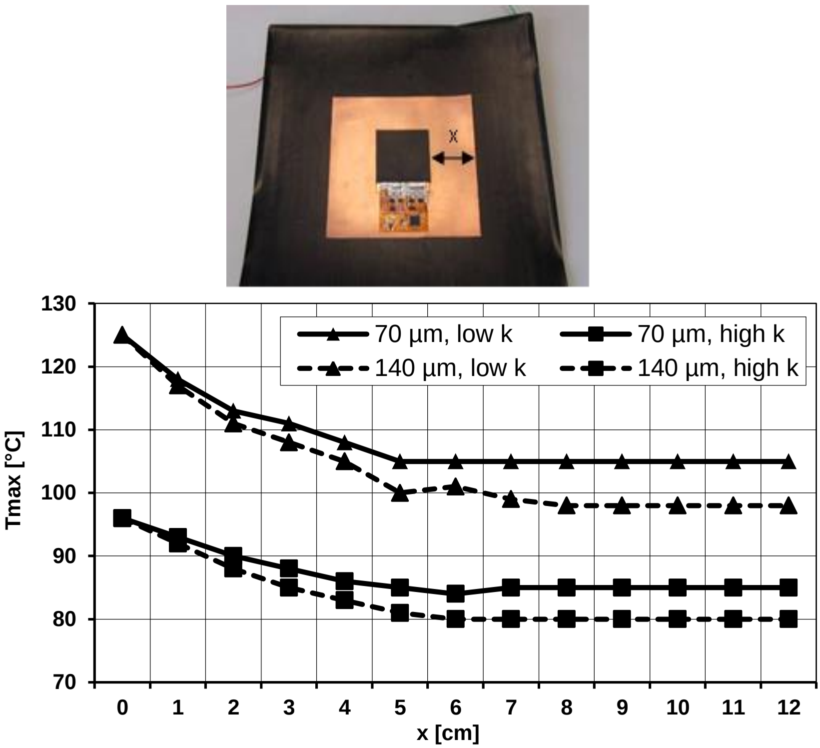

Figure 6.20: Measuring the effectiveness of the heat spreading layer for low and high thermal conductance supporting structure

As it can be seen, for the given heat spreading layer thickness there is an optimum size of the layer after which further improvements are negligible. Increasing the thickness of the heat spreading layer will further improve the system thermal behavior but will also add to the total converter thickness and will reduce the flexibility of the PV module. In the analyzed example, even after applying the thicker (140 µm) heat spreading layer, the overall design still stays fairly flexible.

To test the effectiveness of the heat spreading layer, as predicted by the previous analysis, the experimental setup was once again tested under the same conditions and for the both surface conductivity scenarios using the 16x16 cm2, 140 µm copper layer. Figure 6.21 shows the obtained measurement results and comparison with the analytical model and CFD simulations.

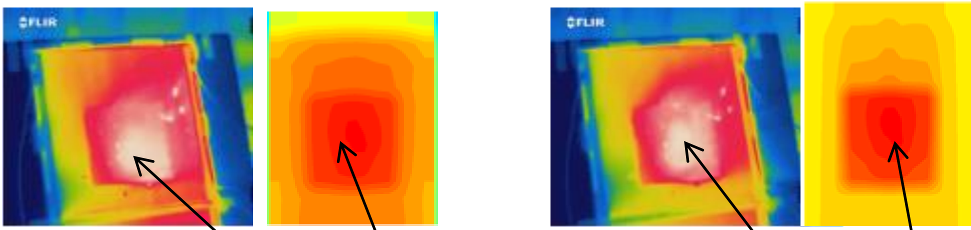

Analytical	Measured	CFD
98°C	93°C	95°C

(a)

Analytical	Measured	CFD
84°C	80°C	79°C

(b)

Figure 6.21: Measuring the effectiveness of the heat spreading layer: (a) High and (b) Low thermal conductance supporting structure

As it can be seen, the achieved maximum hot-spot temperature was decreased by more than 18°C in case of high conductivity supporting surface (Figure 6.21a). As for the scenario with low conductivity surface, the converter is now able to operate under the maximum power level (Figure 6.21b), but the reached hot-spot temperature is very close to the maximum allowed temperature due to the still high converter heat losses transferred to the ambient through the PV module. Nevertheless, the results obtained using the analytical thermal model still prove the effectiveness of the additional heat spreading layers. Once again, the result predicted by the model and Figure 6.20 matches well with the measurement and simulation results.

6.6 Conclusions

This chapter covers the thermal interaction between the PV module and the integrated converter, as well as the necessary conditions to keep the operating temperatures in the system within the safe limits. Thermal modeling of the system was performed in three steps, going from the PV module alone, through the converter as a whole unit, and within the converter for efficient heat spreading.

The thermal model of the PV module gives quick and sufficiently accurate baseline thermal conditions for its operation and for any circuits integrated within the module. The complete model takes into account the integrated converter and estimates the PV module temperatures based on operating conditions, the ways the PV module is mounted, and the amount of non-uniform heat losses coming from the converter. To make the model valid, the guidelines for necessary conditions are given in order to achieve sufficient heat spreading of losses within the converter.

The thermal design might be the most critical design area, since it depends on the way the PV module is mounted and the properties of the supporting structure for the PV module, which is not known in advance. Should this be a problem, alternative solutions for the converter integration are suggested.

6.7 References

[6-1] E. A. Sjerps-Koomen, E. A. Alsema, W. C. Turkenburg, "A Simple Model for PV Module Reflection Losses under Field Conditions," Solar Energy, Vol. 57, No. 6, 1996

[6-2] M. Zeman, O. Isabella, K. Jäger, R. Santbergen, S. Solntsev, M. Topic, J. Krc, "Advanced Light Management Approaches for Thin-Film Silicon Solar Cells," Energy Procedia, Vol. 15, 2012

[6-3] F. Meillaud, M. Boccard, G. Bugnon, M. Despeisse, S. Hanni, F. J. Haug, J. Persoz, J. W. Schuttauf, M. Stuckelberger, C. Ballif, "Recent Advances and Remaining Challenges in Thin-Film Silicon Photovoltaic Technology," Materials Today, Vol. 18, No. 7, 2015

[6-4] T. T. Chow, "A Review on Photovoltaic/Thermal Hybrid Solar Technology," Applied Energy, Vol. 87, No. 2, 2010

[6-5] R. G. Ross, "Interface Design Considerations for Terrestrial Solar Cell Modules," Photovoltaic Specialist's Conference, 1976

[6-6] A.Q. Jakhrani, A.K. Othman, A.R.H. Rigit, S.R. Samo, "Comparison of Solar Photovoltaic Module Temperature Models," World Applied Sciences Journal 14, 2011

[6-7] Ralph Remsburg, "Thermal Design of Electronic Equipment," CRC Press, 2001

[6-8] S. Krauter, "Solar Electric Power Generation," Springer, 2006

[6-9] M. Acanski, J. Popovic-Gerber, J. Ferreira, "Thermal Modeling of the Module Integrated DC-DC Converter for Thin-Film PV Modules," Power Electronics and Motion Control Conference (EPE/PEMC), 2010

[6-10] M. Acanski, J. Popovic-Gerber, J. Ferreira, "Thermal Modeling of the Module Integrated DC-DC Converter for Flexible Thin-Film PV Modules," European Conference on Power Electronics and Applications (EPE) 2011

Chapter 7 Integral Design, Optimization and Experimental Validation

7.1 Introduction

In Chapters 4-6, different design aspects of the PV module integrated converter were investigated. In conventional designs the final procedure would normally be straightforward, from electrical design, over the choice of devices to thermal design and final assembly. As discussed in Chapter 3, tight interdependences between the different design areas caused by shared design parameters will bring in multiple iterations through different design points.

In this chapter, an integrated electrical, technological and thermal design procedure for the PV module integrated converter is presented. Two different converters will be considered, corresponding to two different DMPPT architectures chosen in Chapter 2, one with variable low output voltage (LOV) suitable for series string connection to HV DC buss, and one with fixed high output voltage (HOV) suitable for parallel connection to HV DC bus.

The designs presented here will consider only the power stages of the converters. The rest of the circuit, which is not critical for the PV module integration, is given in Appendix A.

The goals of this chapter are:

- To combine the results from electrical design in Chapter 4, technology platforms from Chapter 5, and thermal management strategies from Chapter 6 into a unified design procedure.
- To optimize the design of the converter in order to achieve the lowest losses and to provide operation within the thermal limits of the components and the PV module.
- To construct and experimentally validate LOV and HOV converter.

The chapter will start with the design and assembly of the LOV converter, where the design procedure will be described. After that the HOV converter will be designed using the same procedure as for the LOV converter. In the end of the chapter, the design and experimental results are discussed.

7.2 Design of the Low Output Voltage Converter

In the considered DMPPT architecture the converters are connected in series to form strings which are further connected in parallel to a central inverter over a common high voltage DC bus. This architecture was already introduced in Chapter 4 and shown on Figure 4.9. This arrangement is the same as in conventional PV systems, but the addition of the converter effectively decouples one PV module from the rest of the system, increasing its flexibility and functionality. The output connectors of the converters are connected in series to form a string connected to a high voltage DC bus, which means that the converters share the same current. Depending on the generated power of each PV module, the output voltage is variable and can be lower or higher than the PV module voltage. To achieve this, a topology able to increase or decrease the voltage has to be used. For this purpose, a synchronous buck-boost converter selected in Chapter 4 was chosen [7-1].

7.2.1 Design Procedure

The flowchart of the integral design process is shown in Figure 7.1. The choice of the switching frequency will have the major impact on the converter size and losses. Therefore it will be the main design parameter used to perform iterations. Rather than going for a predetermined value, a loss analysis will be conducted for a range of switching frequencies f_{sw}, keeping in mind the thermal and spatial constraints. The next parameter to consider is the inductor current ripple. Varying its value, the trade-off between the DC and AC inductor losses can be made.

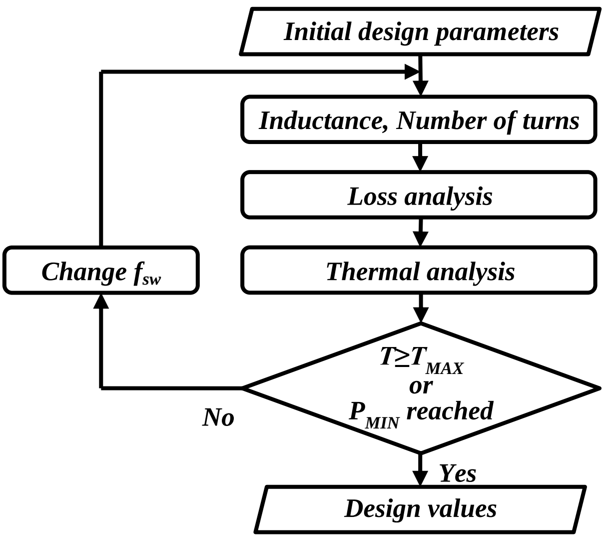

Figure 7.1: Converter design flowchart

Depending on the ratio of the AC-to-DC winding resistance, the optimum current ripple will be somewhere in the CCM mode, moving toward the boundary mode as this ratio decreases. Based on the analysis from Chapter 5, the optimal peak-to-peak current ripple is found to be 150%, and this value will be used in the design procedure. After the switching frequency and the inductor current ripple are known, the converter losses can be estimated. Using the loss values in the thermal model, the operating temperatures can be obtained. The goal is to minimize the losses, while keeping the operating temperatures within the component and material limits. For both versions of the converter, the maximum operating temperatures for different components and materials are given in Table 7.1.

Table 7.1: Maximum operating temperatures for components and materials

PV module	Converter			
	Power switches and diodes	Passives	PCB	Magnetic materials
90°C	150°C	125°C	125°C	90°C

Following the electrical design from Chapter 4, the converter ratings are predetermined by the used PV module. In this case, our reference PV module has a maximum power point voltage in the range from 20 V to 30 V, with scalable current/power rating by changing its length. Figure 7.2 shows the converter circuit schematic. The synchronous buck-boost topology is chosen due to its robustness and low number of components [7-2]. The output voltage from the PV module can be increased or decreased in order to compensate for the voltage changes in the rest of the PV string. The complete schematic of the LOV converter is given in Appendix A.

Taking into account the specifications from Chapter 4 and Table 4.2, the input voltage and current values used in the design are set to 30 V and 4 A respectively, which corresponds to the maximum power point voltage and current under standard test conditions (irradiation of 1000 W/m^2 and ambient temperature of 25 °C) if our reference PV module is 4 m long. The nominal output voltage together with the DC bus voltage is controlled by a central inverter and is set to 50 V. Therefore it is expected that the converter will boost the voltage for the most of the time. For that reason, in the following analysis, it is considered that the converter operates in the boost mode.

To enable efficient high switching frequency operation with small switching losses, GaN devices are employed for $\boldsymbol{Q_{1\text{-}4}}$ (EPC2001C, 100 V, 36 A, by EPC [7-3]). The used switches satisfy the rating requirements defined by Equation 4.12 in Chapter 4. GaN–specific gate drivers were used along with the GaN switches (LM5113, Texas Instruments [7-4]). The switching frequency $\boldsymbol{f_{sw}}$ and the desired inductor current ripple $\boldsymbol{\Delta I_L}$ will set the inductance value $\boldsymbol{L}$ according to the following expression:

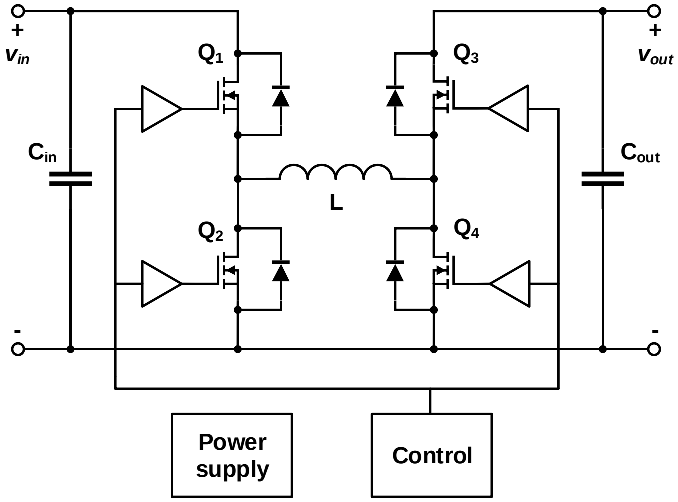

Figure 7.2: LOV converter circuit

$$L = \frac{V_{IN} D}{f_{sw} \Delta I_L} \tag{7.1}$$

Where $\boldsymbol{D}$ is the duty cycle ratio and $\boldsymbol{V_{IN}}$ is the input voltage, and $\boldsymbol{\Delta I_L}$ is set to 6 A. After finding the inductance, the input and output capacitor $\boldsymbol{C_{in}}$ and $\boldsymbol{C_{out}}$ are specified according to the desired input and output peak-to-peak voltage ripple $\boldsymbol{\Delta V_{in,pp}}$ and $\boldsymbol{\Delta V_{out,pp}}$:

$$C_{in} = \frac{\Delta I_L}{8 f_s \Delta V_{in,pp}} \tag{7.2}$$

$$C_{out} = \frac{D I_{out}}{f_s \Delta V_{out,pp}} \tag{7.3}$$

Figure 7.3 shows the inductor cross section and structural parameters with spiral winding layers sandwiched between the IRJ04 ferrite-polymer-composite (FPC) sheets from TDK [7-5]. The permeability of the used material is approximately 40 up to 100 MHz. The inductor windings are arranged in 70 µm copper layers on the 70 µm flexible polyamide film. The windings are covered with two 0.5 mm layers of the FPC laminate.

Since two PCB layers are available, the inductor windings can be arranged in one or two layers. Two layers inductor would result in slightly higher profile but with approximately half the surface area than the one layer inductor. However, that would also result in higher power loss density and higher parasitic capacitances. Nevertheless, both variations will be considered during the design process.

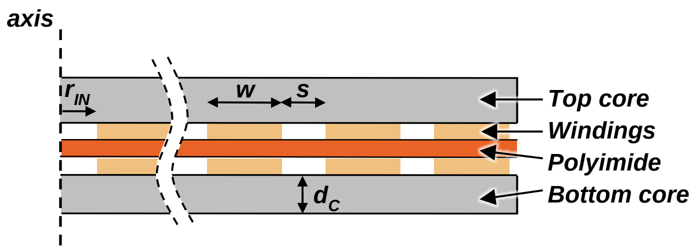

Figure 7.3: Structural parameters of the inductor for the LOV converter

The design of the LOV converter starts with the preset parameters – the converter voltage/current ratings from Chapter 4, Table 4.2, with the addition of current/power levels of the PV module. The turn width for the inductor is set to w=5 mm which sets the current density for the winding to J=11 A/mm^2. Somewhat higher current density is possible due to larger surface available for heat dissipation. The first step done by FEM analysis is to obtain the number of turns in order to achieve the predetermined inductance value and inductor peak-to-peak current ripple of 150% according to Equation 7.1. After that, the input and output capacitances are calculated in order to obtain 1% voltage ripple. Once all the circuit parameters are known, the inductor and switch losses are calculated and used as the input for the thermal model to obtain the operating temperatures. The inductor core and winding losses are obtained by means of FEM simulation, with the datasheet value of relative loss factor tan(δ)/μ' for the core losses. The switch losses are obtained using the piecewise-linear approximation of device's terminal currents and voltages. This iterative process is then repeated for a range of switching frequencies.

The results of this procedure are shown in Figure 7.4. As an optimum between the size and power losses the operating switching frequency is chosen to be 500 kHz with

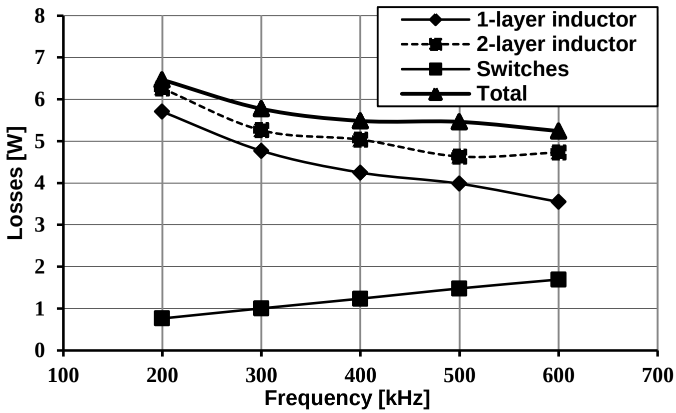

Figure 7.4: Frequency dependent loss breakdown for the LOV converter

overall losses of 5.3 W. This would set the efficiency of the power stage to 95.6%. Increasing the frequency, the losses can be further decreased, but the problem of extracting increased losses from small switches becomes difficult. Furthermore, the analysis shows that the two-layer inductor arrangement has higher losses, which combined with the smaller area increases the loss density even more.

Table 7.2 shows the inductor design values for the chosen frequency, according to the Figure 7.3. With these values the inductance obtained by FEM analysis is 3.3 µH. For the peak-to-peak input and output voltage ripple of 1% of the nominal voltage the required capacitances are $C_{in,min}$=5.9 µF and $C_{out,min}$=4.2 µF.

Table 7.2: Inductor parameters for the LOV converter

L [µH]	n	d_C [mm]	r_{IN} [mm]	w [mm]	s [mm]
3.7	7	0.5	1	5	0.5

For the selected switching frequency, the inductor losses contribute with P_L=3.9 W, while the switch losses are P_{Q1}=0.16 W, P_{Q3}=0.39 W and P_{Q4}=0.93 W. Note that Q1 is always on, while Q_2 turn on only sporadically to charge the bootstrap capacitor for the high side driver of Q_2. The thermal model shows that the maximum achieved PV module and the inductor temperature in that case would be $T_{PV,max}$=T_L=83°C, which is lower than the maximum 90°C. The switch junction temperatures are T_{Q1}=89°C, T_{Q3}=96°C and T_{Q4}=110°C, which is lower than the maximum operating junction temperatures for these devices (150°C).

Table 7.3: Summary of estimated losses and temperatures for the LOV converter

Part/component	Q_1	Q_2	Q_3	Q_4	L	PV module
Losses [W]	0.16	-	0.39	0.93	3.9	-
Temperature [°C]	89	-	96	110	83	83

7.2.2 Experimental Results

Figure 7.5 shows the inductor made according to Table 7.2. The permeability of the core material is very low, with μ_r≈40, but it can still increase the inductance of an equivalent air core inductor by a factor of almost 4 with the achieved inductance of 3.7 µH. This is close to the simulated inductance of 3.3 µH. The diameter of the inductor is approximately 8.2 cm while the thickness is 1.2 mm.

The converter prototype is shown in Figure 7.6. The converter and the inductor are built on a double sided copper (70 µm) cladded polyimide (Kapton). All the converter components were available in SMT packaging with heights up to 1 mm. The overall

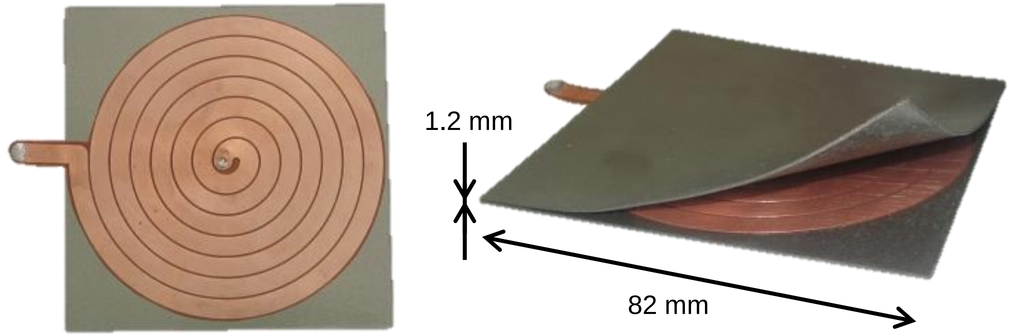

Figure 7.5: Inductor assembly for the LOV converter

achieved thickness is approximately 1.2 mm. The converter measures 14.3x8.5 cm^2 and the power density is approximately 8.2 W/cm^3.

Figure 7.7 shows the measured efficiency curve of the power stage. For the measurements, the input was set to 30 V, changing the duty cycle to achieve 50 V on the output as the input power was changed. The measured efficiency at the maximum power level is 94.1%, which results in 7.3 W of losses. This is higher than the modeled 5.4 W. A potential source of the additional loss is inaccurate switching loss modeling. The used piecewise-linear model assumes that the device capacitances completely determine its switching behavior. However, in practice especially when using high-speed GaN devices, parasitic inductances in the PCB layout can limit the switching speed. Another source of inaccuracies could lay in inductor FEM modeling and simulation results. Figure 7.8 shows the breakdown of calculated losses in the converter prototype.

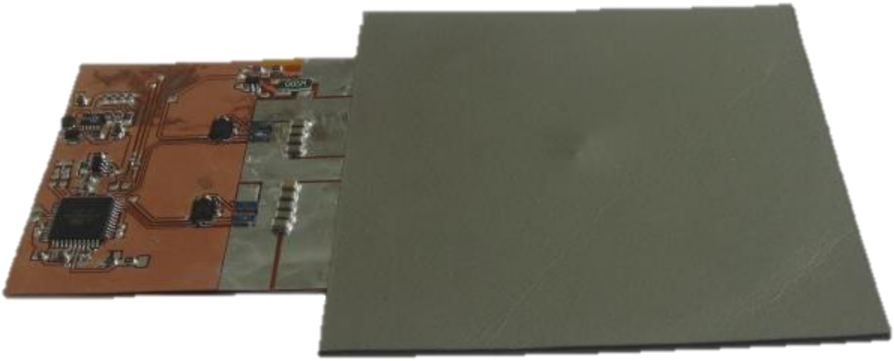

Figure 7.6: Assembled LOV converter

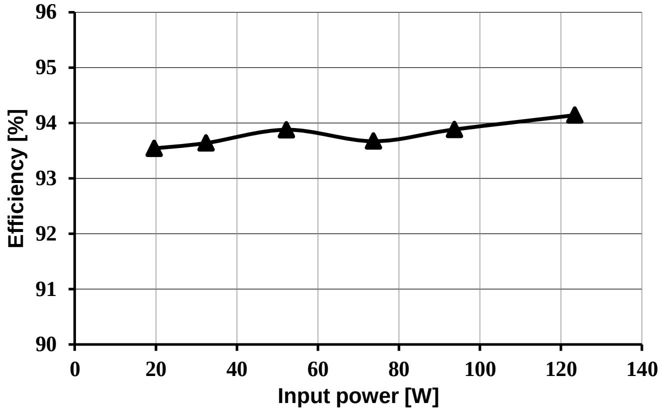

Figure 7.7: Measured efficiency of the LOV converter

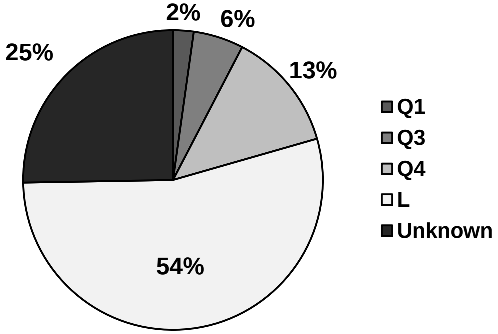

Figure 7.8: Breakdown of modeled loss sources for the LOV converter

The efficiency could be further improved on higher switching frequencies, moving the losses from the inductor to the switches. Changing the turn width will also affect the efficiency. Wider inductor turns decrease the DC and AC resistance, but also decrease the inductance, requiring more area and longer winding. Further improvement would also require better magnetic materials for the core.

The efficiency measurements were performed at the ambient temperature of 24°C and the following component temperatures were measured: T_{Q1}=39°C, T_{Q3}=48°C, T_{Q4}=74°C, T_L=57°C.

Table 7.4: Reached component temperatures at ambient temperature (24°C)

Part/component	Q_1	Q_2	Q_3	Q_4	L
Temperature [°C]	39	-	48	74	57

7.3 Design of the High Output Voltage Converter

In the DMPPT architecture with HOV converters, the converter outputs are connected in parallel to a central inverter over a common high voltage DC bus. This architecture was shown in Chapter 4 Figure 4.9 for N=1. Here, the converters do not share the common output current, and will therefore not influence each other. However, to achieve high voltage required for the central inverter, a large voltage boost is required which can have negative impact on the converter efficiency. For this purpose, a high step-up converter selected in Chapter 4 will be used [7-6].

7.3.1 Design Procedure

The design process flowchart for HOV converter is the same as for LOV converter and is shown in Figure 7.3. The design process is conducted for the full output power, since this scenario corresponds to the worst case conditions with maximum power losses and reached temperatures. The design starts with the predefined parameters - the converter voltage/current ratings and power level set by the PV module and system architecture, and initial variable parameter - switching frequency.

The circuit schematic of the high step-up boost converter with coupled inductors and passive clamp is shown in Figure 7.9 [7-7]. As in the case for the low voltage convert, the converter ratings are predetermined by the same PV module being used. The input voltage and current values used in the design are set to 30 V and 4 A respectively, which corresponds to the maximum power point voltage under standard test conditions for the 4 m long reference PV module from Chapter 4. The nominal output voltage is set to 380 V. The complete schematic is given in Appendix A.

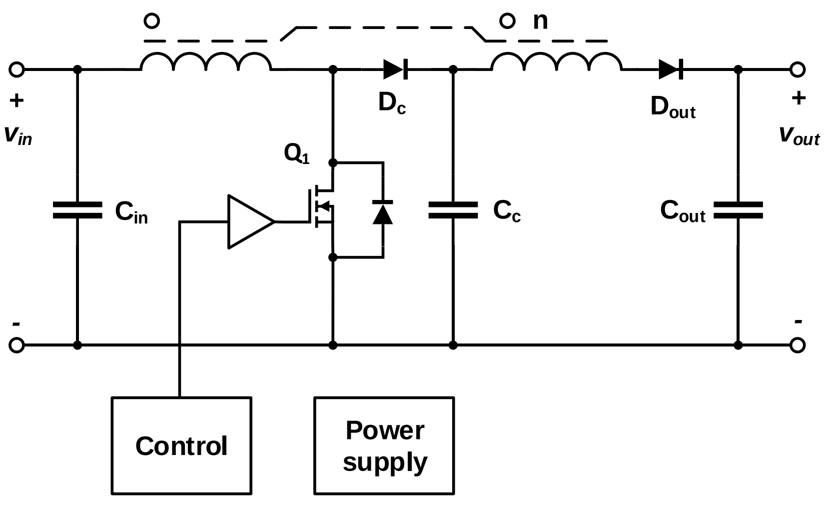

Figure 7.9: HOV converter circuit

The ratings of the switch and diodes are determined by the input/output voltage and the turn ratio $\boldsymbol{n}$, according to the Equation 4.19 from Chapter 4. The required turn ratio can be determined by the required voltage gain. Neglecting the influence of the leakage inductance, the maximum switch voltage is approximately:

$$V_{Q,max} = \frac{V_{in}}{1-D} = \frac{V_{out}}{1+nD} \tag{7.4}$$

where $\boldsymbol{V_{out}}$ is the output voltage and $\boldsymbol{n}$ is the turn ratio. The turns ratio also determines the voltage rating of the clamp capacitor $\boldsymbol{C_c}$. and the clamp diode $\boldsymbol{D_c}$, which are equal to the rating of the transistor $\boldsymbol{Q}$. The voltage gain is given with:

$$M = \frac{1+nD}{1-D} \tag{7.5}$$

where $\boldsymbol{D}$ is the duty cycle. The turn ratio was chosen to be $\boldsymbol{n}$=4, limited by manufacturability of thin secondary windings on the PCB. Considering that the voltage gain is approximately $\boldsymbol{M}$=13, the switch and the clamp diode have to be rated above 100 V, while the output diode has to be rated above 400 V. To enable high switching frequency operation with low switching losses, GaN device is used as the main switch $\boldsymbol{Q_1}$ (EPC2010C, 200 V, 22 A, by EPC [7-8]). For the output diode $\boldsymbol{D_{out}}$, a 600 V SiC device is used (C3D1P7060Q, 600 V, 3 A, by Cree [7-8]). As for the clamp circuit, an ordinary 150 V, 3 A Si Schotky diode is used. All the devices were available in packages with height under 1 mm.

For the magnetizing inductance $\boldsymbol{L}$, the same Equation 7.1 is valid in this case. For the chosen switching frequency $\boldsymbol{f_{sw}}$, the primary magnetizing inductance value L is calculated so that the desired peak to peak current ripple $\boldsymbol{\Delta I_L}$ is obtained. The spatial and material constraints will limit the size of the inductance, leading to higher switching frequencies. The input and output capacitor $\boldsymbol{C_{in}}$ and $\boldsymbol{C_{out}}$ are specified according to the desired input and output peak-to-peak voltage ripple $\boldsymbol{\Delta V_{in,pp}}$ and $\boldsymbol{\Delta V_{out,pp}}$:

$$C_{in} \cong \frac{(n-1)(1+nD)I_{out}}{(n+1)f_s \Delta V_{in,pp}} \tag{7.6}$$

$$C_{out} \cong \frac{2(1-D)I_{out}}{(n+1)f_s \Delta V_{out,pp}} \tag{7.7}$$

and the clamp capacitor Cc is determined by its peak-to-peak voltage ripple $\boldsymbol{\Delta V_{Cc,pp}}$:

$$C_c \cong \frac{I_{out}}{f_s \Delta V_{Cc,pp}} \tag{7.8}$$

The coupled inductors are realized in a similar way as the inductor for the LOV converter, with spiral winding layers sandwiched between the magnetic sheets. In this way the total thickness can be kept low at the expense of the required surface, which is in principle not limited. However, for the particular design an optimal size should be found in order to minimize the total losses. Figure 7.10 illustrates the inductor cross-section and construction parameters for the spiral windings structure. The inductor windings are placed in 70 μm copper layers on the 70 μm flexible polyamide film. The windings are covered with two 0.5 mm layers of FPC laminate [7-5]. The permeability of the used material is approximately $\boldsymbol{\mu_r}$=40. The saturation flux density is close to 0.25 T, but due to the small permeability, the actual flux density levels will be much lower. Furthermore, due to the low permeability and very low inductor thickness, the magnetic field is not completely closed in the core and therefore has complex distribution. This makes the process of analytically determining the inductance and losses rather complex. The exact number of turns required for the inductance is therefore obtained using the 2D FEM analysis. The high frequency winding and core losses are also obtained by means of FEM analysis.

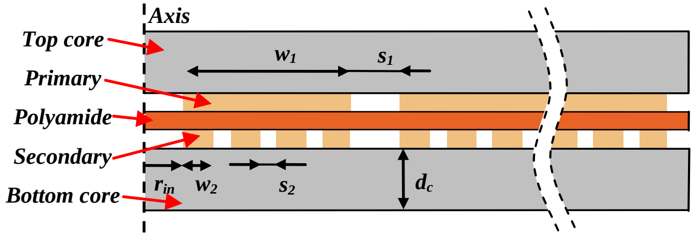

Figure 7.10: Spiral coupled inductor structure for the HOV converter

The current density for the primary winding is again set to $\boldsymbol{J}$=11 A/mm2 which sets the primary turn width to $\boldsymbol{w}$=5 mm. Somewhat higher current density is possible due to the low profile and large surface area. Higher current density would result in decreased required area and high frequency AC effects but increased DC losses. The first step done by FEM analysis is to obtain the number of turns in order to achieve the predetermined inductance value and inductor peak to peak current ripple between of 150%. Afterwards, the inductor and power stage losses are calculated and used as the input for the thermal model to obtain the maximum reached temperatures. This iterative process is then repeated for different switching frequencies until the minimum value for the converter losses is reached.

The bottom limit for the switching frequency is practically limited with the required inductor size. At low frequencies, a large number of turns is required. On the other hand, the maximum switching frequency is limited by losses. Since the inductor has a relatively large surface area, higher losses are allowed, but the problem of extracting increased losses from small elements like switches becomes increasingly difficult.

The loss breakdown for the considered range of switching frequencies is shown in Figure 7.11. According to the analysis, the minimum overall losses are reached around 500 kHz.

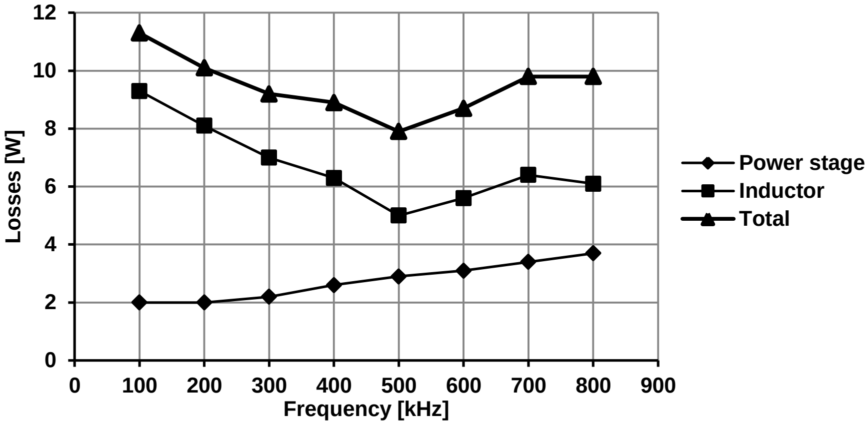

Figure 7.11: Frequency dependent loss breakdown for the HOV converter

Table 7.5 shows the inductor parameters according to Figure 7.10. According to the FEM analysis, the achieved inductance is 3.3 µH. This result is close to the result for the inductance in the LOV converter. In case of coupled inductors, the additional secondary winding puts the cores slightly more apart which results in slightly lower inductance.

Table 7.5: Coupled inductor parameters for the HOV converter

L [µH]	n_1	n_2	d_C [mm]	r_{IN} [mm]	w_1 [mm]	w_2 [mm]	s_1 [mm]	s_2 [mm]
3.3	7	28	0.5	1	5	1	0.5	0.33

The inductor losses contribute with 4.9W while the power stage losses are 2.7 W. According to the thermal model, the maximum achieved inductor temperature in that case is close to 82°C which is acceptable, while the power stage temperature is 69°C. This would set the main switch temperature to 93°C and the output diode temperature to 108°C, which is lower than the maximum operating junction temperatures of these devices.

Table 7.6: Summary of modeled losses and temperatures for the HOV converter

Part/component	Q_1	D_c	D_{out}	L	PV module
Losses [W]	1.6	0.2	0.9	4.9	-
Temperature [°C]	93	84	108	84	84

7.3.2 Experimental Results

Figure 7.12 shows the coupled inductors constructed according to Table 7.5 and Figure 7.10. The used core material has very small permeability ($\mu_r \approx 40$) but can still boost the inductance of an equivalent air core inductor by a factor of almost 6 with the achieved inductance of 3.9 µH. This is close to the simulated inductance of 3.3 µH. Somewhat higher inductance is achieved when compared to the LOV converter since the whole core area is filled with square shaped turns. The inductor measures approximately 80x80x1.2 mm^3.

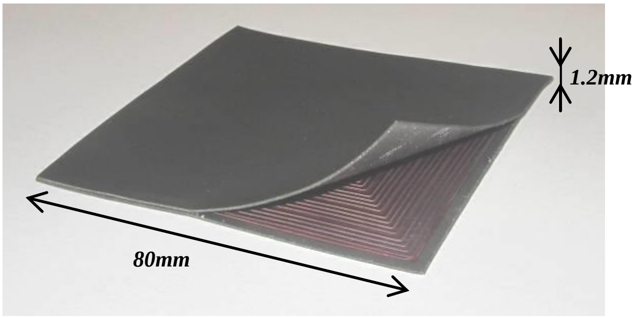

Figure 7.12: Coupled inductors assembly for the LOV converter showing the secondary winding

The converter prototype is shown in Figure 7.13. The converter is built on a double sided copper (70 µm) cladded polyimide. All the converter components were available in SMT packaging with heights up to 1.3 mm. The converter is 1.5 mm thick at most and measures 14x8 cm^2. The power density is 7.3 W/cm^3.

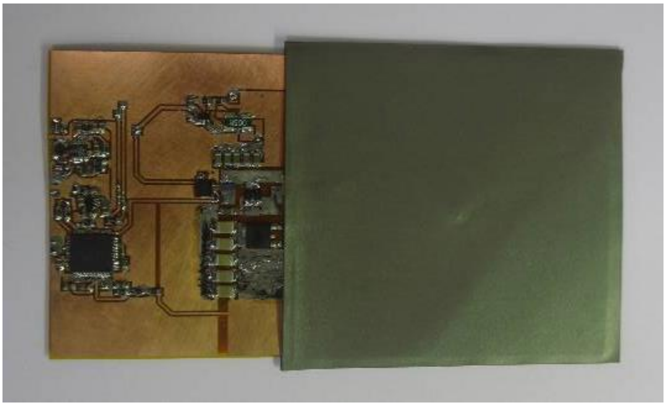

Figure 7.13: Assembled HOV converter

To test the conversion efficiency, the converter was mounted on a heat plate set to 50°C. Figure 7.14 shows the measured efficiency curve, and Figure 7.15 the losses breakdown. The achieved efficiency at the maximum power is close to 87% which is lower than expected and would lead to higher system temperatures if the converter is mounted on a PV module. According to the FEM analysis the main contributor to the losses are the high AC winding losses in the inductor. This is partly due to the wide copper track and the fact that the magnetic field is not closed completely in the core. A possible additional source of losses could be also current ringing on the secondary side, due to the secondary leakage inductance and the capacitance of the output diode.

The measured temperature of the inductor is 85°C, whereas the temperatures of the output diode pads and the main switch and are 98°C and 123°C respectively. Using the datasheet values for the junction to pad and junction to case thermal resistances for the output diode and the switch, the calculated junction temperatures are 117°C and 135°C. The main switch junction temperature is close to the maximum value, but the next generation devices will have maximum junction temperature of 150°C.

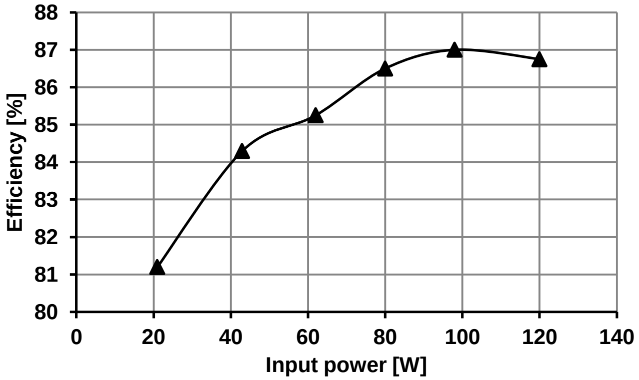

Figure 7.14: Measured efficiency of the HOV converter

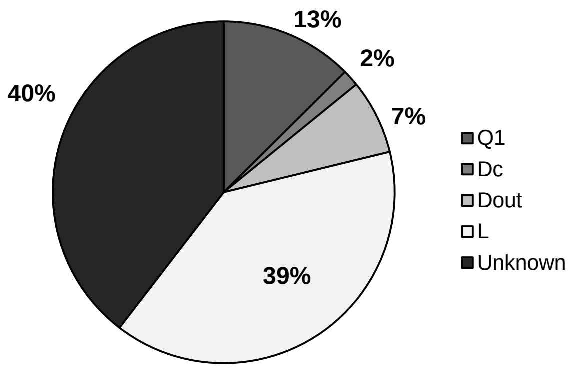

Figure 7.15: Breakdown of modeled loss sources for the HOV converter

Table 7.7: Reached component temperatures at 50°C ambient temperature

Part/component	Q_1	D_c	D_{out}	L
Temperature [°C]	135	117	-	85

According to the measurement results all the components operate within the safe temperature range, however, as already mentioned, the thermal setup assumed the thermally conductive supporting structure for the PV module. If the PV module is to be mounted on a high thermal resistance substrate, this configuration would be thermally unstable and the additional heat extraction and heat spreading strategies should be employed.

7.4 Conclusions

In this chapter, a unifying procedure combining the results from Chapter 4-6 is presented and used to design the PV module integrated converter. The goal of the design procedure is to maximize the efficiency of the converter while keeping the temperatures within the thermal limits for the PV module and the converter components. The trade-of between the efficiency and the size of energy storage components is made by changing the switching frequency. Two demonstrators were constructed using the presented design procedure.

The LOV converter achieved high efficiency of over 94%. There is still a potential for improvements if better magnetic materials are used, through a better optimized design procedure.

The HOV converter on the other side achieved low maximum efficiency of 87%. This was caused in the first place by underperforming magnetic material, which was available at the time. Such a low efficiency could diminish the benefits of DMPPT but could also cause higher temperatures on the PV module, if the converter is to be integrated on the active area. It is advised to use higher permeability magnetic sheets in order to improve the efficiency, or additional heat spreading layers are needed to keep the temperature within the allowed limits.

7.5 References

[7-1] M. Acanski, J. Popovic-Gerber, J. Ferreira, "Flexible Low Profile PV Module Integrated Converter for Distributed MPPT PV System," Power Electronics and Motion Control Conference (EPE/PEMC), 2012

[7-2] L. Linares, R. W. Erickson, S. MacAlpine, M. Brandemuehl, "Improved Energy Capture in Series String Photovoltaics via Smart Distributed Power Electronics," Applied Power Electronics Conference and Exposition (APEC), 2009

[7-3] EPC2001C datasheet, available online at *www.epc-co.com*

[7-4] LM5113 eGaN gate driver datasheet, available online at *www.ti.com*

[7-5] TDK IRJ04 ferrite film datasheet, available online at *www.tdk.com*

[7-6] M. Acanski, J. Popovic-Gerber, J. Ferreira, "Design of a Flexible Very Low Profile High Step-Up PV Module Integrated Converter," Energy Conversion Congress and Exposition (ECCE), 2012

[7-7] Q. Zhao, F. C. Lee, "High-Efficiency, High Step-Up DC-DC Converters," IEEE Transactions on Power Electronics, Vol. 18, No. 1, 2003

[7-8] EPC2010C datasheet, available online at *www.epc-co.com*

[7-9] C3D1P7060Q datasheet, available online at *www.cree.com*

Chapter 8 Conclusions and Recommendations for Future Work

With the recent trends in PV industry, PV energy became cheap enough for end users that the price-per-watt numbers became much less important than they were just a decade ago. At this point, the cost driver shifts to other aspects of PV energy, such as ease of installation, usability, or integrability with the environment. This thesis addresses this transition twofold, by trying to close the price gap, and by bringing power electronics technologies for the next generation PV systems.

Chapter 1 of the thesis identifies the potential to increase the level of penetration of power electronics in PV systems, both physically and on the system level, in order to decrease the cost and improve the system performance.

Chapter 2 shows the evolution that PV systems went through while transitioning from large utility scale to residential and BIPV sector, leading from centralized to distributed MPPT. It was shown that high level of PV system penetration into electrical grid and built environment has to be followed by high level of penetration of power electronics into the PV array. Future trends in power electronics technology for residential PV systems are shown, and drawbacks that still exist in the current solutions are identified.

Chapter 3 presents the concept of power converter integrated into flexible PV module as the next step in future DMPPT PV systems, with the goal of increasing the level of integration by combining packaging layers of the PV module and the converter. Three design areas are identified together with interrelations that connect the electrical performance, thermal stability and the required technology platforms.

Chapter 4 investigates electrical requirements for the PV module integrated converter, from input/output voltage/current specifications, over selection of suitable converter topologies for PV module integration, to relations between system parameters and the size of energy storage components.

Chapter 5 identifies enabling power electronic technologies for PV module integration. In order to overcome requirements for energy storage devices within low profile flexible construction, new magnetic materials and semiconductor devices for high switching frequency operation are considered.

Chapter 6 analyzes thermal interaction between the PV module, integrated converter and the environment, and identifies thermal management strategies for efficient heat extraction and dissipation.

In Chapter 7, the results from electrical design in Chapter 4, technology platforms from Chapter 5, and thermal management strategies from Chapter 6 are combined in a unified design procedure to construct the PV module integrated converter.

8.1 Conclusions

In the following, the conclusions of this thesis are given, organized into groups which address the research questions given in Chapter 1:

- To investigate integration concepts, and to identify possible system architectures for distributed power processing and converter topologies suitable for PV module integration.
- To find suitable technologies for integrating the power electronic converter into the PV module and converter integration concepts to integrate the most suitable topologies using the best technology platforms.
- To identify thermal management strategies for heat extraction and operation under high temperature conditions, to develop a solution for integrated thermal management and to model the system thermal behavior.
- To analyze the interdependence between the electrical, technological and thermal design domains, to develop a multi-objective design procedure, and to design, assemble and test a demonstrator using the developed design concept.

Integration Concepts, System Architectures and Converter Topologies for PV Module Integrated Converter

The practice in present PV systems is to use large arrays of PV modules connected to a central power converter acting as an interface to the utility AC grid. At the same time, the converter performs maximum power point tracking in order to extract the maximum available energy from the electrically nonlinear PV sources. As the PV energy penetrates into urban environment, this approach starts to show its shortcomings since non-uniform operational conditions of the PV modules coupled with the centralized MPPT can decrease the system energy yield.

New PV system architectures have been proposed with power processing on a PV module level, effectively decoupling the PV modules from mutually influencing one another, therefore increasing the system yield. However their acceptance is still low due to the increased investment costs for the individual converters for the PV modules, and additional cables and labor required for assembly and installation.

In this thesis, a new concept for DMPPT systems is proposed with a converter integrated directly into a flexible thin-film PV module. By sharing packaging layers between the converter and PV module, the cost of the system could be decreased, and by optimizing the converters for the particular PV module the yield of the system could be improved.

Among a large number of topologies and several DMPPT architectures available, two possible DMPPT architectures for the PVMIC are proposed, each with its own advantages, resulting in two converter variants based on the output voltage:

- Low output voltage (LOV) converter suitable for series/parallel arrangements in PV array, being easier to accommodate to existing PV systems and having less demanding design procedure,
- High output voltage (HOV) converter suitable for parallel arrangements in PV array, and having better system scalability.

The selection of the suitable topologies for the PVMIC was performed by classifying them on the basis of identified criteria, with different weight factors based on the level of importance for PV module integration. In order of importance, those are:

- Integrability – the ability to achieve low profile components, in the first place energy storage devices,
- Performance – the ability to achieve high conversion efficiency, and the required voltage levels,
- Reliability – the capacity for reliable operation in high temperature conditions,
- Cost – the ability to achieve low cost through low component count,
- Control – the possession of simple, efficient and cost effective control algorithm.

Two robust and simple topologies are proposed as suitable solutions for PVMIC, enabling high switching frequency operation and possibility to achieve small numbers of low value energy storage components. The important equations, connecting the design parameters, the values of energy storage components and the ratings of passive and active devices are provided for the design and optimization procedure to be used along with thermal and technological design.

Enabling Technologies for High Efficiency, Low-Profile, Flexible Converter

The requirement for flexible and low-profile construction of the PV module integrated converter prevents standard technologies for power electronics to be used for all converter parts and components. Three groups of enabling technologies were investigated in order to address and meet these requirements:

- Flexible printed circuit board – to enable flexible, construction of the converter, and to provide additional functionality in the magnetic and thermal design,
- Fast switching devices – to enable high switching frequencies in order to achieve low volume energy storage components,
- New magnetic materials and integrated structures – to enable flexible, low profile power inductors and transformers.

An overview of the flexible circuit technology is presented with possibility to further decrease the cost and increase the level of integration via embedded passive components. Additional functionalities of the flexible circuit carrier are achieved by providing conductors for magnetic components and integrated thermal structures.

Novel wide-bandgap devices for power electronics bring disruptive improvement in switching performance when compared to the traditional silicon devices. GaN based devices considered in this thesis address both the performance and cost effectiveness of the integrated converter. Design guidelines regarding the layout techniques, gate drive circuits and power loss models are presented.

Magnetic components present the major barrier to meet the spatial requirements. An alternative to standard ferrite core inductors, in the form of ferrite-polymer compounds is considered in this thesis. A FEM based design is presented to link the values of (coupled) inductors with the arrangements of the windings and the resulting power losses.

Thermal Management Strategies and Thermal Modeling for PV Module Integration

With its presence and losses, the integrated converter will change the temperature distribution of the PV module, creating a hotspot in the place where it is mounted. While the converter may operate within its temperature limits, the operation and reliability of the PV module should not be compromised. The low-profile requirement for constructing the PV module integrated converter confines the inevitable conversion losses into smaller volumes, increasing the power loss density and putting additional constraints on the thermal design. The environmental conditions, coupled with the electrical and technological limitations impose significant restrictions when dealing with heat losses in the converter. The requirement for flexible construction prevents the use of conventional heatsinks and alternative paths for heat extraction and dissipation have to be found, modeled and analyzed.

The thermal analysis and modeling of the system composed of a PV module and an integrated converter is performed in a three-stage top-down approach through:

- Modelling the PV module alone, to assess the impact of surface power loss density on the PV module temperature and to determine the base operating temperature for any subsequent devices integrated into the PV module,
- Modeling the complete system composed of the PV module and the integrated converter to determine the reached temperatures on the PV module surface and in the converter areas.
- Selection of thermal management strategies to extract and spread the power losses from the converter components, and the component level modeling of the integrated converter to determine the reached temperatures in the converter components.

The developed thermal models are simple, have sufficient accuracy, and are included within a multi-objective design procedure for the PV module integrated converter. Their use is not limited to PV module integration alone, but can be also used for other low profile applications.

Integrated Electrical, Technological and Thermal Design Procedure for PV Module Integrated Converter

Three design areas are identified in the design procedure for the PV module integrated converter: electrical, technological and thermal. The integrated construction of the converter will introduce tight interdependence between the design areas. A multi-objective design procedure is needed in order to balance the stringent requirements for:

- High conversion efficiency – The efficiency of the converter has to be high in order to not diminish the advantages of DMPPT. Moreover, the resulting lower heat losses will aid the thermal design but can lead to larger energy storage components.
- Low-profile, flexible construction – The spatial requirements will limit the size of energy storage components, space for thermal management strategies and their effectiveness, increasing the power loss density.
- Imposed thermal limits – The operation under elevated temperatures with strict thermal limits dictated by the PV module and components of the converter will require efficient topologies, devices and integrated thermal management strategies.

A unifying design procedure for the PV module integrated converter is presented. The procedure intends to maximize the power level of the converter and the conversion efficiency, while keeping the PV module and converter temperatures within the limits. The switching frequency, being the dominant design parameter, is used to make trade-offs in the design between efficiency, losses, size of energy storage components, and the required thermal management. As the result, taking into account the design limitations and interdependences, two demonstrators for LOV and HOV converters were designed, assembled and tested:

- The LOV converter shows promising results with the efficiency around 94%, which could be further increased with better design optimizations and improved magnetic materials.
- The HOV converter achieved efficiency below 90%, in the first place due to inferior magnetic materials and accompanying parasitic components. Nevertheless, the lower efficiency of the HOV converter could still be compensated with higher system yield in some DMMPT cases.

8.2 Recommendations for Future Work

Every answer breeds new questions and this thesis is no exception. In the following, recommendations for future research are given in four groups, motivated by the results from Chapter 4, 5 and 7. The recommendations for future work address the electrical design of the converter, new technologies for high switching frequencies, and design procedure optimization.

Converter Topologies and Control

While by no means extensive, the list of topologies considered in Chapter 4 represents a small group of buck/boost based topologies with proven performance and reliability. Using resonant topologies, power losses are in general shifted from switching devices to magnetic components. When using inferior magnetic materials, such as FPC, resonant topologies start to lose advantage, especially when using devices with lower switching losses, such as GaN transistors. For that reason, the advantage has been given to hard-switched and, where possible, transformerless topologies, which would lead to simpler designs and better operating conditions for the selected magnetic materials. However, low profile design coupled with high current requirements inherently possesses high parasitic capacitances. It would be interesting to investigate possibility to use topologies which could take advantage of both high parasitic inductance and capacitance, such as LLC/LCC-based or other resonant topologies.

Moreover, the topologies considered in Chapter 4 are based on classical ones which have been used, with some alterations, since the dawn of power electronics. With new and improved wide band-gap devices, the switching frequencies are moving to multi-MHz range, especially in case of low power converters. It would be interesting to investigate if some of the topologies and design procedures used for radio frequencies could be applied to power converters.

From the system point of view, a DMPPT PV system consists of multiple smaller converters and a central inverter, each with its own independent control. The central inverter controls the DC bus voltage while, as the response, the PV module integrated converters balance its output voltage while performing MPPT. This will interfere with MPPT operation and might decrease the efficiency in dynamic situations. It would be useful to investigate to what extent the central inverter control affects the DMPPT converters, and if so, to devise a procedure for control parameters, such as MPPT speed and step, depending on dynamic properties of the central inverter.

Technologies and Materials for Very High Switching Frequency Converters

The magnetic materials used for inductors in Chapter 5 are not originally intended to be used as a core for power inductors. Although it was possible to construct an inductor, the achieved inductance was rather low due to the small permeability. It would be beneficial if the manufacturers could sacrifice some amount of material flexibility for an increase in permeability. This might also increase the specific core losses, but could lead to more compact inductors with lower parasitic elements and overall better efficiency. Especially when moving deep into MHz switching frequency range, where low permeability materials could still be of use before the switching frequency is high enough to enable air inductors.

A PV module with its integrated converter is in principle intended to operate “in free air”, or practically mounted on a supporting structure which is usually non-magnetic. In Chapter 5 it was shown that there will be a part of the magnetic field which will not close completely in the core of the power inductor, caused by limited permeability of the used FPC materials. If this would present an issue, it would be useful to investigate the possibilities for shielding, for example adding high-permeability materials as the outer layers of the inductor’s core.

Conventional ferrite materials are not suitable for the size, ratings and mechanical requirements of a power inductor that can be used for the PV MIC. However, it would be interesting to investigate if the power inductor could be substituted with an array of smaller, ferrite core inductors, commonly used in low power POL power supplies. New miniature and low profile power inductors are constantly being improved for very low profile devices, such as mobile phones and laptops. The inductance and current rating required for higher power applications, such as converters in DMMPT systems, could be achieved with series-parallel arrangements of smaller inductors. The challenge here would be providing equal current sharing, minimizing external field, and optimizing such a structure.

Tools for Design Space Exploration in Power Electronics

In Chapter 7, the integral electrical, technological and thermal design for the PV module integrated converter is performed. The converter design is based on finding the maximum power level of the PV module and optimal switching frequency for minimum losses, while keeping the temperatures of the PV module and the converter components within safe limits. It is assumed that the higher power converter will have higher efficiency. Moreover, the optimum inductor current ripple was found in advance in Chapter 5, and set as constant in Chapter 7. It would be useful to devise a procedure with more input parameters and to perform wider design space exploration in order to maximize the efficiency of the converter. This could be applied to the components alone, but also to the whole system, where the parameter could be the number of converters in the DMPPT system and their configuration, or the optimal number and size of PV cells, which is easily reconfigurable for thin-film PV technology. With the recent advances in artificial intelligence and deep learning, it would be interesting to apply new optimization technics to power converters, components, PV modules and systems in general.

Appendix A Schematic of the PV Module Integrated Converter

The block scheme of the PV module integrated converter is shown in Figure A.1. The high voltage and low voltage versions differ only in the power stage and the resistor values in the output voltage divider. The complete schematic of both versions of the converter is shown in Figure A.2.

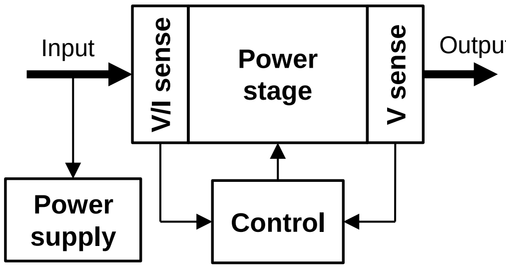

Figure A.1: Block scheme of the PV module integrated converter

The power stages were presented in Chapter 4, shown in Figure 4.27 and Figure 4.29 respectively. For the LOV converter, the power stage is based on EPC2001C GaN transistor and LM5113 gate driver. The HOV converter uses the low side of the same gate driver, a single EPC2010C GaN transistor and C3D1P7060 SiC diode.

The control part of the converter is implemented around 8-bit microcontroller ATxmega32. The microcontroller performs sampling of the input/output voltages and currents and generates the driving PWM signals for the transistors, as well as some additional functions, described in appendix B.

For the purpose of MPPT, the input voltage is measured using a voltage divider. The current is measured using a high-side current shunt amplifier INA195. On the output side, only voltage is measured, while the current is calculated via input power and output voltage, correcting for the estimated conversion efficiency.

The auxiliary power supply is based on a small buck converter built around LT3689 in low profile MSOP package. The accompanying power inductor was available in a low profile package. A linear voltage regulator MIC5219 is used for the microcontroller.

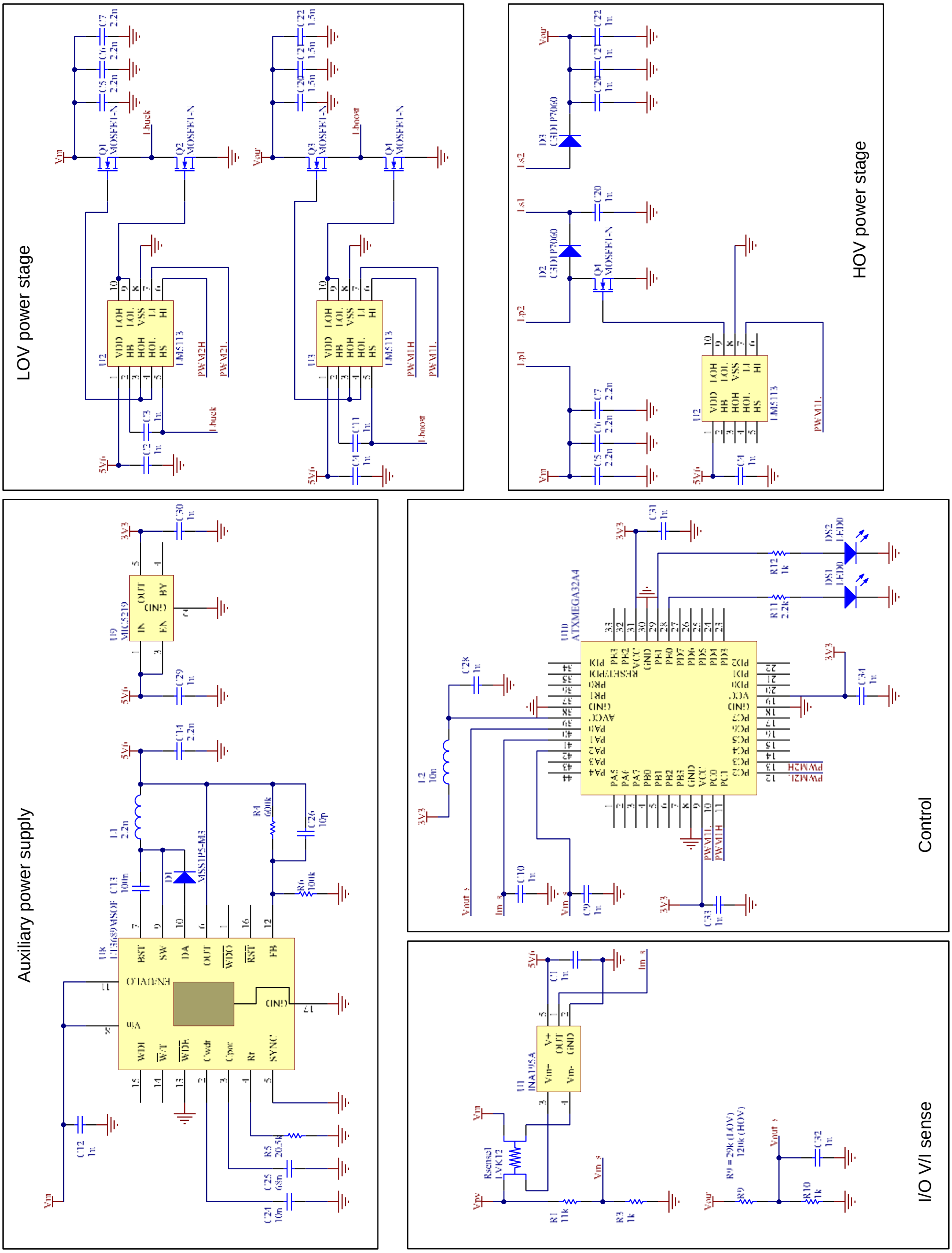

Figure A.2: Schematic of the PV module integrated converter

Appendix B Control Design for the PV Module Integrated Converter

In the following section, the control for the PV module integrated converter is described in more detail. The general control principle and guidelines for its implementation is presented, based on which it can be easily adapted to different platforms.

As discussed in Chapter 4, a digital control is implemented, which offers increased flexibility and improved consistency over traditional analog control. The design presented in this thesis is based on an 8-bit microcontroller (µC) ATxmega32A4U. In general, the converter control is not computationally intensive, which enables relatively slow, low-power and low-cost microcontrollers to be used, instead of implementing the control on an FPGA platform. However, an advanced PWM peripheral stage is required in order to generate all the required gate drive signals. High switching frequency $\boldsymbol{f_s}$ in orders of hundreds of kHz coupled with the need for high step resolution $\boldsymbol{N_{PWM}}$ of the duty cycle $\boldsymbol{D}$ to enable precise MPPT requires that the clock frequency of the PWM stage to be:

$$f_{clk\_PWM} = f_s \cdot N_{PWM} \tag{B.1}$$

With switching frequencies approaching 1 MHz and the need for duty cycle resolution to be at least 8-bit, this leads the PWM clock frequencies in the range of hundreds of MHz. Typically this is higher than the operating frequency of the µC/DSP, requiring fast PWM peripheral with a special PLL stage for PWM clock generation. Fortunately, this was recognized by several manufacturers which equipped standard, low-speed, low performance (but high enough for power electronics purposes) µCs/DSPs with high performance PWM stages. Moreover, in case when there is a half bridge in the power stage, such as the one in the LOV converter, the PWM stage can also provide dead-time generation to prevent shoot through and damage the converter. In our case, the ATxmega32 can provide the PWM frequency of 512 kHz with 8-bit resolution (256 steps) for duty cycle $\boldsymbol{D}$, and generate multiple PWM signals together with dead-time control.

The general algorithm for the control is shown in figure B.1. It covers both the LOV and the HOV converter, which differ in the way the gate driver signals are generated.

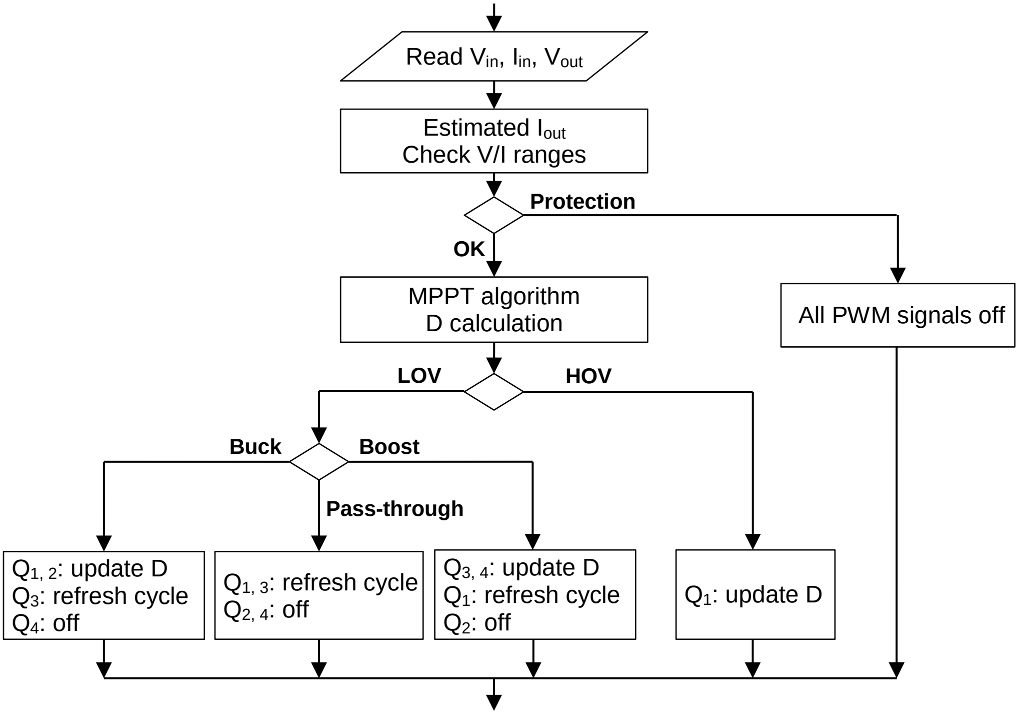

Figure B.1: Algorithm for the PVMIC control

The procedure shown in Figure B.1 is interrupt driven at frequency f_{int}, which then dictates the time step for the MPPT algorithm. As noted in Chapter 4, the converter merely transforms the PV module into a constant power source, and there is no feedback for the output voltage control. The control procedure can be divided into four stages:

- **Input/output voltage/current readouts** – The input and output voltages and currents are measured for two purposes. First, the input voltage and current measurements are required to perform the MPPT algorithm. Second, all voltages and currents are monitored for protection, as described below. In our case, the measurement is performed using the 12-bit ADC peripheral. Since the output current is not measured, its value is estimated based on the input power, output voltage and the converter efficiency.
- **Input/output protection** – All voltages and currents are monitored in order to keep them within safe range, prevent damage of the converter. For example if the load current decreases to zero, the converter acting as a constant power source will force the output voltage to rise, as shown in Figure 4.11. If any voltage or current reaches the predetermined maximum value, the power stage is temporarily turned off, until the next control cycle begins. In the meantime, the duty cycle remains the same, and the converter continues operating at MPP.

- **MPPT algorithm** – In each control cycle one iteration of the MPPT algorithm is performed and the PWM duty cycle is updated. As described in Chapter 4, an ordinary P&O MPPT algorithm is implemented as shown in Figure 4.24. In our case f_{int} is set to 1 kHz and the step size ΔD is set to minimum possible, determined by the PWM resolution N_{PWM} together with the switching frequency f_s, and corresponds to approximately 0.4% (8-bit resolution).
- **PWM signal update** – For the power stage to operate, one or more PWM signals have to be generated for the gate drivers. The number of signals depends on the number of switches in the power stage. In case of the HOV converter, there is only one low-side transistor Q_1 (Figure 7.9), which is driven straightforward by one PWM signal. In case of the LOV converter there are four PWM signals, with three additional features:
    - Depending on the input and output voltage, the LOV converter can operate in buck or boost mode, generating PWM signals for only one of the $Q_{1,2}$ or $Q_{3,4}$ half-bridges, as shown in Figure 7.2. Additionally, a pass-through mode can be added when the output voltage should be close to the operating V_{MPP} voltage of the PV module, in order to eliminate switching losses.
    - When the $Q_{1,2}$/$Q_{3,4}$ half-bridge is inactive, the low-side transistor is turned off whereas the high-side transistor is constantly on. Since the high-side gate drive circuit is operated via a bootstrap circuit, the bootstrap capacitor needs to be recharged periodically to keep Q_1/Q_3 on. The maximum refresh period ΔT is determined by the bootstrap capacitor C_{bs} (C_3/C_{11} in Figure A.2), allowed voltage drop of the high-side supply voltage ΔV_{hs}, and the current consumption of the high-side gate drive circuit I_{hs}:

      $$\Delta T = \frac{C_{bs} \cdot \Delta V_{hs}}{I_{hs}} \qquad \text{(B.2)}$$

      In our case, allowing ΔV_{hs} to be 0.5 V, and considering that C_{bs}=1 µF, I_{hs}<0.1 mA, the maximum required period ΔT is approximately 6 ms. Since the control routine is performed at each 1 ms (f_{int}=1 kHz), the bootstrap capacitors are recharged sufficiently often, by turning off high-side and turning on low-side transistor of the inactive half bridge during one PWM period.
    - Dead-time has to be generated for the operating half bridge in order to prevent shoot-through. This is done automatically in the PWM stage. In our case, the dead time is equal to the smallest duty cycle step, and is equal to approximately 0.4%.

As a final note, for even higher performances in terms of computational power, duty cycle and dead-time resolution, a C2000 microcontroller from Piccolo series (Texas Instruments) is recommended.

Summary

PV Module Integrated Converter for Distributed MPPT PV Systems

PhD thesis
By Miloš Ačanski

Driven by constant advances and cost reductions in photovoltaic (PV) technology, together with incentive government policies toward cleaner environment, the PV energy became one of the fastest growing market in the world. In many countries the amount of installed PV power is increasing at an exponential rate, in all sectors from large utility scale power plants to small residential PV systems.

Large research and development efforts are being made to decrease the cost and to improve the performance of PV modules and electronic converters for PV systems. On the PV module side, recently developed flexible thin-film photovoltaic modules have the potential to lower the manufacturing costs. Furthermore, such lightweight and flexible devices offer additional cost benefits in terms of transportation and installation. To achieve cost reduction on the power electronics side, there is a trend toward higher power density and higher conversion efficiency. Despite advances in PV and power electronics technology, the basic PV system architecture has changed little. In urban areas and especially in building integrated PV systems, due to nonoptimal module placement and environmental impact, the traditional way of processing the power from PV modules can introduce significant losses in the system.

New modular distributed architectures were recently proposed where each PV module has its own maximum power point tracking (MPPT) unit. In that way the power output of each module is maximized, regardless of the performance of other modules connected to the same PV system. To decrease the cost, it would be desirable to increase the level of integration by positioning the converter as close as possible to the PV module not only from the electrical point of view but also the mechanical, combining functional and electrical with physical integration. By integrating the converter directly into the PV module, the PV-module-converter system could be considered as a single building block in a PV system. By specifying which encapsulation and packaging layers can be shared among the PV module and the converter, one could also consider different integration levels.

This thesis presents the design considerations for an optimized converter intended for integration into a low cost thin-film flexible PV module. The converter is designed through an integral design procedure, combining design areas in order to satisfy the stringent requirements for PV module integration, in particular those related to the magnetics design and high operating temperatures.

Integration of the converter into the PV module will impose harsh environmental conditions on the converter operation with elevated temperatures and large temperature swings. PV modules are relatively simple and robust devices and it is a challenge to design a converter that can meet their reliability and lifetime. Furthermore, a tight thermal coupling between the converter and the PV module and the requirements for a low profile, flexible construction introduces interdependences between the design areas. Three groups of specifications can be identified in the design process of the module integrated converter, each with its own goals:

- Electrical design with the goal of maximizing the conversion efficiency,
- Technological design with the goal of achieving low profile and flexibility,
- Thermal design with the goal of keeping the operating temperatures safe.

The electrical design relies on classifying and ranking the existing topologies on the basis of electrical performance and suitability for integration in order to come to the most suitable topologies. Different possible system architectures are considered, resulting in different topologies selected for the PV module integrated converter.

An overview of existing technologies and defining new packaging and integration concepts as the most suitable platforms to implement a PV module integrated converter is given. The existing suitable technologies are ranked on the basis of thermal, electrical and mechanical performances, limitations, cost and reliability. Special attention is given to ability for high switching frequency operation and the enabling semiconductor devices based on GaN and SiC technologies; and to magnetic components as the most critical part for achieving low profile integration.

The existing thermal management strategies suitable for low profile converters are analyzed and categorized on the basis of technological and electrical requirements. The thermal model of the combined PV module and the integrated converter is presented, from the system level down to the component level.

Finally, the individual design areas are combined into a unified design procedure, based on defining converter electrical specifications and electrical design, choosing the technology platform and defining thermal requirements using the developed thermal model. Based on the optimization parameters the most suitable combination of topology, technology and thermal management parameters is obtained. As the result, the chapter presents two possible solutions through the assembly, experimental validation and performance evaluation of the integrated converter design.

Samenvatting

FV-module Geïntegreerde Omvormer voor Gedistribueerde MPPT FV-systemen

PhD thesis
Door Miloš Ačanski

Gedreven door constante vooruitgang en kostenbesparingen in fotovoltaïsche (FV) technologie, samen met een stimulerend overheidsbeleid voor een schoner milieu, werd de FV-energie één van de snelst groeiende markten ter wereld. In veel landen neemt de hoeveelheid geïnstalleerd FV-vermogen exponentieel toe, in alle sectoren, van grote elektriciteitscentrales tot kleine residentiële FV-systemen.

Er worden grote inspanningen geleverd op het gebied van onderzoek en ontwikkeling om de kosten te verlagen en de prestaties van FV-modules en elektronische omvormers voor FV-systemen te verbeteren. Aan de kant van de FV-module kunnen onlangs ontwikkelde flexibele dunne fotovoltaïsche modules de productiekosten verlagen. Bovendien bieden dergelijke lichtgewicht en flexibele apparaten extra kostenvoordelen in termen van transport en installatie. Om kostenvermindering aan de kant van de vermogenselektronica te bereiken, is er een trend naar hogere vermogensdichtheid en hogere conversie-efficiëntie. Ondanks de vooruitgang in FV- en vermogenselektronica-technologie, is de architectuur van het basis FV-systeem weinig veranderd. In stedelijke gebieden en met name bij het bouwen van geïntegreerde FV-systemen, vanwege de niet-optimale plaatsing van modules en de gevolgen voor het milieu, kan de traditionele manier om de energie van FV-modules te verwerken aanzienlijke verliezen in het systeem veroorzaken.

Nieuwe modulaire gedistribueerde architecturen werden onlangs voorgesteld, waarbij elke FV-module zijn eigen maximale PowerPoint tracking (MPPT)-eenheid heeft. Op die manier wordt de vermogensoutput van elke module gemaximaliseerd, ongeacht de prestaties van andere modules die op hetzelfde FV-systeem zijn aangesloten. Om de kosten te verlagen, zou het wenselijk zijn het integratieniveau te verhogen door de omvormer zo dicht mogelijk bij de FV-module te plaatsen, niet alleen vanuit elektrisch oogpunt maar ook mechanisch, waarbij functioneel en elektrisch wordt gecombineerd met fysieke integratie. Door de omvormer rechtstreeks in de FV-module te integreren, kan het FV-module-omvormersysteem worden beschouwd als

één enkele bouwsteen in een FV-systeem. Door te specificeren welke inkapseling en verpakkingslagen kunnen worden gedeeld tussen de FV-module en de omvormer, zou men ook verschillende integratieniveaus kunnen overwegen.
Dit proefschrift presenteert de ontwerpoverwegingen voor een geoptimaliseerde omvormer die bedoeld is voor integratie in een goedkope, flexibele FV-module met dunne film. De omvormer is ontworpen door middel van een integraal ontwerpproces, waarbij ontwerpgebieden worden gecombineerd om te voldoen aan de strenge vereisten voor de integratie van FV-modules, met name die met betrekking tot het magnetisch ontwerp en hoge bedrijfstemperaturen.

Integratie van de omvormer in de FV-module zal zware omgevingsvoorwaarden opleggen aan de werking van de omvormer met verhoogde temperaturen en grote temperatuurschommelingen. FV-modules zijn relatief eenvoudige en robuuste apparaten en het is een uitdaging om een omvormer te ontwerpen die aan hun betrouwbaarheid en levensduur kan voldoen. Bovendien zorgt een strakke thermische koppeling tussen de omvormer en de FV-module en de vereisten voor een laag profiel en flexibele constructie voor onderlinge afhankelijkheid tussen verschillende ontwerpgebieden. Drie hoofdgroepen van specificaties kunnen worden geïdentificeerd in het ontwerpproces van de module geïntegreerde omvormer, elk met zijn eigen doelen:

- Elektrisch ontwerp met het doel de conversie-efficiëntie te maximaliseren,
- Technologisch ontwerp met het doel om een laag profiel en flexibiliteit te bereiken,
- Thermisch ontwerp met als doel de bedrijfstemperaturen veilig te houden.

Het elektrische ontwerp is afhankelijk van het classificeren en rangschikken van de bestaande topologie op basis van elektrische prestaties en geschiktheid voor integratie om tot de meest geschikte topologie te komen. Verschillende mogelijke systeemarchitecturen worden overwogen, wat resulteert in verschillende topologie opties die zijn geselecteerd voor de geïntegreerde omvormer van de FV-module.

Er wordt een overzicht gegeven van bestaande technologieën en het definiëren van nieuwe verpakkings- en integratieconcepten als de meest geschikte platforms om een FV-module geïntegreerde omvormer te implementeren. De bestaande geschikte technologieën worden gerangschikt op basis van thermische, elektrische en mechanische prestaties, beperkingen, kosten en betrouwbaarheid. Speciale aandacht wordt besteed aan de mogelijkheid van een hoge schakelfrequentie en de inschakeling van halfgeleiderapparaten op basis van GaN- en SiC-technologieën; en aan magnetische componenten als het meest kritische onderdeel voor het bereiken van integratie met een laag profiel.

De bestaande thermische beheerstrategieën die geschikt zijn voor omvormers met een laag profiel worden geanalyseerd en ingedeeld op basis van technologische en elektrische vereisten. Het thermische model van de gecombineerde FV-module en de geïntegreerde omvormer wordt gepresenteerd, vanaf systeemniveau tot componentniveau.

Tot slot worden de individuele ontwerpgebieden gecombineerd in een uniforme ontwerpprocedure, gebaseerd op het definiëren van elektrische specificaties van omvormers en elektrisch ontwerp, het kiezen van het technologieplatform en het definiëren van thermische vereisten met behulp van het ontwikkelde thermische model. Op basis van de optimalisatieparameters wordt de meest geschikte combinatie van topologie, technologie en thermomanagementparameters verkregen. Als resultaat presenteert het hoofdstuk twee mogelijke oplossingen door de assemblage, experimentele validatie en prestatie-evaluatie van het ontwerp van de geïntegreerde omvormer.

Publications

[1] M. Acanski, J. Popovic-Gerber, J.A. Ferreira, “Next Generation Power Electronics Technology for Photo Voltaic Systems,” Young Researchers Symposium, 2010

[2] M. Acanski, J. Popovic-Gerber, J. Ferreira, “Thermal Modeling of the Module Integrated DC-DC Converter for Thin-Film PV Modules,” Power Electronics and Motion Control Conference (EPE/PEMC), 2010

[2] M. Acanski, J. Popovic-Gerber, J. Ferreira, “Thermal Modeling of the Module Integrated DC-DC Converter for Flexible Thin-Film PV Modules,” European Conference on Power Electronics and Applications, 2011

[3] M. Acanski, J. Popovic-Gerber, J. A. Ferreira, “Comparison of Si and Gan Power Devices Used in PV Module Integrated Converters” Energy Conversion Congress and Exposition (ECCE), 2011

[4] M. Acanski, J. Popovic-Gerber, J. Ferreira, “Flexible Low Profile PV Module Integrated Converter for Distributed MPPT PV System,” Power Electronics and Motion Control Conference (EPE/PEMC), 2012

[5] Z. Ouyang, M. Acanski, J. Popovic, J. Ferreira, O. Thomsen, M. Andersen, “Design Considerations of Very Low Profile Coupled Inductors for Flexible Photovoltaic Module,” International Conference on Integrated Power Electronics Systems (CIPS), 2012

[6] M. Acanski, Z. Ouyang, J. Popovic, J. Ferreira, O. Thomsen, M. Andersen, “Very Thin Flexible Coupled Inductors for PV Module Integrated GaN Converter,” International Power Electronics and Motion Control Conference (ECCE/PEMC), 2012

[7] M. Acanski, J. Popovic-Gerber, J. Ferreira, “Design of a Flexible Very Low Profile High Step-Up PV Module Integrated Converter,” Energy Conversion Congress and Exposition (ECCE), 2012

[8] M. Acanski, J. Popovic-Gerber, J. Ferreira, “Design of a Flexible Low-Profile PV Module Integrated Converter,” manuscript in preparation

Curriculum Vitae

Miloš Ačanski was born in Kula, Yugoslavia on March 11, 1983. He graduated from the Faculty of Electrical Engineering, Department of Electronics, Telecommunications and Control, University of Belgrade, Serbia in 2008. In March 2009, he started working towards his PhD degree at the Delft University of Technology in the Netherlands. His PhD project focuses on design of DC-DC converters for photovoltaic systems.

His research interests include high switching frequency power converters, control theory and high precision measurements.